Charles University in Prague

Faculty of Science

Geology

Mgr. Lucie Nováková

Brittle tectonics in the NE Bohemian Massif as related to recent tectonic movements indicated by GPS measurements

Ph.D. Thesis

Supervisor: Prof. RNDr. František Hrouda, CSc.

Consultant: RNDr. Jiří Málek, Ph.D.

Prague, 2013

Declaration

The contents of this thesis are all my own work, except otherwise stated. The views and opinions expressed herein are mine and not necessarily those of any other person or anybody unless so attributed. This thesis or its major part has never been used to obtain any different or same academic degree.

Declaration [in Czech]

Prohlašuji, že jsem závěrečnou práci zpracovala samostatně a že jsem uvedla všechny použité informační zdroje a literaturu. Tato práce ani její podstatná část nebyla předložena k získání jiného nebo stejného akademického titulu.

Tupadly, 15.3.2013 Mgr. Lucie Nováková

Contribution of co-authors

Two of the papers included in the thesis, had been prepared in cooperation with my colleagues from the Institute of Rock Mechanics and Structure, Academy of Sciences of the Czech Republic, v.v.i. These are:

(1) Nováková, L., Hájek, P., Šťastný, M., 2010. Determining the relative age of fault activity through analyses of gouge mineralogy and geochemistry: a case study from Vápenná (Rychlebské hory Mts.), Czech Republic. International Journal of Geosciences, 1, 2, 66–69.

(2) Nováková, L., Balek, J., Active tectonics and paleostress reconstruction of Hronov – Poříčí Fault Zone, NE part of the Czech Republic. Studia Geophysica et Geodetica. Under review.

The paper (1) confronts relative age determination of faults based on geochemical analysis of the fault gauges with the intersection law. The paper co-authors Mgr. Hájek and Dr. Štastný were responsible for geochemical interpretation and chemical analysis, respectively. Regarding this article, I did the field work, including identification of the faults and gauge sampling, as well as geological data interpretation.

The paper (2) deals with tectonic history of the Hronov – Poříčí Fault Zone area. The paper co-author Ing. Balek proceeded raw GPS data, calculated GPS movements and evaluated measurement errors. On the other hand, I set the concept of the work, including choosing of the GPS stations and geological interpretation of the movements. I also handled all brittle tectonics related issues of the paper.

It is obvious that the team work included joint discussion on the topic of the papers. I am grateful to all co-authors for their ideas and comments during this process.

Abstract

North-eastern part of the Bohemian Massif is characterised by many NW-SE striking faults. The Sudetic Marginal Fault Zone (SMFZ) and Hronov – Poříčí Fault Zone (HPFZ) represent the major seismoactive dislocations in this area. Field structural investigations, including fault-slip data collection were carried out on a number of natural outcrops and quarries with the aim of establishing a robust and field-constrained model for the local brittle structural evolution of the studied areas. Almost 5000 faults and fractures have been measured and studied in 116 localities. Two principle sets of faults within the SMFZ are oriented in the N-S and W-E directions. The faults are mainly dipping under 80-90°. The lineations found on the fault planes are mainly trending to the SW and W. The kinematic frequent analysis was performed due to the distribution of the fault types in the orientations.

The faults were divided into the different tectonic phases based on their origin or reactivation and their relative age using the calculation of paleostress analysis. The paleostress analysis of the fault-slip data within the SMFZ resulted identification of six tectonic phases from the youngest to the oldest: strike-slip regime with maximum compression σ_1 in the NNW-SSE direction, compressional regime with σ_1 in the WNW-ESE direction, extensional regime with subvertical σ_1, extensional regime with σ_3 in the ENE-WSW direction, strike-slip regime with σ_1 in the NNE-SSW direction, strike-slip regime with σ_1 in the NW-SE direction. The faults within the HPFZ are mostly oriented in NW-SE direction, nevertheless in minor they also occur in NE-SW direction. The faults are mainly vertical or subvertical dipping 70-90°. The lineations found on the fault planes are mainly trending to the NE, S, SSW and SW. The paleostress analysis of the fault-slip data within the HPFZ resulted in indentification of four tectonic phases from the youngest to the oldest: compressional regime with σ_1 in NE-SW direction, compressional regime with σ_1 in WNW-ESE direction, strike-slip regime with σ_1 in NW-SE direction, strike-slip regime with σ_1 in NNE-SSW direction.

Six GPS stations (BISK, PETR, LANS, VIDN, STAM and VRES) were employed for long-term GPS monitoring in the SMFZ area. Five GPS stations (BEZD, MOKA, TURO, UPIC a ZOLE) monitored the HPFZ area. Both horizontal and vertical components of the movements were calculated from long-term GPS monitoring data. Standard errors calculated for individual stations pointed out the permanent GPS stations provide up to a hundred times more precise positioning than the campaign stations. To highlight the local component of station movements three various methods were applied to set the regional component. The highest local horizontal velocity within the SMFZ area was found for the GPS station VIDN (1.33 mm/y). The highest local vertical velocity within the SMFZ area

was calculated for the GPS station PETR (2.54 mm/y) upwards. Generally, comparing to the whole area, stations BISK and PETR move downwards, while the stations LANS, VIDN, STAM and VRES move upwards. The highest local horizontal velocity within the HPFZ area was calculated for GPS station MOKA (2.18 mm/y). The highest local vertical velocity within the HPFZ area was calculated for GPS station TURO (2.61 mm/y) upwards. The stations BEZD, MOKA and TURO move downwards, while the stations UPIC and ZOLE move upwards.

The brittle tectonic data has been related to the recent tectonic movements indicated by the GPS measurements. Both structural and GPS data were compared and the actual activity and stress conditions of the SMFZ and HPFZ areas were constructed. The SMFZ has been a sinistral fault zone with strike-slip regime recently. The HPFZ has been a dextral transpressive fault zone in compressional regime recently. In both studied areas, the youngest tectonic phase defined by the paleostress analysis corresponds to the actual movements found by the GPS monitoring. Thus the employed methods provided useful complementary results.

Abstract [in Czech]

Pro severovýchodní část Českého masívu je charakterická řada zlomů ve směru SZ-JV. Sudetské okrajové zlomové pásmo (SMFZ) a Hronovsko-Poříčské zlomové pásmo (HPFZ) představují hlavní seismicky aktivní poruchy v oblasti. S cílem vytvořit robustní, geologické realitě odpovídající, model tektonické situace studované oblasti byl proveden terénní strukturně-geologický průzkum zaměřený na křehké porušení hornin. V průběhu průzkumu bylo na 116 lokalitách, na přirozených výchozech i v lomech, změřeno téměř 5000 zlomů a puklin. V zóně SMFZ jsou dvě základní skupiny zlomů orientovány ve směru S-J a Z-V. Tyto zlomy většinou strmě upadají pod úhlem 80-90°. Lineace nalezené na zlomech přitom obvykle směřují k JZ a Z. Pro jednotlivé typy zlomů byla provedena analýza četnosti orientací zlomových ploch.

Zlomy byly pomocí paleonapěťové analýzy rozděleny do šesti různých tektonických fází, v nichž vznikaly nebo byly reaktivovány, a fáze byly seřazeny podle relativního stáří. V oblasti SMFZ byly identifikovány následující tektonické fáze (od nejmladší po nejstarší): strike-slip režim s maximální kompresí (σ_1) ve směru SSZ-JJV, kompresní režim s σ_1 ve směru ZSZ - VJV, dva následující extenzní režimy s minimální kompresí (σ_3) ve směru VSV- ZJZ (s lišícími se kvazi-vertikálními σ_1), strike-slip režim s maximální kompresí (σ_1) ve směru SSV-JJZ a další strike-slip režim s maximální kompresí (σ_1) tentokrát ve směru in SZ-JV. Zlomy uvnitř HPFZ jsou orientovány zejména ve směru SZ-JV. Pouze v menší míře se vyskytují i zlomy orientované SV-JZ. Zlomy jsou obvykle vertikální nebo subvertikální upadající pod úhlem 70–91°. Lineace na zlomových plochách směřují především k SV, J, JJZ a JZ. Paleonapěťová analýza indikovala v oblasti HPFZ tyto čtyři tektonické fáze (od nejmladší k nejstarší): kompresní režim s maximální kompresí σ_1 ve směru SV-JZ, další kompresní režim s maximální kompresí σ_1 ve směru ZSZ-VJV, strike-slip režim se σ_1 ve směru SZ-JV a další strike-slip režim s maximální kompresí σ_1 ve směru SSV-JJZ.

Šest GPS stanic bylo použito k dlouhodobému monitoringu v okolí SMFZ (BISK, PETR LANS, VIDN, STAM a VRES), pět pro monitoring oblasti HPFZ (BEZD, MOKA, TURO, UPIC a ZOLE). Dlouhodobý GPS monitoring poskytl data pro výpočet horizontální i vertikální složky pohybů. Vyčíslení směrodatných odchylek pro jednotlivé GPS stanice zřetelně ukázalo, že přesnost stanovení polohy je u permanentních stanic proti kampaňovým až o dva řády vyšší. Pro zvýraznění lokálních pohybů byla v obou oblastech zavedena oprava o generelní trend pohybu. Použity byly tři různé varianty stanovení opravy: (1) oprava o hodnoty vyplývající z modelu NNR-NUVEL1A, (2) aritmetický průměr pohybů stanic v oblasti a (3) vážený průměr pohybů stanic v oblasti. Relativní směr pohybu v horizontální rovině byl vyjádřen geografickým azimutem. Po zavedení opravy

vykazují v oblasti SMFZ největší odchylku stanice VIDN v horizontálním směru (až 1.33 mm/rok) a PETR ve vertikálním směru (až 2.54 mm/rok). Obecně, v porovnání s celou oblastí okolí SMFZ, stanice BISK a PETR zaklesávají, zatímco stanice LANS, VIDN, STAM a VRES stoupají. V oblasti HPFZ byly po zavedení oprav největší pohyby zaznamenány na stanicích MOKA (v horizontální rovině až 2.18 mm/rok) a TURO (až 2.61 mm/rok ve vertikálním směru). Stanice BEZD, MOKA a TURO v porovnání s generelním trendem oblasti zaklesávají, zatímco stanice UPIC a ZOLE stoupají.

Výsledky paleonapěťové analýzy byly konfrontovány s aktuálními pohyby v okolí obou zlomových zón zaznamenanými GPS monitoringem. Ze srovnání strukturních a GPS dat byla stanovena aktuální aktivita a napěťové podmínky obou oblastí. SMFZ je tak v současné době sinistrální zlomovou zónou ve strike-slip režimu. HPFZ je dextrálně transpresní zóna v kompresním režimu. Nejmladší dokumentovaná tektonická fáze přitom v obou oblastech koresponduje s aktuálními pohyby podle GPS monitoringu. Provedené práce tak ukázaly komplementární povahu obou použitých metod.

Acknowledgements

I gratefully acknowledge the Grant Agency of the Charles University for funding the project "Comparative study of the directions of recent tectonic activity according to structural geology research and long-term GPS monitoring in the Rychlebské hory Mts., Czech Republic" during the years 2008-2009 (43-258020), Ministry of Education, Youth and Sports for funding the project "Recent dynamics of Earth" during the years 2005-2008 (LC 506), Grant Agency of the Czech Republic for funding the project " Nature of seismicity in the Hronov – Poříčí Fault area" during the years 2010-2012 (205/09/1244), Institute of Rock Structure and Mechanics Academy of Sciences of the Czech Republic, v.v.i. (IRSM AS CR) for funding within a research plan during the years 2005-2010 (A VOZ 30460519).

I would like to thank Institute of Rock Structure and Mechanics Academy of Sciences of the Czech Republic (IRSM AS CR), v.v.i. where I have been working since 2005 that enabled me to study my PhD. I also thank to Institute of Petrology and Structural Geology, Faculty of Science, Charles University where I have been studying since 2006 that enabled me to study my PhD. My special thanks go to Doc. Mgr. David Dolejš, Ph.D., Head of the Institute, for valuable suggestions.

I thank to National Research Council of Italy for funding my stage in Third Rome University and field courses in Central Apennines, L´Aquilla region during the years 2007-2010. Prof. Fabrizio Storti and Dr. Fabrizio Balsamo took care about me during the stages and taught me many things about brittle tectonics and field work.

A large number of people have worked in GPS campaigns arranged by Institute of Rock Structures and Mechanics Academy of Sciences of the Czech Republic, v.v.i. during 15 years of GPS campaigns in the years 1997-2012. Without them it would not be possible to write this thesis. My thanks go to all of them. I personally have attended many GPS campaigns during the years 2001-2008. I thank to Dr. Vladimír Schenk and Dr. Zdeňka Schenková for organising the campaigns and endless energy to the work. I thank to my colleagues from the Department of Geogynamics IRSM AS CR, v.v.i., especially Dr. Milada Cajthamlová and Dr. František Mantlík for their helpful advice, Ing. Jan Balek for compilation of the GPS data and Mr. Zdeněk Fučík for all technical stuff relates to GEONAS network.

I am grateful to Prof. František Hrouda for supervising my thesis. I am also grateful to my consultant Dr. Jiří Málek, Head of the Department of Seismotectonics, for his critical review of the thesis, many advice and comments.

Many thanks go to my colleagues from Department of Seismotectonics IRSM AS CR, v.v.i. and to my friends for their help with the finishing the thesis, endless optimism and friendship. I also thank to Dr. Petra Štěpančíková for useful comments and suggestions and Dr. Jiří Žák for his priceless field lessons.

I am grateful to Dr. Jure Žalohar for free use of software T-Tecto 3.0 Professional, Dr. Jiří Zachariáš for useful discussions related to this software and Prof. Francesco Salvini for free use of software Daisy3. ASTER GDEM, I used to visualize my results, is a product of METI and NASA.

The last but not least thank belongs to my parents, my sister, my husband´s parents and to my husband Petr for their patience and comprehension with my study. My son Petr helped me to finish the thesis with his unconquerable smiles and first steps.

Table of Contents

List of Figures

List of Tables

Table of Abbreviations

AGNES… Automated GPS Network for Switzerland

CEGRN…Central European GPS Geodynamic Reference Network Consortium

CODE… Center of Orbit Determination in Europe

DPGA… Dutch Permanent GNS Array

EFS…Elbe Fault System

EPN...European Permanent Network

ETRS89…European Terrestrial Reference System 89

EUREF… European Geodetic Reference Systems

GDEM…Global Digital Elevation Model

GEONAS…Geodynamic Network of Academy of Sciences

GEONET… GPS Earth Observation Network

GLONASS…Global Navigation Satellite System

GNSS…Global Navigation Satellite Systems

GPS…Global Positioning System

HPF…Hronov – Poříčí Fault

HPFZ…Hronov – Poříčí Fault Zone

HPT…Hronov – Poříčí Trough

IAG… International Association of Geodesy

ISF…Intra – Sudetic Fault

ITRF…International Terrestrial Reference Frame

IRSM AS CR, v.v.i…Institute of Rock Structure and Mechanic Academy of Sciences of the Czech Republic, v.v.i.

NAVSTAR…Navigation Signal Timing and Ranging Global Positioning System

NNR-NUVEL1A…No net rotation Northwestern University Velocity model

RDM…Right Dihedra Method

SMF…Sudetic Marginal Fault

SMFZ…Sudetic Marginal Fault Zone

TGO…Trimble Geomatics Office

VGF…Visualization of the Gauss function

Chapter 1

Introduction

1.1. Brittle tectonics and long-term GPS monitoring

In geology, a combination of various methods is, in general, a useful tool for analysing the development of the structures and actual conditions of a studied area. Obviously, the most promising approach is the using of complementary methods from various disciplines, providing different points of view.

Brittle tectonics is a powerful tool for studying rock characteristics in the field. During brittle conditions a rock matrix tends to a deformation of the structure and even to the fracturation. Results of a brittle deformation are tensional or shear fractures and faults. During fracturing, typically only sliding has significant effects on the reactivation on existing shear fractures. These structures tend to repeat the fracturation when the conditions are favourable and reactivated fractures are developed. The kinematic indicators on fault planes are a sign of movements along these planes. On the base of fractures orientation of the fractures and indicators of the movements along the planes, it is possible to determine the stress conditions during which the studied fractures have been developed or reactivated. The multiple lineation systems allow separating different tectonic phases and, where possible, even to determine the relative age of the phases. This method is called the paleostress analysis. With this approach, the youngest tectonic phase can be described and confronted with the actual movements and tectonic stress conditions determined by another method e.g. long-term GPS monitoring.

Long-term GPS monitoring is a method used for precise geodetic position measurements. Low cost handheld GPS receivers have become increasingly popular to a big amount of users providing position, velocity and navigation information under all weather conditions. Moreover, continuous observations of permanent GPS stations provide information about changes of position due to lithosphere continental plate motions, regional and local geodynamics and periodical variations of geocentric coordinates.

1.2. Scope of the thesis

Scope of the thesis covers two principal areas. First, on the methodological level, the thesis confronts two methods for studying of tectonic movements, while in the second part, an idea of a tectonic development on the regionally geological level, is suggested.

Geological mapping focused on the brittle tectonic structures provides input data for a kinematic analysis. The analysis points out stress history of a locality or area. Eventually, several tectonic phases and the timing might be defined. It is obvious that any kinematic indicator found during mapping represent a movement, which took place in past. Long-term GPS monitoring, on the other hand, delineates actual movements in the area. The tectonic interpretation of GPS data, however, requires at least basic idea of the tectonic situation. The thesis highlights a complementary character of both methods. The approach is demonstrated on, tectonically speaking, less known area of the Bohemian Massif. Two parallel, regionally important, tectonic structures were chosen in the NE part of the Massif. The Sudetic Marginal Fault is a large active fault which is situated in the northeast border of the Bohemian Massif. The Hronov – Poříčí Fault Zone is a seismically active structure with documented earthquake of magnitude 4.7 in the historical catalogue. The thesis points out a current movement along the structures as well as the actual and historic stress conditions.

1.3. Main aims of the thesis

The main aim of the thesis has been to contribute to the rare geological information about NE part of the Bohemian Massif. Geological mapping has been done during 90th years of the 20th century. However, no detailed structural geological and tectonic investigation had been done before. Two parallel, regionally important, tectonic structures were chosen in the NE part of the Bohemian Massif. The Sudetic Marginal Fault Zone (SMFZ) is a large active fault zone which makes northeast border of the Bohemian Massif. The Hronov – Poříčí Fault Zone (HPFZ) is a seismically active structure with documented M4.7 earthquake. To achieve the set objectives, it was necessary to proceed paleostress analysis to determine different stages of the development of the studied geological structures.

Data from long-term GPS monitoring provided precise location of the locality with the GPS station and allowed to estimate the mean directions of the geological unit actual movements.

The other aim has been to test a possibility of correlation the data and the results of the paleostress analysis and long-term GPS monitoring. Two distinct methods from different science disciplines, geology and geodesy, were brought together to confront and compare. The interpretation of the data from both methods provided a multidisciplinary study of the studied fault zones. Correlation between these two methods provided complex information of the tectonic history and the actual stress conditions of the studied areas. Moreover, complementary results have been expected.

Chapter 2

State of the art

2.1 Fundamentals of the brittle tectonic and paleostress analysis

Faults are weak zones in the brittle part of the lithosphere, along which movement can take place in a response to applied stress. When fault undergoes a displacement, strain markers can be formed on its surface. These markers are used in brittle tectonics, which is widely used as a tool for studying a paleostress evolution of big geological units (e.g. Bergerat et al., 1992; Lee et al., 1996; Bistachi and Massironi, 2000; Strzerzynski et al., 2004; Khanbari and Huchton, 2010; Viola et al., 2011) as well as small areas (e.g. Havíř, 2002; Popotnig et al. 2007; Komárek, 2009; Kounov et al., 2011; Zachariáš and Hübst, 2012). The paleostress reconstruction is an important technique because it allows an interpretation of the stress conditions in the past. It is therefore important to collect in field as many measurements as possible. Field observations is important in separating sets that homogeneously represent the same deformation event because they provide independent information that may support or help to correct calculation inconsistencies (Burg, 2012).

There are many authors who described methodology of the brittle tectonic or collecting data in field (e.g. Hancock, 1985). He suggested collecting microstructural data from small sampling stations (stations) that are structurally homogeneous domains. Doblas (1998) described new classification of the sliskensides. He used 61 criteria to subdivide them to 11 major groups. Usually there are three or four types of the kinematic indicators in field. Finding the fault planes with two or more sets of slickensides enables to determine the relative age of the paleostress phases. Where complex fault pattern occurs, the recognition of phases of faulting has been invoked as a tool to reconstruct the faulting history (Angelier, 1994). Moreover, non-striated faults can be used to make a paleostress analysis and determine stress field (Arlegui et al., 2006). Viola et al. (2011) paid specific attention to direct crosscutting relationships among several generations of faults because this helped to add constraints to the relative time sequence of events. In conjugate fault systems, the orientations of fault planes as well as slickensides are determined by the principle stress axes, because the same tectonic event induces both formation of faults and movements along them. However, faulting commonly uses previous discontinuities as older faults or joints (Angelier, 1979). Salvini and Storti (2005) suggested framing a conjugate set of

faults to the boxes. They used this methodology in strike-slip fault network in Ross Sea Region in Antarctica (Salvini et al., 1997).

Since the 1970s a variety of methods have been proposed for estimating paleostress phases from field measurements of fault striations on fault planes (e.g. Carey and Brunier, 1974; Angelier and Mechler, 1977, Nemcok and Lisle, 1995; Yamaji, 2000; Žalohar and Vrabec, 2007). One of the best known and a widely used graphical technique to visualize paleostress phases is the Right Dihedra Method developed by Angelier and Mechler (1977). This method is based on the idea that orientation of the maximum principal stress axis is constrained to the pressure quadrant (P), while orientation of the minimum principal stress axis is constrained to the tension quadrant (T) associated with a chosen fault. Spatial orientation and position of the P and T quadrants is defined by orientation of the fault plane and the slip direction along it. This enables to construct the approximate direction of the principal stresses as the geometrical centre of the common intersection of the P and T quadrants (Žalohar, 2009). Existing methods can be roughly divided into two categories according to a data character. The first category assumes that the stress field is homogeneous (e.g. Angelier, 1984; Nieto-Samaniego, 1998). The second category of the methods is concerned with heterogeneous sets of the field data (e.g. Yamaji 2000; Liesa and Lisle, 2004; Kernstocková and Melichar, 2006; Žalohar and Vrabec, 2007; Melichar and Kernstocková, 2008).

One of the methods used for calculating paleostress analysis is the Gauss method. This method is based on the philosophy of the fault-slip data inversion, which involves the concept of the best fit stress tensor (Žalohar and Vrabec, 2007). The T-Tecto program enables classical analysis of heterogeneous and even homogeneous fault-slip data using several different numerical methods including the Gauss method. The program is based on the fault-slip data inversion which involves the concept of best-fitting stress and strain tensors (Žalohar, 2009).

2.2 Fundamentals of the GPS and its correlation with geology

In the past it was not possible to watch the tectonic plates moving. The geologists accepted that they moved, but all the evidence was indirect. Now, thanks to the Global Navigation Satellite Systems (GNSS) everyone can see the plates are moving. Currently operating GNSS's are NAVSTAR GPS (U.S. Navigation Signal Timing and Ranging Global Positioning System) and GLONASS (Russia's Global Navigation Satellite System). Another GNSS planned for the future is Europe's Galileo.

GPS are used worldwide and especially for the structural geologists are very useful. By repeatedly measuring distances between specific points, geologists can determine the movement along faults or between the plates. Usually arrays of few to tens of GPS stations are used to investigate the active tectonics of the studied area (e.g. Dixon et al., 1997; Calais et al., 2000; Caporali et al., 2003; Bechtold et al., 2009; Styron and Taylor, 2009).

There are many local GPS networks and arrays (e. g. AGNES, DPGA, GEONAS, GEONET) (e.g. Mantlík et al., 2005; Dach et al., 2009). There are also European GPS stations covering some of the small ones (Grenerczy et al., 2005) (Fig. 1). The Central European GPS Reference Network established in 1993 (Fejes et al., 1993) is operated by the CEGRN Consortium and covers 14 countries of the region. The European Terrestrial Reference System 89 (ETRS89) is used as the standard precise GPS coordinate system throughout Europe. The ETRS89 is maintained by the IAG sub-commission EUREF. It is accessed through the EUREF Permanent Network (EPN), a science-driven network of continuously operating GPS reference stations (Bruyninx et al., 2001; Bruyninx, 2004; Bruyninx, 2006).

It became very important to post-process raw GPS data using software that gives the desired accuracy for estimating the crustal deformations. A variety of software is available on the market today for processing the GPS observations. The GPS data processing software like commercial GPSurvey, Trimble Geomatics Office (TGO), SKI, etc., and academic Bernese, GAMIT are available. Likhar et al. (2002) dealt with the performance of different software used for processing GNNS data. They stated the Bernese post-processed baseline results are more precise, as compared to GPSurvey and TGO. Grácová et al. (2005) calculated GPS station movements in the Bohemian Massif determined by the GAMIT/GLOBK and BERNESE GPS software.

GPS enables to determine current stress rate (Calais et al., 2000), displacement of the stations (Bock et al., 1997) or velocities of the stations (e.g. D'Agostino et al., 2008). Bock et al. (1997) measured crustal deformation between two big earthquakes occurred within two years in California. They compared displacement rates at four GPS stations. Nevertheless, they stated their data are limited by the small number of continuous GPS stations and relatively short time interval. Calais et al. (2000) used a rigorous combination of GPS and triangular data collected within 50 years in the Western Alps. They estimated slip rates 2 - 4 mm a year. However, they mentioned a necessity of identification of potentially active faults and importance of integration of geodetic, geological and seismological information. Styron and Taylor (2009) established kinematics of active faults in the Himalayan arc using GPS geodesy and structural geology. Using 130 Himalayan and south Tibetan GPS geodetic vectors they were able to calculate the GPS station velocities, varying from zero to >30 mm a year. They also presented the results of the field mapping of the active, subvertical, right-slip, Tibrikot fault. Styron et al. (2010)

emphasized understanding the knowledge of the region's geologic structures. Finally, they predicted a model and tested it against structural and geodetic observations (Styron et al., 2011). It is clear that continuous data from a denser array need to be collected over longer periods of time in order to better sample crustal deformation in time and space (Bock et al., 1997).

Fig. 1 GPS velocities with respect to Euroasia (Grenerczy et al., 2005). Station GOPE and TUBO (operated by EPN) are situated in the Czech Republic.

2.3 GEONAS

Geodynamic Network of the Academy of Sciences of the Czech Republic (GEONAS, Fig. 2) has been established in 1997. All information is available online at geonas.irsm.cas.cz. The network contains 34 campaign (Fig. 2) and 20 permanent stations (Fig. 3). Permanent GNNS stations were set up in 2001 within the framework of the national Centre of Earth Dynamics Research activities. All stations register both NAVSTAR and GLONASS satellite signals. Four stations (MARJ, BISK, VACO and POUS) belong to the EUREF network of the permanent stations (EPN) since 2005. The

GNNS data are processed using the Bernese GPS software 5.0 (Beutler et al., 2007). The GEONAS network covers area of 400x220 km. The network enables monitoring of the effects of the dynamic processes going on inside the Earth's crust, as well as the upper lithosphere (Schenk et al., 2010). All stations have corresponding choke-ring antenna with snow domes. In addition, selected mountain stations are equipped with a web camera and meteorological sensors to monitor snow coverage at the antenna (Schenk et al., 2004).

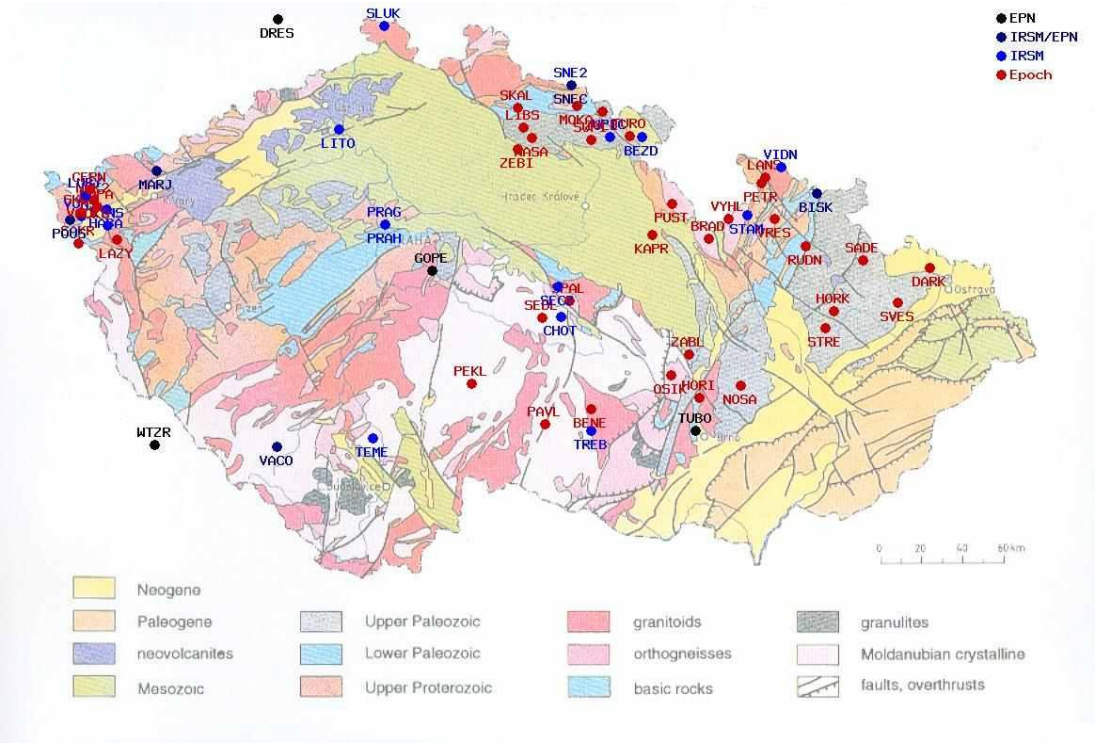

Fig. 2 GEONAS GPS stations (http://geonas.irsm.cas.cz).

2.3.1 Permanent stations

Since 2001 the permanent stations were established within the Bohemian Massif (Fig. 3). The aim of this work was the monitoring of the recent geodynamic movements. The stations are distributed in respect to the main fault zones and areas with detected earthquakes. Stations MARJ, LUBY, KYNS, POUS, HABA and VONS are situated in Western Bohemia in the seismic area of the Nový Kostel fault zone. Stations VIDN, BISK and STAM are positioned in the eastern part of the Bohemian Massif on the both sides of the Sudetic Marginal Fault Zone. Stations UPIC and BEZD are placed in East Bohemia each on the both sides of the Hronov – Poříčí Fault Zone. Stations SECZ and CHOT are situated in the Českomoravská Vysočina Highlands to monitor the Železné hory Mts. Fault Zone. Station PRAG is to be found on the building of IRSM AS CR, v.v.i. in Prague.

Station SNEC was abolished when the building of the Old Czech Post Office was demolished on the summit of Sněžka, the highest mountain of the Czech Republic. New station SNE2 has been established.

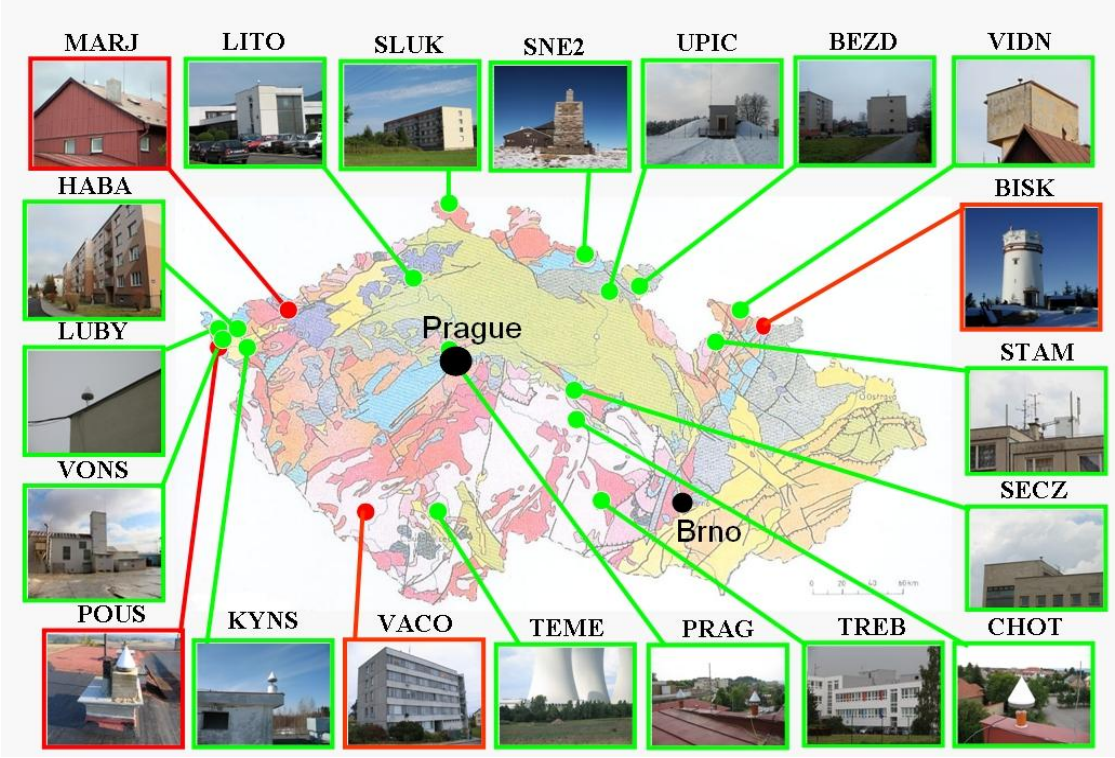

Fig. 3 GEONAS permanent stations (photographs by Z. Fučík). Red colour – EPN stations, green colour – others.

Fig. 4 Antennas and receivers used on the permanent stations. From left ASHTECH Z18 receiver with ASH701946.2 SNOW antenna, TPS GB-1000 receiver with TPSCR3_GGD CONE antenna, TOPCON NET-G3 receiver with TPSCR_G3 CONE (photographs by Z. Fučík).

Three types of antennas and three types of receivers are used on the permanent stations (Fig. 4). The most common receiver TPS GB-1000 (TOPCON) is located on 15 stations. The other receiver from the TOPCON company is TOPCON NET-G3 located on 4 stations. The remaining 2 stations employ the ASHTECH Z18 receiver. Antennas with CONE and SNOW type are used on all stations. Stations located in mountain areas are also equipped with a meteorological unit and webcamera because of the snow coverage monitoring on the antennas (Grácová et al., 2007).

2.3.2 Regional campaign network

The geodynamic network East Sudeten was established in 1997. It contains 12 stations for campaign GPS measurements. Fifteen GPS campaigns were realised at this network. After three campaigns Schenk et al. (2000) identified three geodynamic terrains in the northern part of the Moravo-Silesian region: the Moravo-Devonian terrane, the thrusting zone terrane located around the contact between the Hrubý Jeseník Mts. and the Rychlebské Hory Mts. – Králický Sněžník Mts., and the Outer (the NE part) Bohemian Massif terrane outside the Sudetic Marginal Fault. The geodynamic network West Sudeten was established in 2001. It contains 11 stations for campaign GPS measurements. Fourteen GPS campaigns were realised at this network. These two networks monitor the geodynamic movements between Lugian and Moravo-Silesian area.

The geodynamic network Highlands has been established in 2005. It contains 8 stations for campaign GPS measurements. Seven GPS campaigns were performed here. The network tends to monitor the geodynamic movements between the Moravo-Silesian area and structural blocks of Moldanubian. The geodynamic network West Bohemia was established in 2007. It contains 7 stations for campaign GPS measurements. Seven GPS campaigns were realised there. The network monitors the geodynamic movements in the seismogenic area of West Bohemia, particularly earthquake zones on the eastern edge of the Cheb Basin.

All the networks were set up to monitor the geodynamic movements with the aim to study recent activity on fault zones. The position of campaign stations was claimed with respect to the geological situation of the studied areas. Cement concrete pillars were built for every station to guarantee long-term stability. Pillars with 40x40 cm base are from 60 to 100 cm high (Fig. 5) (Cajthamlová, 2010). Each of concrete pillars is founded under the Earth's surface up to a depth that to secures its contact with bedrock (Schenk et al., 2000).

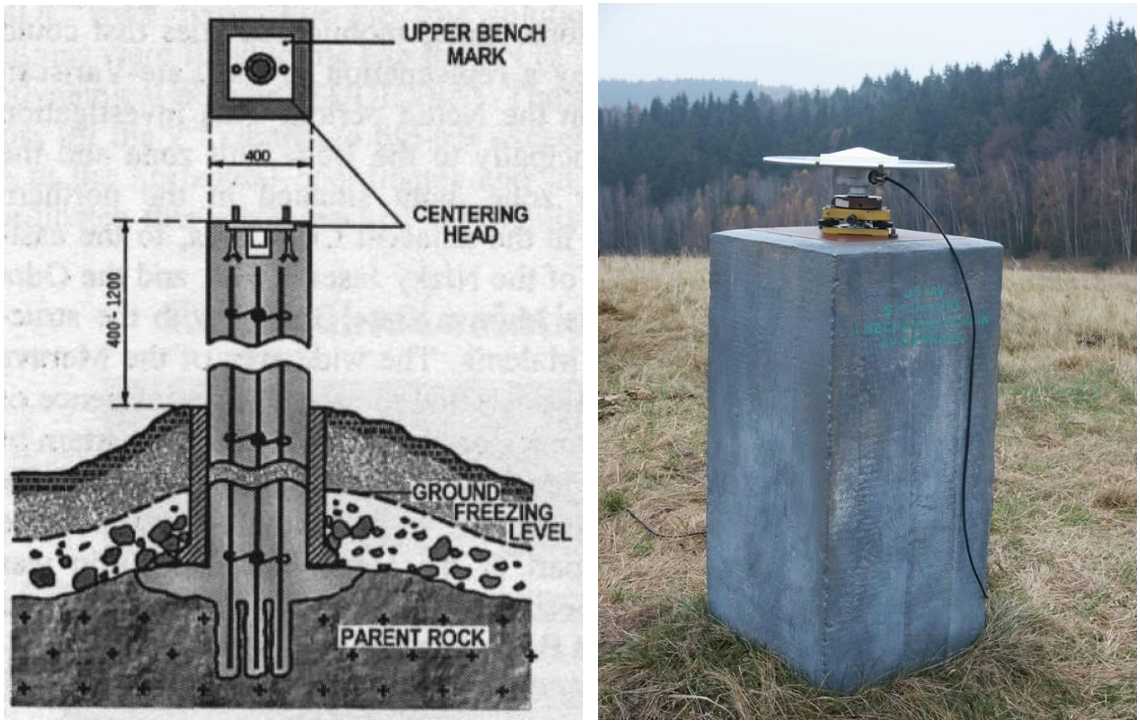

Fig. 5 Conctruction scheme of GPS station (left) (Schenk et al., 2000), photograph of the GPS station TURO (right) (autor L. Nováková).

2.4 NE part of the Bohemian Massif

2.4.1 Geology and tectonics

Two principal geological units, Lugian and the Moravo-Silesian area, form the studied area in the northeastern part of the Bohemian Massif. Lugian (Fig. 6), occurring in the north of the Bohemian Massif is dominant. This heterogeneous region contains mostly metamorphic Proterozoic and Paleozoic plutons of Cadomian and Variscan granitoids. It represents the northern border part of the Bohemian Massif from Elbe Line in the W and SW up to the Nýznerov and Ramzová Overthrusts in the E (Chlupáč et al., 1994). The Ramzová overtrust is the tectonic border between Lugian and Silesicum, a part of the Moravo-Siesian area (Opletal and Pecina, 2004).

The Moravo-Silesian area covers only the south and southeastern part, where it is divided by the Elbe fault. These units are also called West and East Sudetic System, respectively (Opletal and Pecina, 2004). The substantial part of the Lugian is situated in Germany and Poland (Góry Kaczwskie Mts., Góry Sowie Mts., Góry Bardzké Mts., part of the Krkonoše Mts., Orlické hory Mts, Králický Sněžník Mts., etc.). The Lugian Plutonic Complex, Krkonoše-Jizera Crystalline Complex, Krkonoše-Jizera Pluton, Orlice-Sněžník Crystalline Complex and Rychlebské hory Mts. can be found in the Czech Republic.

The most common rocks of the Lugian are as follows: various types of orthogneises, biotitic paragneises and two-mica schists. Crystalline limestones (marbles), phyllites, amphibolites and green schists occur in less metamorphosed areas.

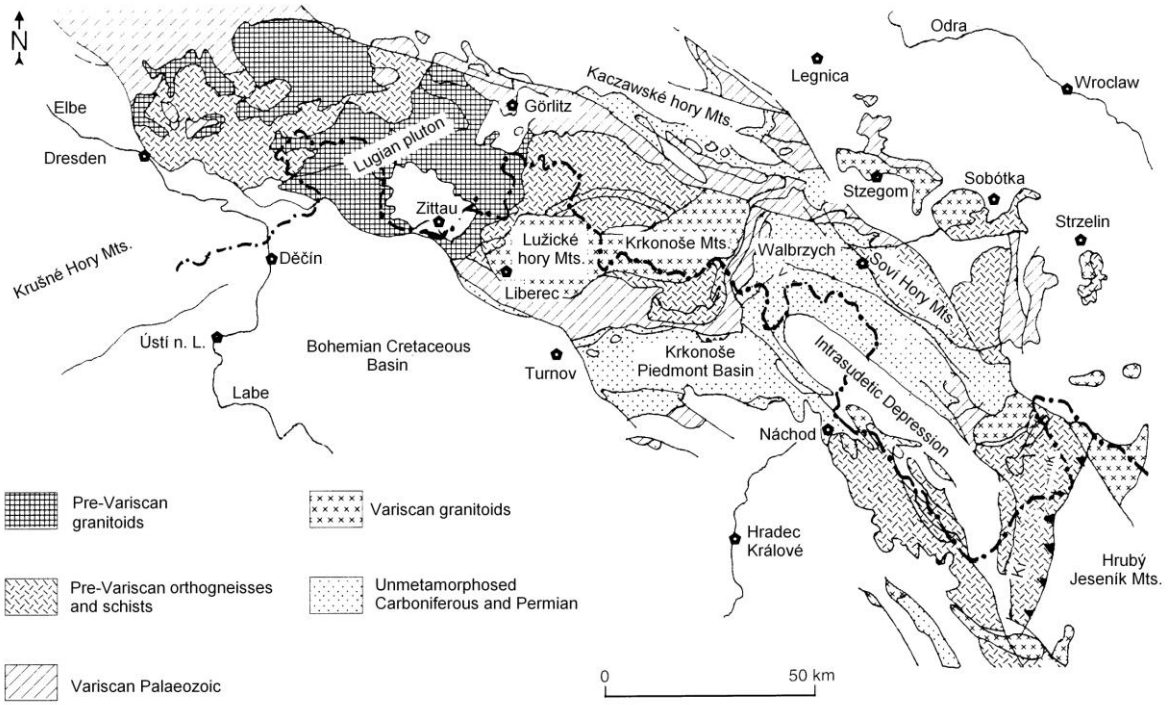

Fig. 6 Geological map of Lugian (after Chlupáč et al., 2002).

The Moravo-Silesian area (Fig. 7) represents the eastern part of the Bohemian Massif. It contains Brunovistulicum (the Upper part of the Proterozoicum and its younger sediments), Moravian (the crystalline parts forming the east border of the Moldanubian overthrusting Brunia), Silesian (the crystalline parts of the Hrubý Jeseník Mts.), Žulová Plutonic Complex (Variscan pluton) and the Moravo-Silesian Paleozoic (mainly Devonian and Lower Carboniferous). The boundary between the Moldanubian and Brunia Units was defined by Suess (1912) as a zone of severely deformed and metamorphosed continental rocks, termed as the Moravo-Silesian Zone. Schulmann and Gayer (2000) interpreted the Moravo-Silesian Zone as a NNE-SSW trending belt being the result of the oblique Variscan collision between the Moldanubian terrain and the Brunovistulian domain. Cymermann et al. (1997) described its sense of displacement from dextral related to oblique, northeasternward displacement of the crystalline Moldanubian nappes over the Moravian, to extensional sinistral movements.

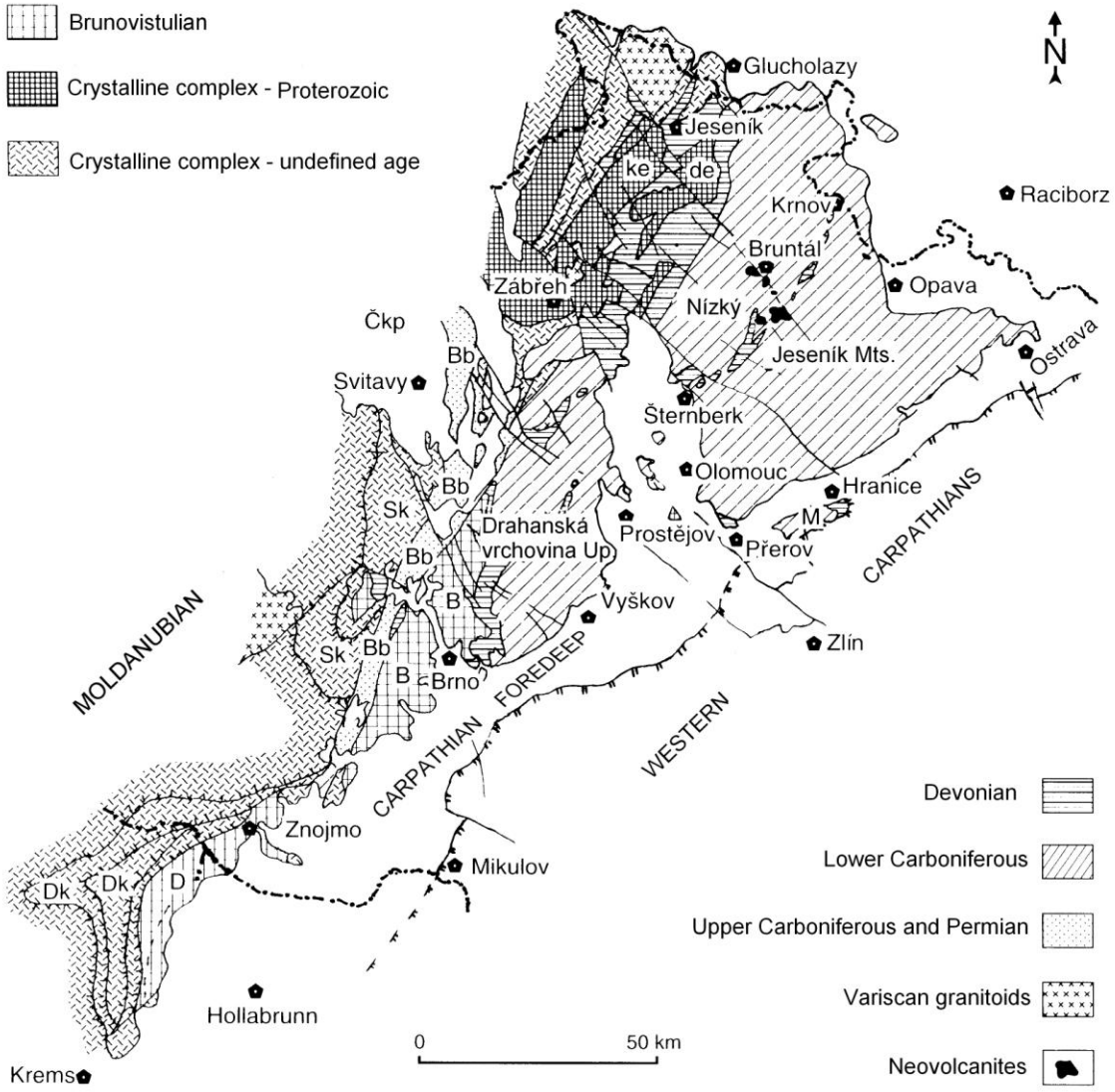

Fig. 7 Geological map of the Moravo-Silesian area (after Chlupáč et al., 2002).

The Variscan orogenesis is of a fundamental importance for the area. Effects of the Variscan deformation and metamorphism are the most significant in the western parts. From west to east the effects of Variscan orogenesis are more intensive in Brunovistulicum (Chlupáč et al., 2002). After the main Varican orogenesis the geological units were not significantly folded and represent a relatively consolidated base. The younger Alpine orogenic processes (in Mesozoicum and Tertiary) formed areas extendidng from Alps to Carpathians. In the Silesian area, this orogenesis is represented by many faults with vertical component of movement, up-thrusts or down-thrust of large units. Younger sediments formed after the Variscan orogenesis are named as platform ones.

2.4.2 Theory about SMFZ and HPZ

Wojewoda (2007) stated the Sudetic Marginal Fault and Hronov-Poříří Fault are the major dislocations in the Sudetes. The seismoactive zone on the NE margin of the Bohemian Massif is approximately 40-60 km wide and 150 km long and comprises a number of NW-SE and NNW-SSE striking faults (Valenta et al., 2008) (Fig. 8).

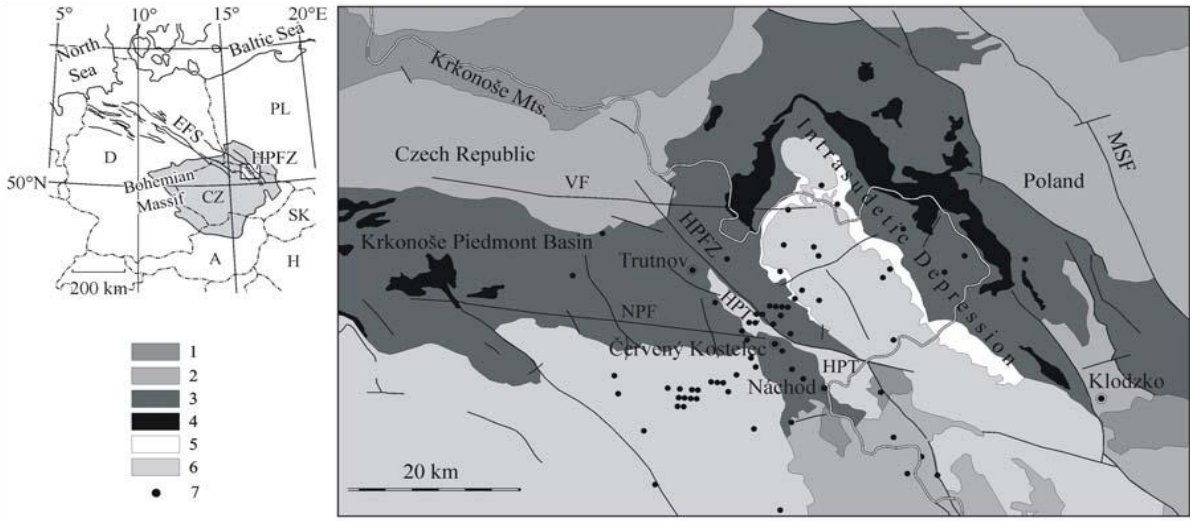

Fig. 8 Geology and tectonics of the study area. 1 – plutonic rocks (granites, granodiorites), 2 – metamorphites (gneisses, schists, granulites, migmatites), 3 – Permian and Carboniferous sediments, 4 – Permian volcanites, 5 – Triassic sediments, 6 – Cretaceous sediments, 7 – epicentres of seismic events recorded from 1985 to 2005 (after Catalogue of regional seismic events, published by the Geophysical Institute AS CR at http://web.ig.cas.cz/en/seismic-service/catalogs-of-regional-seismic-events/). HPFZ – Hronov – Poříčí Fault Zone, HPT – Hronov – Poříčí Trough, VF – Vrchlabí Fault, NPF – Nová Paka Fault, MSF –Sudetic Marginal Fault, EFS – Elbe Fault System (see the small-scale map in the upper left corner) (after Valenta et al., 2008).

This structure represents a regional zone of weakness within the SE termination of the Elbe Fault System, defined by a mesh of interconnected faults associated with historical earthquakes (Špaček et al., 2006). The Elbe Fault System (EFS) is a WNW-striking zone extending from the southeastern North Sea to southwestern Poland along the present southern margin of the North German Basin and the northern margin of the Sudetes Mountains (Scheck et al., 2002).

2.4.2.1 Sudetic Marginal Fault

The Sudetic Marginal Fault (SMF) is a 250 kilometres long fault zone. It is generally oriented NW-SE to N-S. It is located in Poland and passes close to the towns Javorník, Jeseník and Vrbno pod Pradědem before terminating near the town Opava on the Lateral Marginal Jeseník Fault (Buday at al., 1995). The northwestern part (150 km in length) is markedly visible within the terrain morphology (Skácel, 2004). The Sudetes Mts. and the Fore-Sudetic block build the footwall and hangingwall of this fault, respectively. The fault zone is accompanied by Late Oligocene-Miocene basaltoid volcanism as well as numerous troughs and grabens (Badura and Zuchiewicz, 2008). Many authors studied the evolution and history of faulting of the SMF. Despite its distinctness, the evolutionary history of this fault is still matter of the debate (e.g. Badura et al., 2007; Kaplon and Cacoń, 2008; Štěpančíková et al., 2011).

The SMF was traditionally considered (Cloos, 1922) as an important structural boundary during the Paleozoic evolution of the Sudetes. The SMF is thought to have originated from ductile flexure (Oberc, 1967) during Variscan orogenesis (Alexandrowski at al., 1997). Oberc and Dyjor (1969) discussed the different types of movements within the tectonic history of the SMF. Oberc (1977) assumed that the fault was normal and steeply dipping. Down thrust of 200-1000 m has been estimated (Grocholski, 1977; Oberc and Dyjor, 1969) and documented from boreholes (Skácel, 1989). Cháb (1987) and Skácel (1989) established the thickness of 10-12 km of cover the down-faulted block. Krzyszkowski and Bowman (1997) have analysed two sets of extensional deformation features in the Polish part of the SMF. The SMF was Variscan strike-slip reactivated as a normal fault (Krzyszkowski et al., 1995). Cymermann et al. (1997) stated the SMF is of Tertiary age. Skácel (2004) showed that area around the SMF must have been more seismically active during the Variscan and Saxonian orogenic events. The maximum throw in the middle and SE parts of the SMF in 1000-1200 m, range in the remaining segments between 400 and 800 m. The staircase-like pattern of triangular facets points to at least five episodes of uplift of the footwall (Badura and Zuchiewicz, 2008). Štěpančíková (2005) mentioned the reactivation of the SMF during Neogene. The clear difference in the morphology of the uplifted blocks of the Sudetic Mountains and the downthrust Fore-Sudetic block reflects the evidence for a long polygenetic history within the entire study area (Štěpančíková and Rowberry, 2008). In the NE part of the Bohemian Massif, the NW-SE compression occurred not less than four times from Carboniferous to recent. Similarly, the NE-SW compression occurred at least three times during this period (Havíř, 2011). The newest studies were done by Danišík et al. (2012). They made a termochronological reconstruction of history of the Sudetes and faulting along the SMF based on zircon (U-Th)/He, apatite fission track and apatite (U-Th)/He dating. They have stated that the studied part of the SMF acted as a normal fault during early Late Cretaceous burial, as a

reverse fault during subsequent extensive European basins inversion and exhumation, and finally as a normal fault in the late Cenozoic.

2.4.2.2 Hronov – Poříčí Fault Zone

The Hronov – Poříčí Fault Zone (HPFZ) is located in the easternmost part of the Trutnov – Náchod Depression. It is approximately 30-40 km long and up to 500 m wide system of parallel fractures, dividing two important structural units - the Intra Sudetic Basin and the Krkonoše Piedmont Basin (Stejskal at al., 2009). The NW-SE striking structure was formed due to the post-Cretaceous flexural folding and is filled with the Upper Cretaceous sediments (Valenta et al., 2008) and the Permo-Carboniferous volcano-sedimentary complex (Skácelová et al., 2009). It is bounded by the Vrchlabí Lineament in the north and by the Nová Paka Lineament in the south (Stejskal et al., 2007).

The HPFZ had a complicated tectonic evolution, started in the late Paleozoic. Since then, several tectonic phases have taken place (Valenta et al., 2008). The fault zone has been successively developed from an asymmetric anticline, whose steeply inclined SW part was axially disrupted due to the regional compression by a reverse fault (Fig. 9, Tásler et al., 1979). The main reverse fault (thrust) is accompanied by parallel or oblique normal or reverse faults (Valenta et al., 2011).

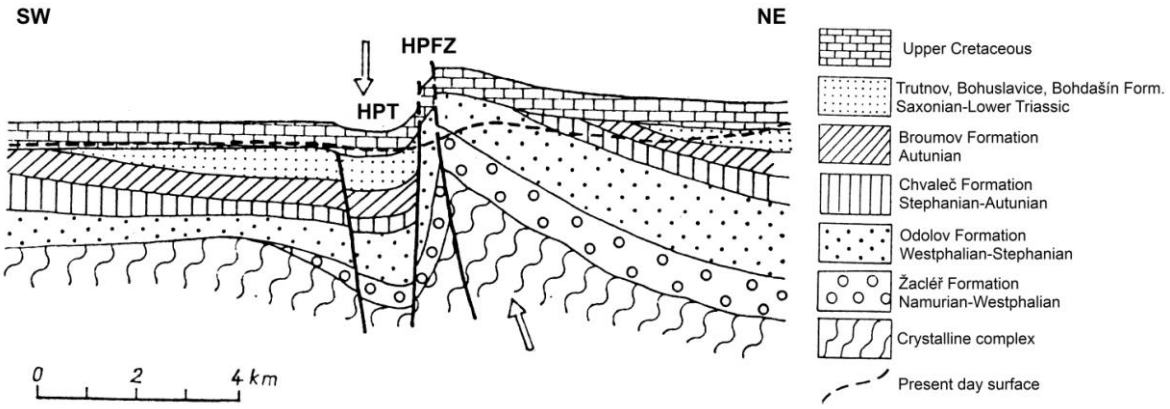

Fig. 9 Development of the HPFZ after Saxonian tectogenesis (according to Tásler et al., 1979). HPT-Hronov – Poříčí Trough, HPFZ-Hronov – Poříčí Fault Zone.

Along the main fault the NE block was relatively uplifted (Kolínský et al., 2012). The reactivation of the HPFZ is recorded after the Upper Cretaceous sedimentation during the Late Saxonian tectogenesis. Not only the previous faults were reactivated, but also short

orthogonal normal faults originated locally (Stejskal et al., 2006). According to Tásler et al. (1979) normal faults in the area of the HPFZ represents younger tectonic elements, i.e. younger normal faults are morphologically more distinct than the older reverse fault. The major dislocations in the Sudetes as SMF, ISF and HPFZ either follow the dominant shear direction or they are oblique, which explains varying kinematics evidenced in various segments of these faults, ranging from dip-slip to strike-slip transpressional faults (Wojewoda, 2007).

2.4.3 Recent tectonic activity

Evidence of the present tectonic activity in the northeastern part of the Bohemian Massif has recently been demonstrated by investigations of:

- Microearthquakes and seismotectonic activity (e. g. Skácelová et al., 1997; Guterch and Lewandowska-Marciniak, 2002; Kaláb et al., 2002; Havíř, 2004; Havíř and Špaček, 2004, Špaček et al., 2005; Havíř et al., 2006; Málek et al., 2008; Zedník and Hudová, 2008; Kolínský et al., 2012)
- Gravimetric monitoring (Barlik, 2002; Blachowski and Cacoń, 2002; Švábenský et al., 2002; Barlik et al., 2004, Cacoń et al., 2007)
- GPS measurements (e.g. Schenk et al, 2000; Bosy et al., 2002; Schenk et al., 2003; Kontny, 2004; Badura et al., 2007; Cacoń et al., 2007; Švábenský and Weigel, 2007; Nováková and Schenk, 2008; Kaplon and Cacoń, 2008; Schenková et al., 2009)
- 3D monitoring of microdisplacements on tectonic structures (Stemberk and Štěpančíková, 2003; Cacoń et al., 2007; Štěpančíková, 2008; Štěpančíková et al., 2008a)
- Trenching within the Sudetic Marginal Fault Zone (Štěpančíková et al., 2008b; Štěpančíková and Hók, 2009; Štěpančíková et al., 2010; Štěpančíková et al., 2011) and within Ramzová fault zone (Opletal and Pecina, 2004)
- Groundwater level variations (Stejskal et al, 2007; Valenta et al., 2011; Kolínský et al., 2012)
- CO_2 rich mineral springs (Buday et al., 1995; Stejskal et al., 2007; Brož et al., 2009; Valenta et al., 2011)

The earthquakes in the northern part of the Bohemian Massif are linked to the crossings of the Variscan fault systems in the NNE-SSW direction and the Sudetic faults in the NW-SE direction (Skácelová et al., 1997). The results of stress analysis of the focal mechanisms show NNW-SSE maximum compression and WSW-ENE maximum extension in the Jeseníky region. This stress field allows the easy reactivation not only of the steep WNW-ESE to NW-SE trending „Sudetic" faults, but also of the contingent steep NNE-SSW trending faults. The reactivation of the NNE-SSW faults becomes less easy with decreasing value of dip (Havíř, 2004). The recent tectonic sinistral (oblique or horizontal) movements along the steep NNE-SSW faults are highly probable (Havíř and Špaček, 2004). The strongest historical earthquake was on 10th January 1901 and reached the magnitude of 4.6 (Woldřich, 1901). During last 300 years (1705-2005), 30 earthquakes of macroseismic effects have been recorded within HPFZ (Stejskal et al., 2006).

The trenching as a method to determine the paleoseismic activity of faults has been performed within the SMFZ. Štěpančíková et al. (2010) constrained a SMF faulting history based on the age of deformed sediments, radiocarbon dating of charcoals and paleosoils covering the deformed sediments in the trenches close to the village of Vlčice. They found four types of a deformation – reverse faulting, horizontal movements, reverse faulting, and normal faulting, subsequently. According to Štěpančíková et al. (2011) the results from the trenches at the Bílá Voda locality show potentially four to five movements on the SMF during late Quaternary (Holocene). Nevertheless, the sense of strike-slip could not be determined due to lack of the kinematic indicators. Štěpančíková et al. (2010) estimated the paleoearthquake minimum moment magnitude as Mw6.3 and slip rate 0.03 mm/y expected on the SMF.

A possible explanation of the present mobility of the HPFZ was given by Schenk et al. (1989). According to their geodynamic model, the HPFZ, as a reverse fault, balances the compression caused by the movements along the Nová Paka and Vrchlabí faults, bounding the HPFZ in the north and the south. This presumption is supported by the analyses of repeated triangular and precise levelling performed in the broader vicinity of the HPFZ by Vyskočil (1988).

During the 1953-2012 period numerous geodetic measurements related to the SMF were done. Their results are accurate enough to detect the relative changes of the fault's sides of 0.5-1 mm a year. The main direction of registered horizontal changes is perpendicular to the SMF line (Kaplon and Cacoń, 2008). It is in agreement with Kontny (2004), who stated about preliminary results of the GPS monitoring, that indicate NE-SW compression tendencies, perpendicular to the SMFZ and HPFZ. Schenk et al. (2003) defined on the base of GPS data two main dominant movement directions in the NE part of the Bohemian Massif – the Sudetic one (NW-SE) and the Moravo-Silesian one (NNE-SSW). Schenk and Schenková (2008) modelled the recent geodynamic pattern of the NE part of the Bohemian

Massif based on the GPS measurements. They showed the sinistral movements on the NW-SE faults, especially along the SMF, as well as on the NNE-SSW faults of the Moravo-Silesian tectonic system. Nevertheless, they stated that nobody can exclude dextral movements in this area. Kaplon and Cacoń (2008) showed that slip along the SMF is not constant and is directed right-lateral in its NW part and left-lateral in the SE part. Cymermann (1999) postulated left-lateral Alpine transpression for the Sudety Mts. Results of repeated GPS measurements indicate compressional regime within the HPFZ.

Chapter 3

Methodology

Field structural investigations, including fault-slip data collection were carried out on a number of natural outcrops and quarries with the aim of establishing a robust and field-constrained model for the local brittle structural evolution of the studied areas. Almost 5000 faults and fractures have been measured and evaluated within the Sudetic Marginal Fault Zone and Hronov – Poříčí Fault Zone in 116 localities. For the demonstrable reason the localities have been divided into three categories: (1) a small natural outcrop/quarry - up to 50 m^2, (2) a midsize natural outcrop/quarry - from 50 m^2 to 500 m^2, (3) a large natural outcrop/quarry - over 500 m^2.

The fault planes have been searched for kinematic indicators, such as mineral accretion steps, grooves or small steps with sharp borders (see Doblas, 1998). The kinematic indicators were used to determine the senses on the fault planes. Four basic types of faults – reverse, normal, dextral, sinistral were described for kinematic frequency analysis. In some cases, the multiple lineation systems with two or three slickenlines were found. Thus the sets of faults could have been assigned to the different tectonic phases.

The phases have been determined by the calculation of the paleostress analysis. For the separation of heterogeneous fault-slip data the software T-Tecto 3.0 Professional have been used (Žalohar, 2009). The faults were divided into the different tectonic phases according to their origin or reactivation and their relative age using the Gauss method. The Gauss method is based on fault-slip data inversion, which involves identifying best-fit stress and strain tensors (Žalohar and Vrabec, 2007). The assumption that a slip on a plane occurs in the direction of the maximum resolved shear stress was given by Bott (1959). Validity of this analysis from the Gauss numerical method was tested against the graphical Right Dihedra Method (RDM) (Angelier and Mechler, 1977). The Visualisation of the Gauss object function (VGF) method has been calculated to find the most probable orientation of the maximum and minimum principle stress axes for several differently orientated faults that were active in the common stress field. The VGF method shows the kinematic axes and PT fields detached by contours. The Mohr diagrams were constructed to visualise the shape of Mohr circles and the positions of "Mohr points" illustrating the state of stress along the faults. The shape of the Mohr diagram (but not the position of the Mohr circles) is defined by the parameter D, where $D = (\sigma_2-\sigma_3)/(\sigma_1-\sigma_3)$ (Žalohar, 2009). The results of various methods were used for the final description of the actual stress conditions of the studied areas during the geological history.

If determined, relative age of kinematic indicators found on the same fault plane enabled line up the tectonic phases. Time succession provided by the T-Tecto software was verified using field data directly. Relation of a pair of indicators was considered as a relation between the corresponding phases. Consequently, complete time line was attained when all paired phases were compared. Number of fault included in a phase was scrutinized as well since younger phases tend to cover the older. Therefore the indicators belonging to younger phases are, in general, more common. Because of empirical, strongly generalizing character of the rule, the number of faults in a phase was, off course, conceded an informative criterion only.

Recent tectonic movements have been studied using long-term GPS monitoring. Data has been acquired from the GPS measurements in the network GEONAS (Mantlík et al., 2005). The permanent and campaign GPS stations situated in the studied areas were chosen to describe the actual movements within the HPFZ and SMFZ. The stations were equipped with receivers capable to register signals of both GPS and GLONASS and to produce two different types of observed data. Permanent GNSS stations produce continuous stream of GNSS measurements. Data from campaign measurements is available for two days per year, while data from permanent measurements are only limited by the construction of the GPS station. The station velocity is generally represented by a change of its position in time. To compute the station coordinates for every measured campaign, double differences-based strategy has been applied. Daily processing was performed in GPS software Bernese v. 5.0 (Dach et al., 2007). The input data were used to enable successful calculation, including final orbit and satellite clocks and final Earth orientation parameters. These files were downloaded from CODE European Centre for Orbit Determination.

To obtain horizontal and vertical velocity components, geocentric Carthesian coordinates have been transformed to topocentric NEU (North, East, Up) Carthesian coordinates (Drake, 2002). Then the velocities of stations and their uncertainties have been determined by the Least Squares regression. Outliers have been removed from time series before processing, because they negatively affect accuracy of approximation and decrease the accuracy of the resulting velocity. Outliers have been cyclically eliminated, so that each value has been compared to three times the sample standard deviation. It corresponds to the 99.7% confidence level. The exceeding value has been excluded from dataset.

Three types of models have been used to subtract the influence of common movements of the stations or movements of the Euroasian tectonic plate. However, every model has a limitation for a local usage conditions. To test the variability and weight of the final velocities and the azimuths, the arithmetical and weighted average has been computed. An average movement of the studied areas of all individual station’s movements has been deducted as well to highlight movements between the stations. To subtract the influence of movement of Euroasian tectonic plate, global motion model NNR-NUVEL 1A has been

applied. Final velocities and their azimuths obtained by deduction of NNR-NUVEL 1A model have been compared with the final velocities and their azimuths obtained by deduction of arithmetical average of all individual station's movements and by deduction of weighted average of all individual station's movements. Thus, all movements described hereafter are, in fact, relative to the average movement of the areas.

Finally, all results from brittle tectonic filed studies, paleostress analysis and GPS measurements have been compared and interpreted. The actual stress condition and actual movements within the SMFZ and HPFZ areas were displayed into ASTER Global Digital Elevation Models.

Chapter 4

Results

4.1 Sudetic Marginal Fault Zone

Almost 4000 faults and fractures have been measured and studied within the Sudetic Marginal Fault Zone. The lithology of the localities is variable and abundant, nevertheless metamorphites and granites occur mostly (Tab. 1). The velocities of the GPS stations from the permanent and campaign GPS observations have been utilized to investigate the active tectonics of the SMFZ area (Tab. 2). The fault zone is clearly visible in the digital model relief. The studied localities and GPS stations were places in the vicinity of the main fault zone (Fig. 10).

Tab. 1 List of the localities studied within the SMFZ with the geographic coordinates, description and lithology

Locality	N latitude	E longitude	Description	Lithology
L1	50°24'54"	16°56'19"	a small natural outcrop	gneiss
L2	50°26'30"	16°53'01"	a large quarry	crystalline limestone
L3	50°24'31"	16°53'45"	a midsize natural outcrop	gneiss
L4	50°25'19"	16°53'30"	a small natural outcrop	gneiss
L5	50°21'59"	16°58'59"	a small natural outcrop	gneiss
L6	50°22'28"	16°56'06"	a small natural outcrop	gneiss
L7	50°22'26"	16°56'56"	a small natural outcrop	gneiss
L8	50°21'17"	16°55'14"	a midsize quarry	basalt
L9	50°19'54"	17°04'56"	a large quarry	granite
L10	50°19'28"	17°05'32"	a large quarry	granite
L11	50°17'41"	17°01'58"	a midsize natural outcrop	metaquartzite
L12	50°17'41"	17°01'52"	a small natural outcrop	gneiss
L13	50°17'46"	17°02'17"	a small natural outcrop	granite
L14	50°14'50"	17°01'22"	rocks	amphibolite
L15	50°15'09"	17°01'21"	a small natural outcrop	amphibolite
L16	50°16'01"	17°01'60"	a small natural outcrop	amphibolite
L17	50°16'25"	17°03'00"	a large natural outcrop	amphibolite
L18	50°21'20"	17°04'27"	a midsize natural outcrop	gneiss
L19	50°16'38"	17°03'29"	a midsize natural outcrop	paragneiss

L20	50°16'39"	17°03'08"	a small natural outcrop	gneiss
L21	50°17'02"	17°15'02"	a midsize quarry	limestone
L22	50°22'07"	16°59'34"	a small natural outcrop	gneiss
L23	50°15'22"	17°15'58"	a small natural outcrop	gneiss
L24	50°17'23"	17°07'18"	a large quarry	granite
L25	50°22'05"	16°59'27"	a large natural outcrop	gneiss
L26	50°13'21"	17°05'30"	a large quarry	crystalline limestone
L27	50°13'20"	17°05'31"	a small natural outcrop	gneiss
L28	50°21'31"	17°10'55"	a large quarry	granite
L29	50°20'07"	17°08'49"	rocks	granite
L30	50°20'09"	17°09'09"	a large quarry	granite
L31	50°21'42"	16°58'50"	a midsize natural outcrop	gneiss
L32	50°26'25"	16°53'09"	a large quarry	limestone
L33	50°26'28"	16°53'04"	a large quarry	limestone
L34	50°23'06"	16°55'22"	rocks	gneiss
L35	50°23'02"	016°57'35"	a small natural outcrop	gneiss
L36	50°20'08"	17°00'38"	a small natural outcrop	gneiss
L37	50°21'08"	17°00'22"	a small natural outcrop	gneiss
L38	50°20'53"	16°59'57"	a small natural outcrop	gneiss
L39	50°18'57"	16°59'39"	a small natural outcrop	gneiss
L40	50°18'60"	16°59'55"	a midsize natural outcrop	granodiorite
L41	50°19'56"	17°05'09"	a midsize natural outcrop	granite
L42	50°17'09"	17°05'21"	a large quarry	crystalline limestone
L43	50°16'57"	17°05'27"	a large quarry	crystalline limestone
L44	50°16'55"	17°05'30"	a large quarry	crystalline limestone
L45	50°18'31"	17°06'54"	a large quarry	granite
L46	50°15'25"	17°11'35"	a small natural outcrop	gneiss
L47	50°15'11"	17°11'05"	a large natural outcrop	gneiss
L48	50°17'26"	17°14'56"	a large quarry	limestone
L49	50°16'54"	17°12'41"	rocks	gneiss
L50	50°16'41"	17°05'32"	a large quarry	crystalline limestone
L51	50°16'39"	17°05'34"	a large quarry	crystalline limestone
L52	50°16'35"	17°07'49"	a large quarry	granite
L53	50°15'24"	17°08'56"	a small natural outcrop	gneiss
L54	50°17'05"	17°07'46"	a large quarry	granite
L55	50°25'03"	16°52'33"	a small natural outcrop	gneiss
L56	50°15'40"	17°07'57"	a small natural outcrop	granite
L57	50°15'41"	17°08'02"	a small natural outcrop	granite

L58	50°15'28"	17°06'45"	a small natural outcrop	phyllite
L59	50°14'46"	17°08'18"	a small natural outcrop	crystalline limestone
L60	50°14'45"	17°08'11"	a small natural outcrop	crystalline limestone
L61	50°17'52"	17°02'08"	a large quarry	granite
L62	50°24'20"	16°55'53"	rocks	two-mica gneiss
L63	50°24'52"	16°55'50"	a small natural outcrop	gneiss
L64	50°26'18"	16°54'22"	a small natural outcrop	gneiss

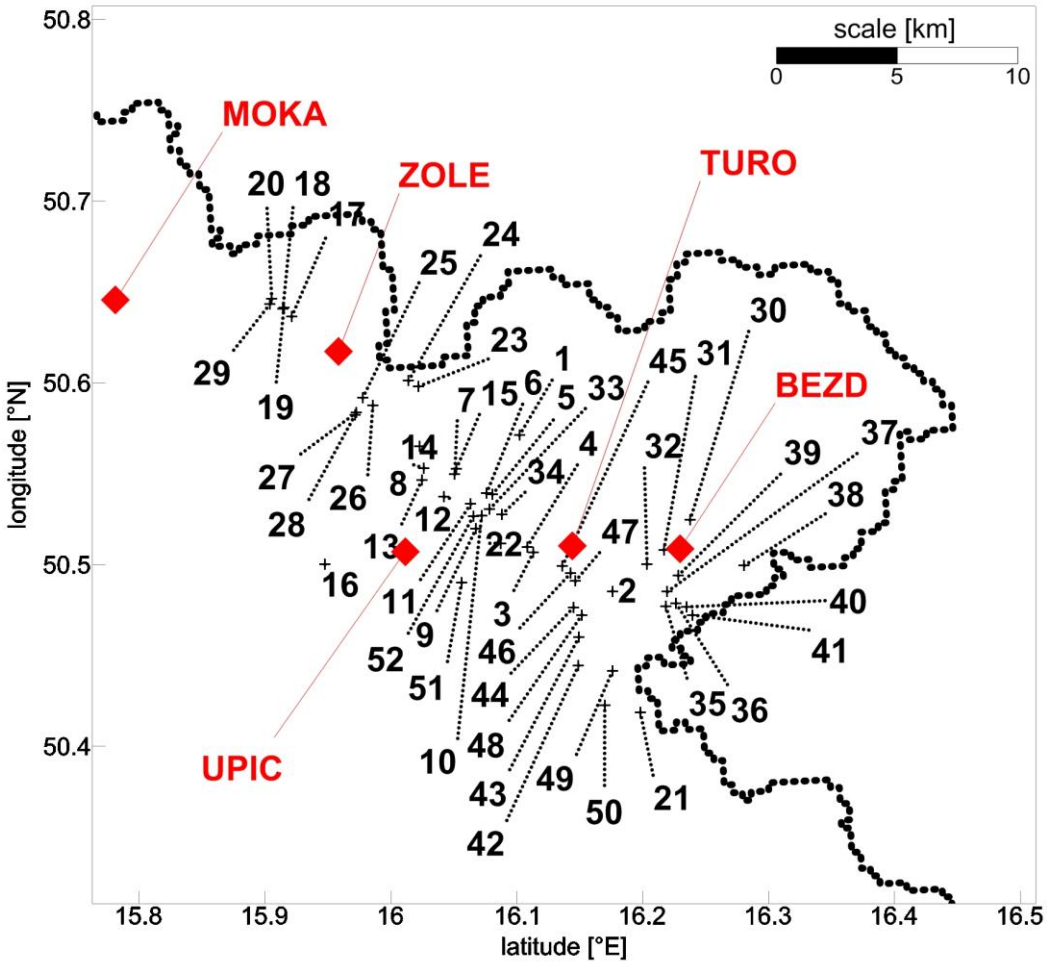

Fig. 10 The map of the SMFZ area. The studied localities are marked by crosses and numbers. Red squares represent the GPS stations.

Tab. 2 Selected stations and their characteristics

		Station location			Observations
Station	**Type**	**N latitude**	**E longitude**	**Ellipsoid heigh [m]**	**Start**
BISK	P	50° 15´ 24.12"	17° 25´ 42.96"	950.867	Aug 2001
LANS	C	50° 19' 34.68"	17° 04' 18.12"	466.031	Aug 1997
PETR	C	50° 18' 13.32"	17° 02' 57.48"	590.829	Aug 1997
STAM	P	50° 09' 44.28"	16° 56' 52.08"	598.976	Aug 2006
VIDN	P	50° 22' 22.44"	17° 11' 07.44"	287.546	Aug 2006
VRES	C	50° 08' 45.96"	17° 08' 10.32"	1364.700	Sep 2000

P: Permanent station, C: Campaign station

Strike and dip of the faults have been measured, as well as trend and plunge of the lineations occurring on the fault planes. The lineations are represented by kinematic indicators, mostly striations, calcite steps and asymmetric elevations. Two principle sets of faults have been determined within the SMFZ (Fig. 11 left). The prevailing orientations are W-E and N-S. However, to a lesser extent the faults are striking in all directions. Fault planes are mainly dipping under 80-90°, which means they are vertical (Fig. 11 right). In general, almost no horizontal or subhorizontal faults occur in the area.

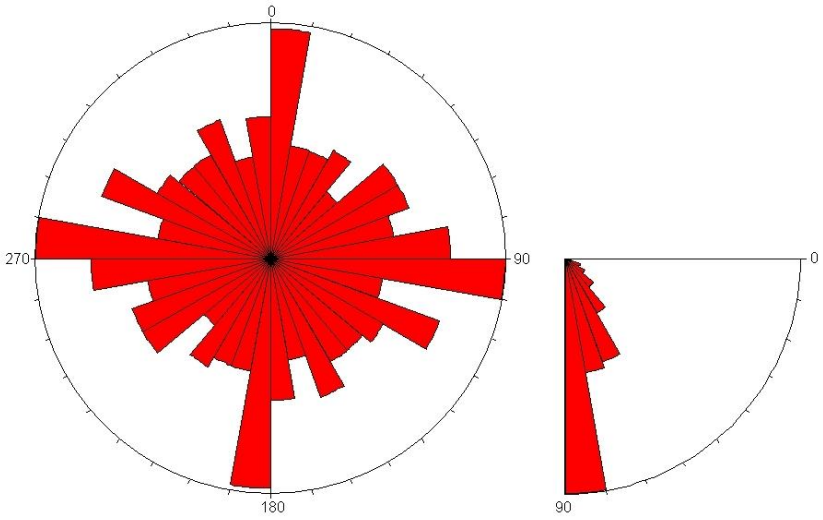

Fig. 11 Rose diagrams of the fault planes within the SMFZ. Left: strike of the planes. Right: dip of the planes. N=470.

Figure 12 (left) shows the trends of lineations (mainly striations or calcite steps) on the fault planes. The prevailing trend is about 210° with subvertical plunge (Fig. 12 right). The sense of the movements has been determined in almost all faults. The kinematic analysis was performed due to the distribution of the fault types in the orientations. Strike-slip faults (dextral and sinistral) are mainly oriented in N-S and W-E directions. On the other hand, normal and reverse faults occur in two perpendicular directions NW-SE and NE-SW (Fig. 13). These data have been used for the construction of the schematic draft of the actual tectonic situation within the SMFZ.

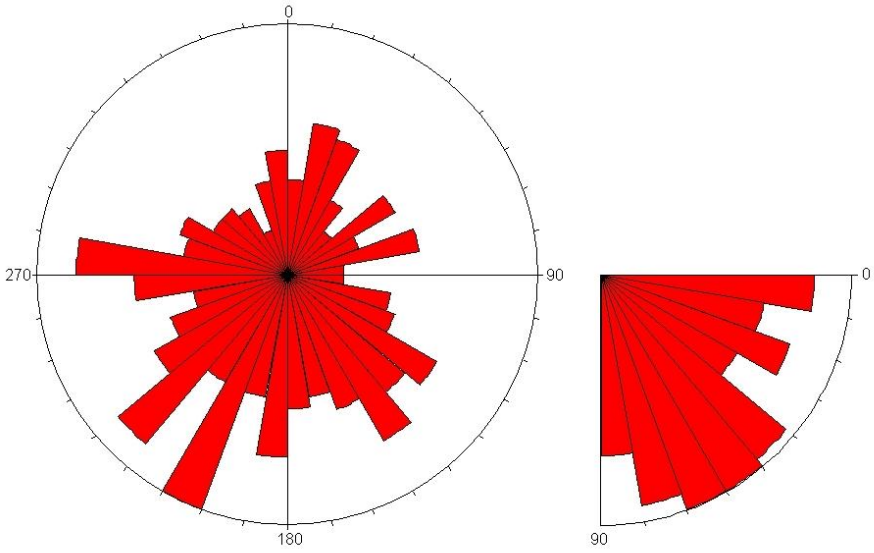

Fig. 12 Rose diagrams of the lineations on the fault planes within the SMFZ. Left: trend of the lineations. Right: plunge of the lineations. N=470.

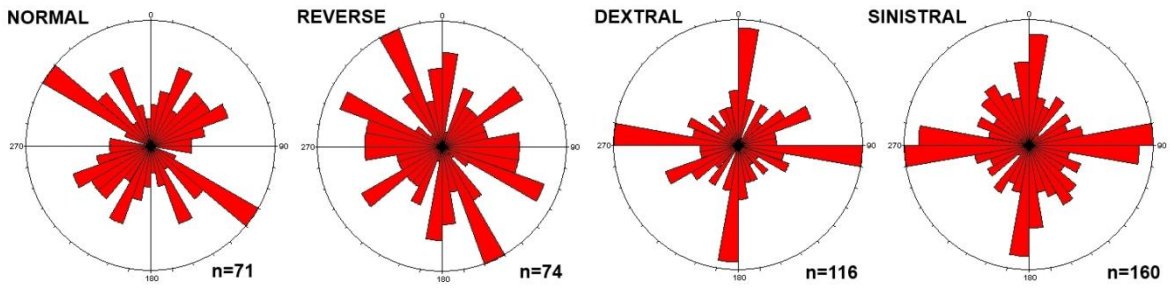

Fig. 13 Kinematic analysis of the fault types within the SMFZ.

Rose diagram of all fractures (Fig. 14 left) shows they have a predominant W-E orientation. Nevertheless, they occur in all directions. Fractures without visible slip have been divided into five groups according to its origin: bedding, foliation, extension/tension fractures, shear fractures and joints. Vertical fractures have been found within the SMFZ mainly (Fig. 14 right).

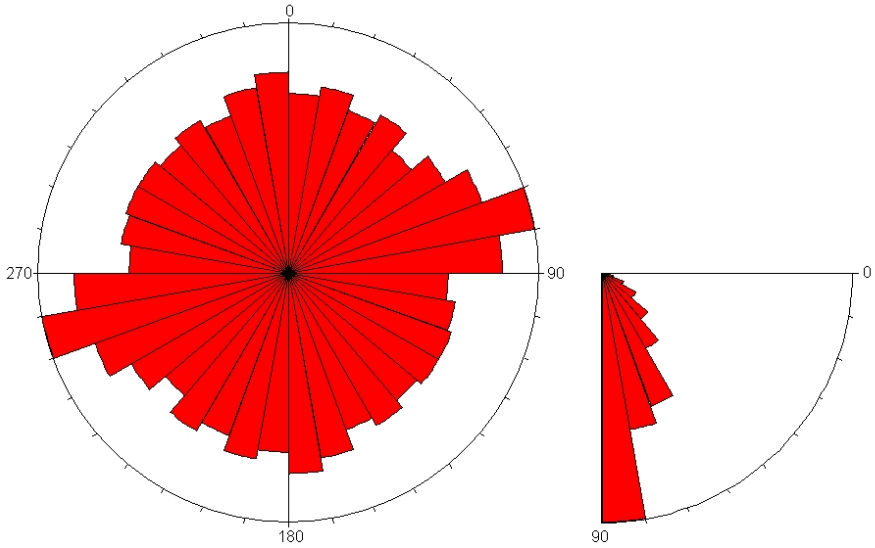

Fig. 14 Rose diagrams of the fracture planes within the SMFZ. Left: strike of the planes. Right: dip of the planes. N=3362.

Paleostress analysis of the fault-slip data based on the Gauss method (Žalohar and Vrabec, 2007) within the SMFZ resulted in identification of six tectonic phases. The phases have been ordered by the geological age on the base on the faults with multiple lineation systems and cross-cutting lineations from the first and youngest to the sixth and oldest.

The youngest phase represents 206 faults. These faults were formed in the strike-slip regime with maximum compression (σ_1) in the NNW-SSE direction and minimum compression (σ_3) in NW-SE direction. The maximum compression axis is trending 251° and plunging 34° subhorizontally (Fig. 15a). This direction is the same as the main fault orientation. The RDM provided same results as the Gauss method. The position of P (pink) and T (blue) quadrants indicated also the strike-slip tectonic regime (Fig. 15b). The VGF documents confidence of stress tensor (contoured plot) where magnitudes of individual stresses are highlighted by colours (red-maximum compression, blue-minimum compression, maximum extension, green-intermediate stress). The calculated stress field is the same as that for RDM (Fig. 15c). The Mohr diagram illustrates the faults reactivated

during the second phase. Faulting occurs when the largest Mohr circle defined by the maximum and minimum principal stresses touches the Mohr envelope (Žalohar, 2009). Eight Mohr points illustrating the state of stress along the faults in the Mohr diagram are positioned under the line representing the Amontons's law of friction (Fig. 15d). This phase is supposed to be the active one, whereas there is no evidence of other younger kinematic indicators. The SMF has been a sinistral fault zone with the maximum compression oblique to the main direction of the fault during the youngest tectonic phase.

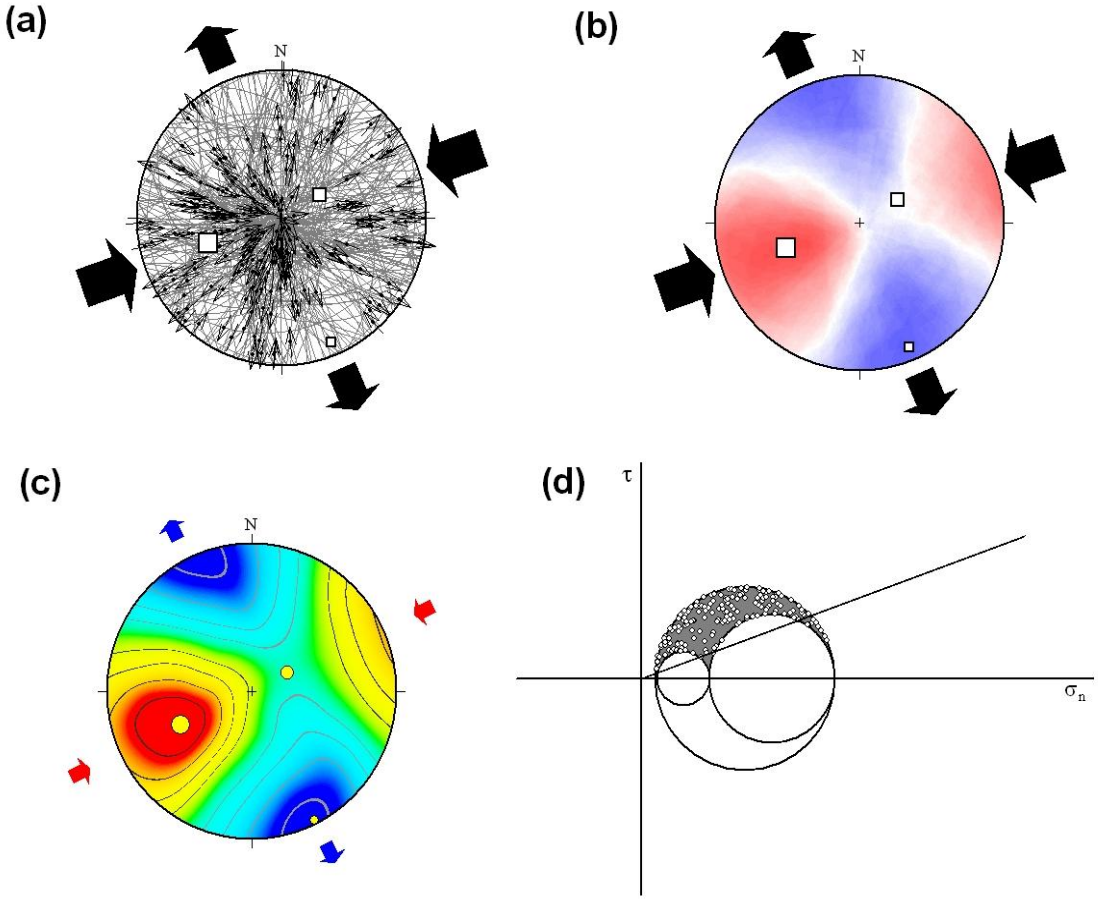

Fig. 15 The youngest phase of fault-slip data separation within the SMFZ. a) Paleostress analysis of the faults based on Gauss method (Žalohar and Vrabec, 2007), paleostress axes: σ_1-a large square, σ_2-a midsize square, σ_3-a small square, arrows are showing the maximum compression and maximum extension; b) Paleostress analysis of the faults based on Right Dihedra Method (Angelier and Mechler, 1977); c) VGF of the faults, kinematic axes: σ_1-a large circle, σ_2-a midsize circle, σ_3-a small circle, red arrows are showing the maximum compression, blue arrows are showing the maximum extension; all stereonets represent lower hemisphere, equal angle projection; d) Mohr diagram. n=206.

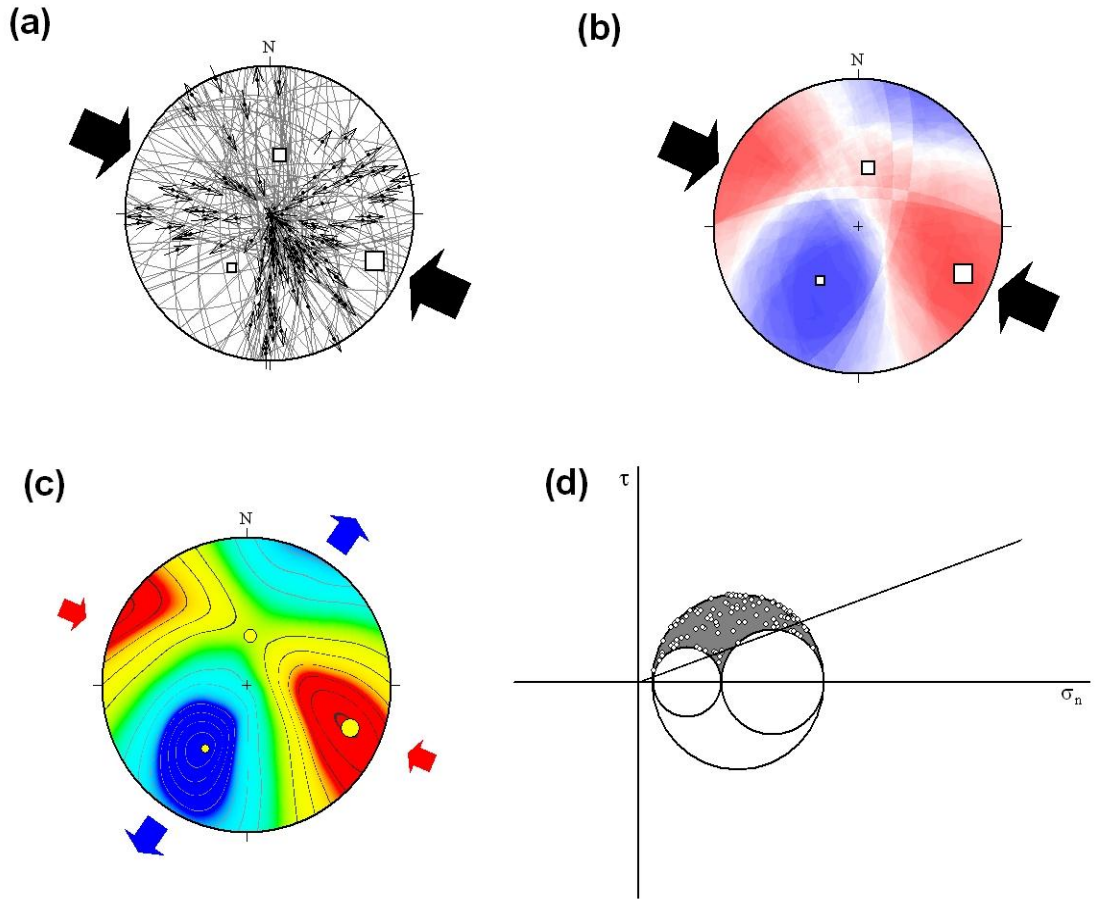

Fig. 16 The second phase of fault-slip data separation within the SMFZ. a) Paleostress analysis of the faults based on Gauss method (Žalohar and Vrabec, 2007), paleostress axes: σ_1-a large square, σ_2-a midsize square, σ_3-a small square, arrows are showing the maximum compression and maximum extension; b) Paleostress analysis of the faults based on Right Dihedra Method (Angelier and Mechler, 1977); c) VGF of the faults, kinematic axes: σ_1-a large circle, σ_2-a midsize circle, σ_3-a small circle, red arrows are showing the maximum compression, blue arrows are showing the maximum extension; all stereonets represent lower hemisphere, equal angle projection; d) Mohr diagram. n=116.

Separation of the faults belonging to the second phase resulted in the compressional tectonic regime. The maximum principle stress was oriented in the WNW-ESE direction. Both intermediate and minimum principle axes were subvertical, dipping 47° and 41° respectively (Fig. 16a). The RDM provided the same results, however the P and T quadrants are rather typical for the strike-slip conditions (Fig. 16b). The position of contours in stereogram calculated by VGF is almost the similar as calculated by RDM. The kinematic axes show the orientation of maximum and minimum compression. The

intermediate stress was almost vertical (Fig. 16c). Nine "Mohr points" illustrating the state of stress along the faults are positioned under the line representing Amontons's law of friction (Fig. 16d). These stress conditions resulted the SMF was a reverse fault zone during the second phase.

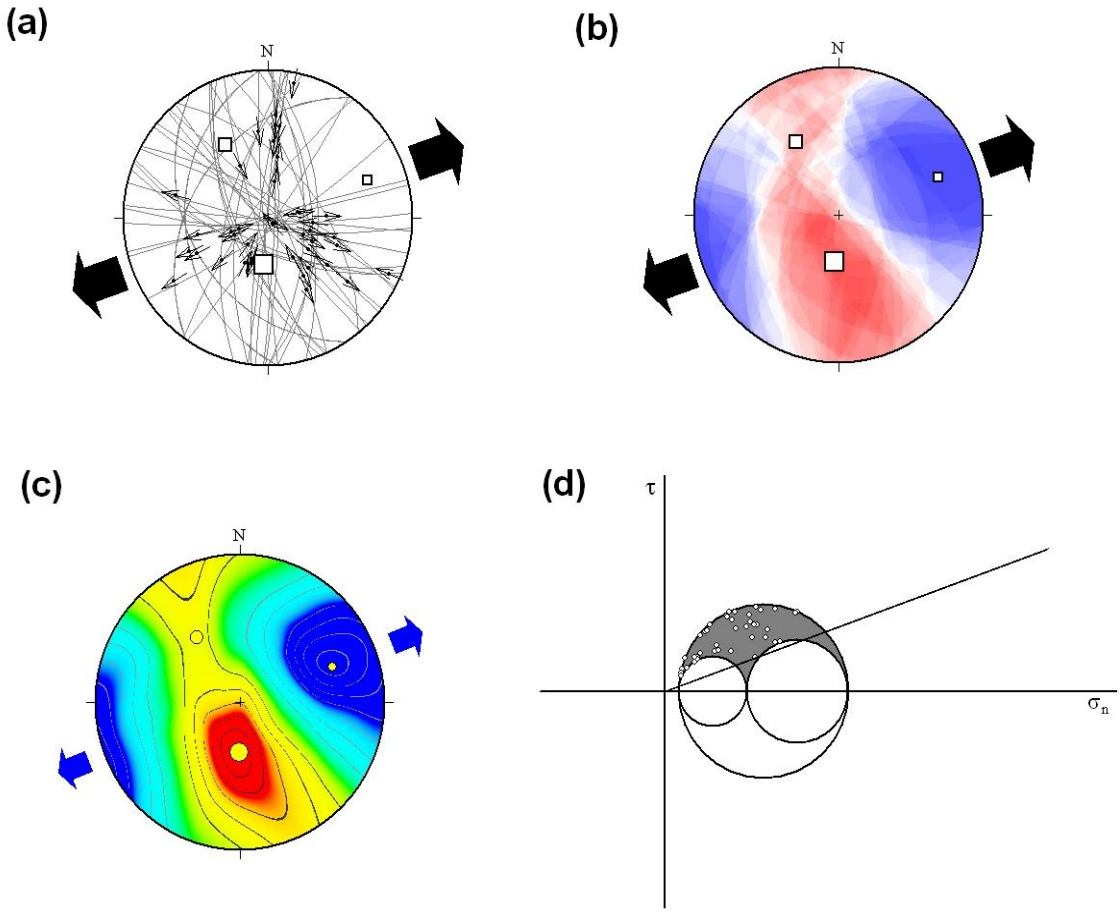

Fig. 17 The third phase of fault-slip data separation within the SMFZ. a) Paleostress analysis of the faults based on Gauss method (Žalohar and Vrabec, 2007), paleostress axes: σ_1-a large square, σ_2-a midsize square, σ_3-a small square, arrows are showing the maximum compression and maximum extension; b) Paleostress analysis of the faults based on Right Dihedra Method (Angelier and Mechler, 1977); c) VGF of the faults, kinematic axes: σ_1-a large circle, σ_2-a midsize circle, σ_3-a small circle, blue arrows are showing the maximum extension; all stereonets represent lower hemisphere, equal angle projection; d) Mohr diagram. n=42.

The third phase is characterised by extensional stress conditions. It contains 42 faults, mostly the normal ones. The maximum extension was oriented ENE-WSW almost perpendicular to the main fault zone. The maximum compression was subvertical to the

main fault zone (Fig. 17a). RDM provided the same stress field as the Gauss method. The P quadrant was clustered around the maximum principle stress and intermediate principle stress, while the T field was situated along the P field containing the minimum principle stress (Fig. 17b). Contoured stereogram made by the VGF method shows the same position of coloured PT field (Fig. 17c). There are no "Mohr points" situated under the line representing Amontons's law of friction in Mohr diagram (Fig. 17d). During the third phase the SMF was a normal fault and extensional tectonic regime occurred.

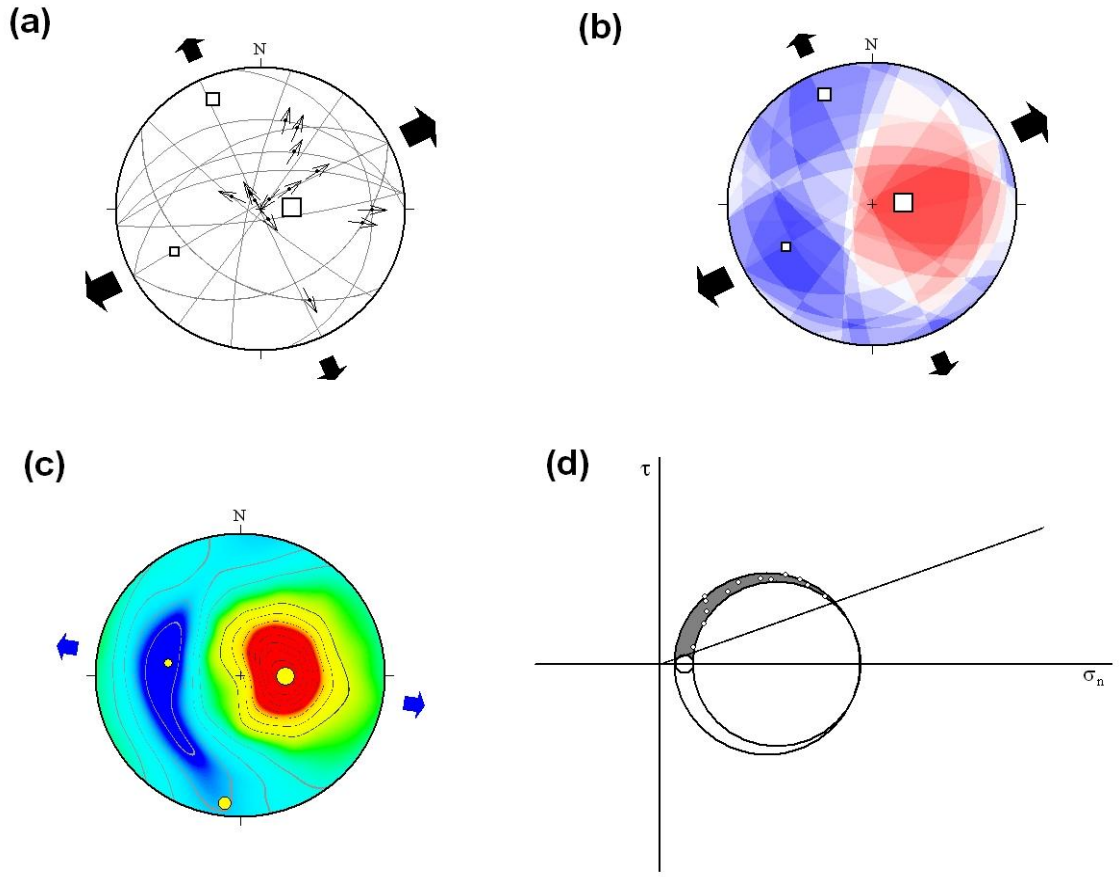

Fig. 18 The fourth phase of fault-slip data separation within the SMFZ. a) Paleostress analysis of the faults based on Gauss method (Žalohar and Vrabec, 2007), paleostress axes: σ_1-a large square, σ_2-a midsize square, σ_3-a small square, arrows are showing the maximum compression and maximum extension; b) Paleostress analysis of the faults based on Right Dihedra Method (Angelier and Mechler, 1977); c) VGF of the faults, kinematic axes: σ_1-a large circle, σ_2-a midsize circle, σ_3-a small circle, blue arrows are showing the maximum extension; all stereonets represent lower hemisphere, equal angle projection; d) Mohr diagram. n=13.

The fourth phase seems to be similar as the third phase. It is also characterised by extensional stress conditions. During the fourth phase 13 studied faults have been reactivated or developed. The strike-slip faults have occurred there, nevertheless the normal faults are frequent too. The maximum extension was oriented ENE-WSW, the intermediate stress axis was oriented NNW-SSE (Fig. 18a). RDM provided the same results as the Gauss method. The P field containing all P axes was clustered around the maximum principle stress, while the T field was situated around the P field containing the minimum principle stress and intermediate principle stress (Fig. 18b). The results calculated by VGF method are rather different. The position of the intermediate and minimum principle stress caused the orientation of maximum extension in WNW-ESE direction (Fig. 18c). The Mohr circles are also rather different than in the previous tectonic phases. There is one big circle, and one small circle. All "Mohr points" are positioned above the line representing Amontons's law of friction. The area where possible mechanically compatible faults could have been reactivated is rather small (Fig. 18d). During this phase the SMF was a normal fault and extensional tectonic regime occurred.

During the fifth phase 81 faults have been developed or reactivated. This phase is characterised by strike-slip regime. The maximum compression is oriented NNE-SSW, the maximum extension is oriented in WNW-ESE direction. The maximum principle stress is subvertical dipping 13° to NNE (Fig. 19a). The RDM provided the same results as the Gauss method. The P and T quadrants are rather typical for the strike-slip conditions (Fig. 19b). The results calculated by the VGF method are same as those calculated by RDM (Fig. 19c). There is only one Mohr circle in the Mohr diagram. All "Mohr points" are situated on the Mohr circle moreover four points are positioned above the line representing Amontons's law of friction. The area where possible mechanically compatible faults could have been reactivated is only on the Mohr circle (Fig. 19d). These stress conditions resulted during this phase the SMF was a dextral fault.

The sixth and the oldest phase seems to be rather similar as the fifth phase. The stress conditions were similar however the orientation of maximum principle stress had rotated. Nevertheless, this reliability of this phase is debatable because of the small amount of the faults. During this oldest phase 9 faults were developed, mainly the sinistral faults. This phase is also characterised by strike-slip regime. The maximum compression was oriented NW-SE almost parallel to the main fault (Fig. 20a). The RDM provided same results as the Gauss method. The P field was clustered around maximum principle stress, while the T field was clustered around the minimum and intermediate principle stress (Fig. 20b). The VGF method provided similar results. The maximum extension is oriented in the same direction as in the stereogram calculated by the RDM. However, the direction of the maximum compression stress was not marked there (Fig. 20c). All "Mohr points" are positioned above the line representing Amontons's law of friction. The area where possible

mechanically compatible faults could have been reactivated is rather small (Fig. 20d). During this last phase, the SMF was a normal fault zone with sinistral component.

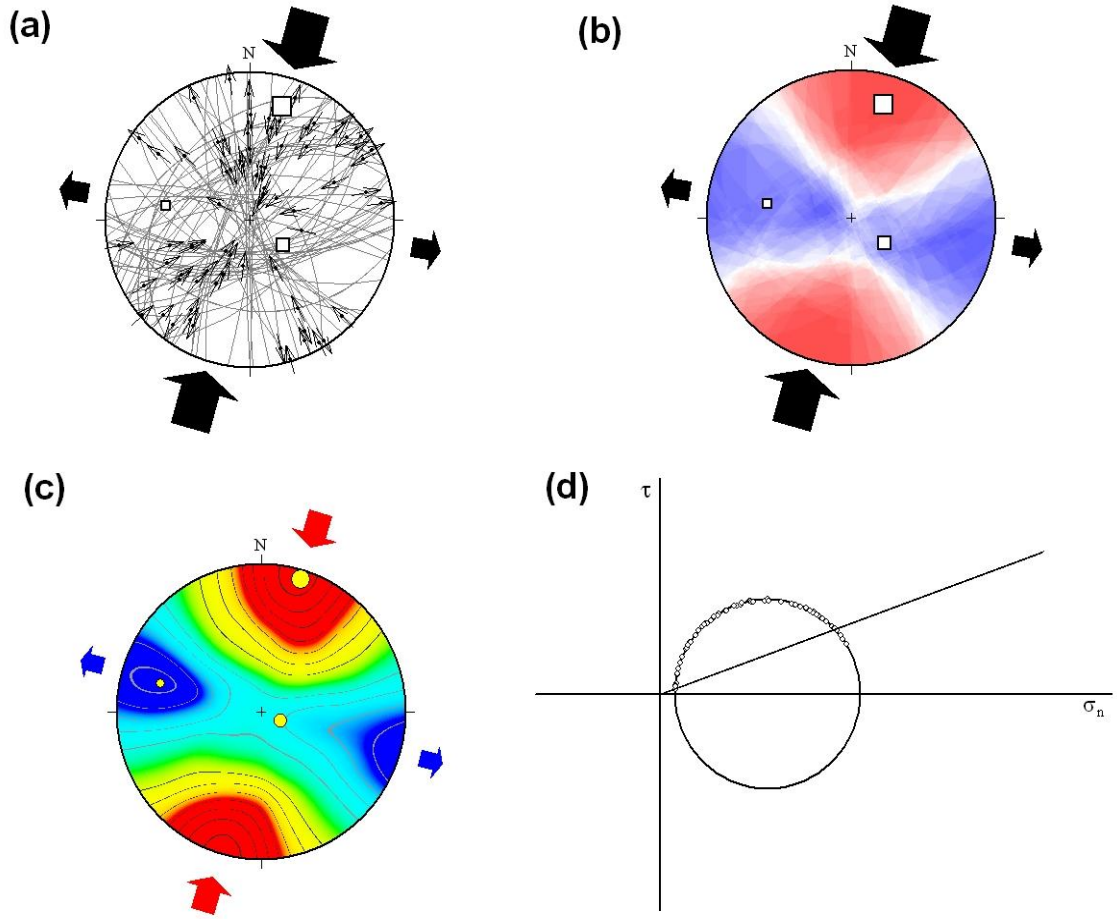

Fig. 19 The fifth phase of fault-slip data separation within the SMFZ. a) Paleostress analysis of the faults based on Gauss method (Žalohar and Vrabec, 2007), paleostress axes: σ_1-a large square, σ_2-a midsize square, σ_3-a small square, arrows are showing the maximum compression and maximum extension; b) Paleostress analysis of the faults based on Right Dihedra Method (Angelier and Mechler, 1977); c) VGF of the faults, kinematic axes: σ_1-a large circle, σ_2-a midsize circle, σ_3-a small circle, red arrows are showing the maximum compression, blue arrows are showing the maximum extension; all stereonets represent lower hemisphere, equal angle projection; d) Mohr diagram. n=81.

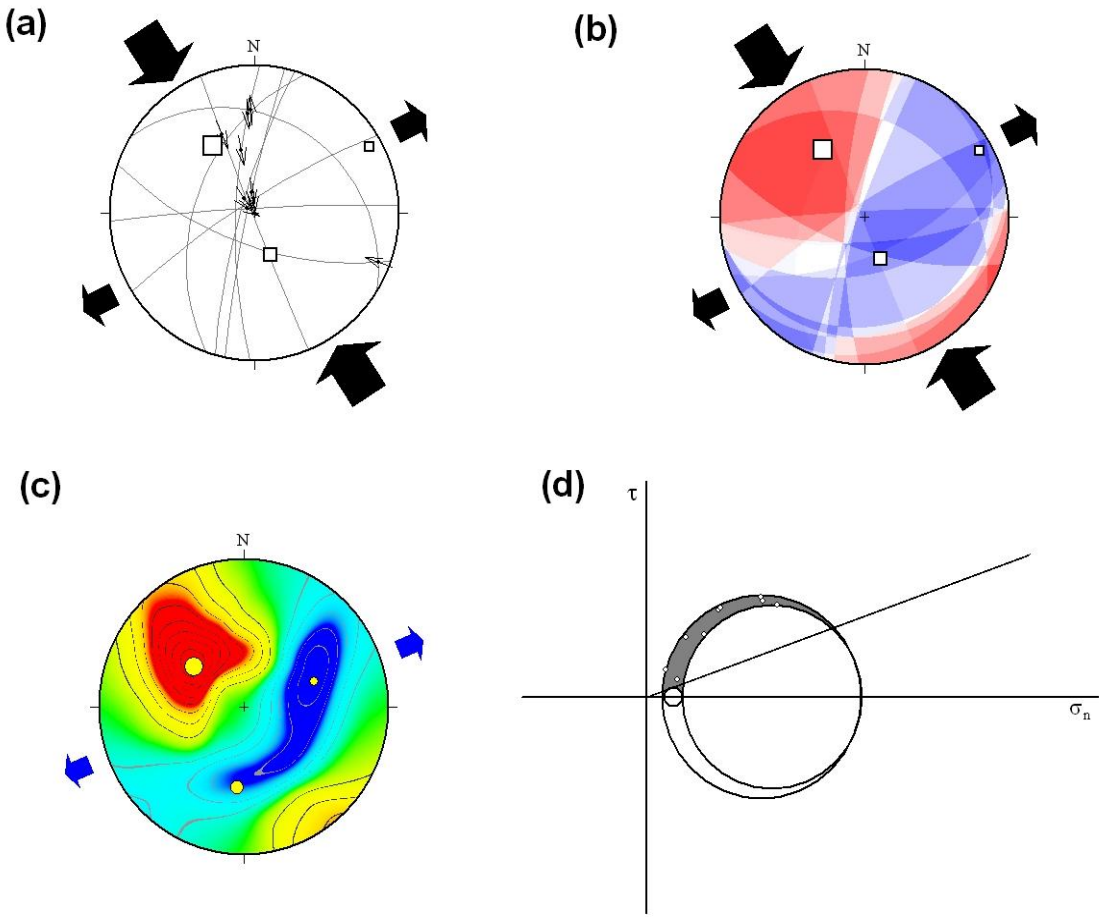

Fig. 20 The sixth phase of fault-slip data separation within the SMFZ. a) Paleostress analysis of the faults based on Gauss method (Žalohar and Vrabec, 2007), paleostress axes: σ_1-a large square, σ_2-a midsize square, σ_3-a small square, arrows are showing the maximum compression and maximum extension; b) Paleostress analysis of the faults based on Right Dihedra Method (Angelier and Mechler, 1977); c) VGF of the faults, kinematic axes: σ_1-a large circle, σ_2-a midsize circle, σ_3-a small circle, blue arrows are showing the maximum extension; all stereonets represent lower hemisphere, equal angle projection; d) Mohr diagram. n=9.

Data from 3 campaign GPS stations and 3 permanent GPS stations were used to calculate the horizontal and vertical movements, azimuths (strikes) of the horizontal movements and the standard deviations within the SMFZ area. Three types of models have been used to test the variability and weight of the final movements and the azimuths. First model is based on the deduction of arithmetic average movement of all individual station's movements from the primary GPS station velocities. The arithmetic average movement for N velocities = 13.61 mm/year, for E velocities = 20.79 mm/year and for vertical

velocities = -0.23 mm/y downwards. The relative horizontal velocities (V_H) are not higher than 1.2 mm/y. The highest value 1.2 mm/y represents the VIDN station, the lowest velocity 0.43 mm/y represents the PETR station. The vertical velocities (V_{UP}) are two times higher than the horizontal. The maximum vertical velocity 2.32 mm/y represents PETR station. Comparing to the whole area, stations BISK and PETR are move downwards, while the other stations move upwards. The standard deviations for both horizontal and vertical movements are much lower for permanent stations than for the campaign stations (Tab. 3). The azimuths of the horizontal movements are marked in Fig. 21, as well as the 95% confidence error ellipses (2σ).

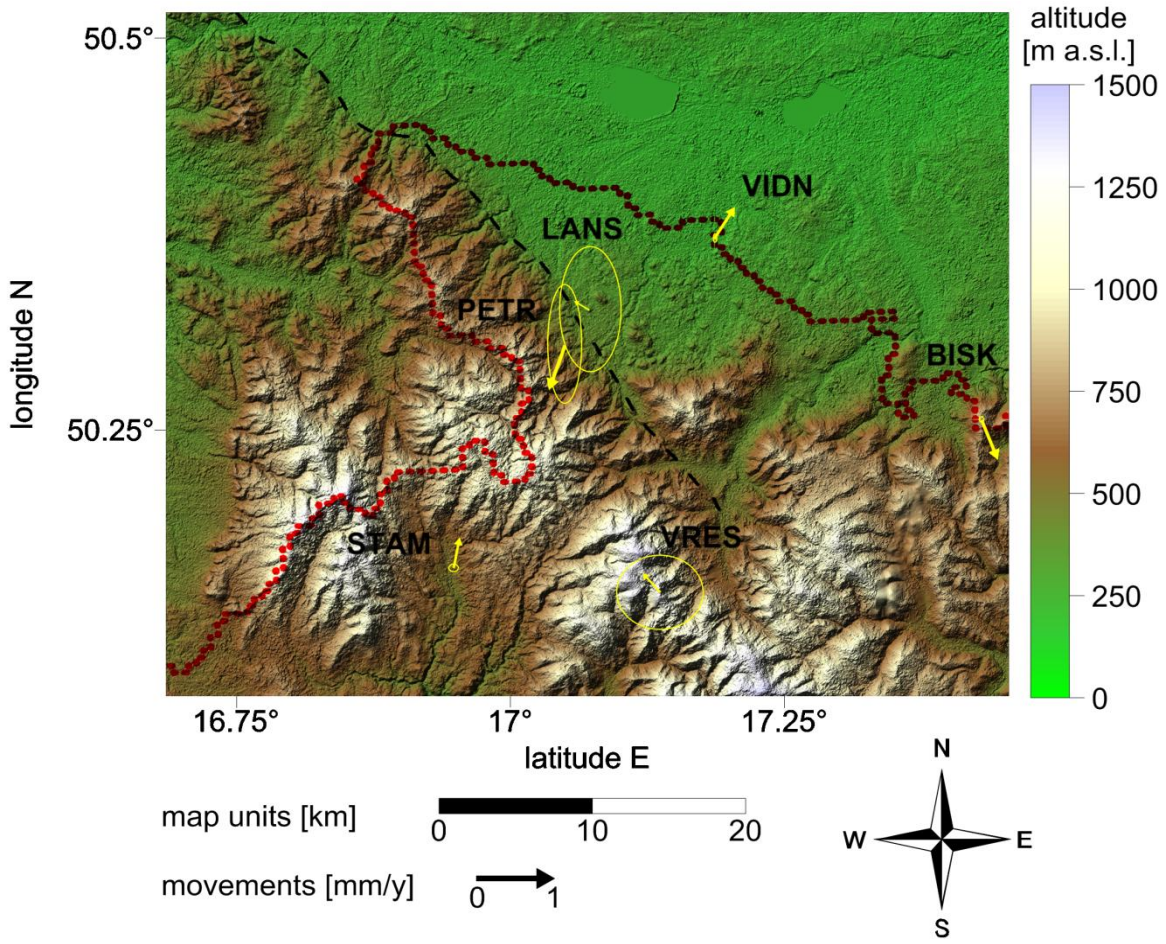

Fig. 21 Model 1: GPS stations with arrows showing strike of horizontal movements and 95% confidence error ellipses. The length of the arrow corresponds to the amplitude of the horizontal velocity.

Tab. 3 Station movements and their uncertainties based on model 1, where V are velocities in N (north), E (east), H (horizontal) UP (up) direction and σ are standard deviations comes from least square estimation, A represents azimuth of the velocity

	Horizontal								Vertical	
Station	V_N [mm/y]	σ_{VN} [mm/y]	V_E [mm/y]	σ_{VE} [mm/y]	V_H [mm/y]	σ_{VH} [mm/y]	A [°]	σ_A [°]	V_{UP} [mm/y]	σ_{UP} [mm/y]
BISK	-0.47	0.01	0.19	0.01	0.51	0.01	158	1	-0.21	0.02
LANS	0.11	0.51	-0.20	0.27	0.22	0.58	299	119	0.75	0.42
PETR	-0.58	0.49	-0.20	0.13	0.61	0.51	199	19	-2.07	0.90
STAM	0.39	0.02	0.07	0.02	0.40	0.03	11	3	0.04	0.07
VIDN	0.40	0.02	0.25	0.01	0.47	0.02	32	2	1.08	0.06
VRES	0.16	0.30	-0.13	0.36	0.20	0.47	321	95	0.39	0.64

Second model is based on the deduction of weighted average movement of all individual station's movements from the primary GPS station velocities. Supposing the results from permanent stations are more precise than from campaign stations, the high weight has been assigned to three used permanent stations. The weighted average movement for N velocities = 13.46 mm/y, for E velocities = 20.98 mm/y and for vertical velocities = -0.54 mm/y downwards.

Tab. 4 Station movements and their uncertainties based on model 2, where V are velocities in N (north), E (east), H (horizontal) UP (up) direction and σ are standard deviations comes from least square estimation, A represents azimuth of the velocity

	Horizontal								Vertical	
Station	V_N [mm/y]	σ_{VN} [mm/y]	V_E [mm/y]	σ_{VE} [mm/y]	V_H [mm/y]	σ_{VH} [mm/y]	A [°]	σ_A [°]	V_{UP} [mm/y]	σ_{UP} [mm/y]
BISK	-0.29	0.01	-0.01	0.01	0.29	0.01	182	2	-0.14	0.02
LANS	0.29	0.51	-0.40	0.27	0.49	0.58	306	51	0.82	0.42
PETR	-0.40	0.49	-0.40	0.13	0.57	0.51	225	36	-2.00	0.90
STAM	0.57	0.02	-0.13	0.02	0.58	0.03	347	2	0.11	0.07
VIDN	0.58	0.02	0.05	0.01	0.58	0.02	5	1	1.15	0.06
VRES	0.34	0.30	-0.33	0.36	0.47	0.47	316	40	0.46	0.64

The relative horizontal velocities (V_H) are not higher than 0.58 mm/y. The highest value represents the VIDN and STAM stations, the lowest velocity 0.29 mm/y represents the BISK station. The vertical velocities (V_{UP}) are more than three times higher than the horizontal. The maximum vertical velocity 2 mm/y represents PETR station. Comparing to the whole area, stations BISK and PETR move downwards, while the other stations move

upwards (Tab. 4). The azimuths of the horizontal movements are marked in Fig. 22, as well as the 95% confidence error ellipses (2σ).

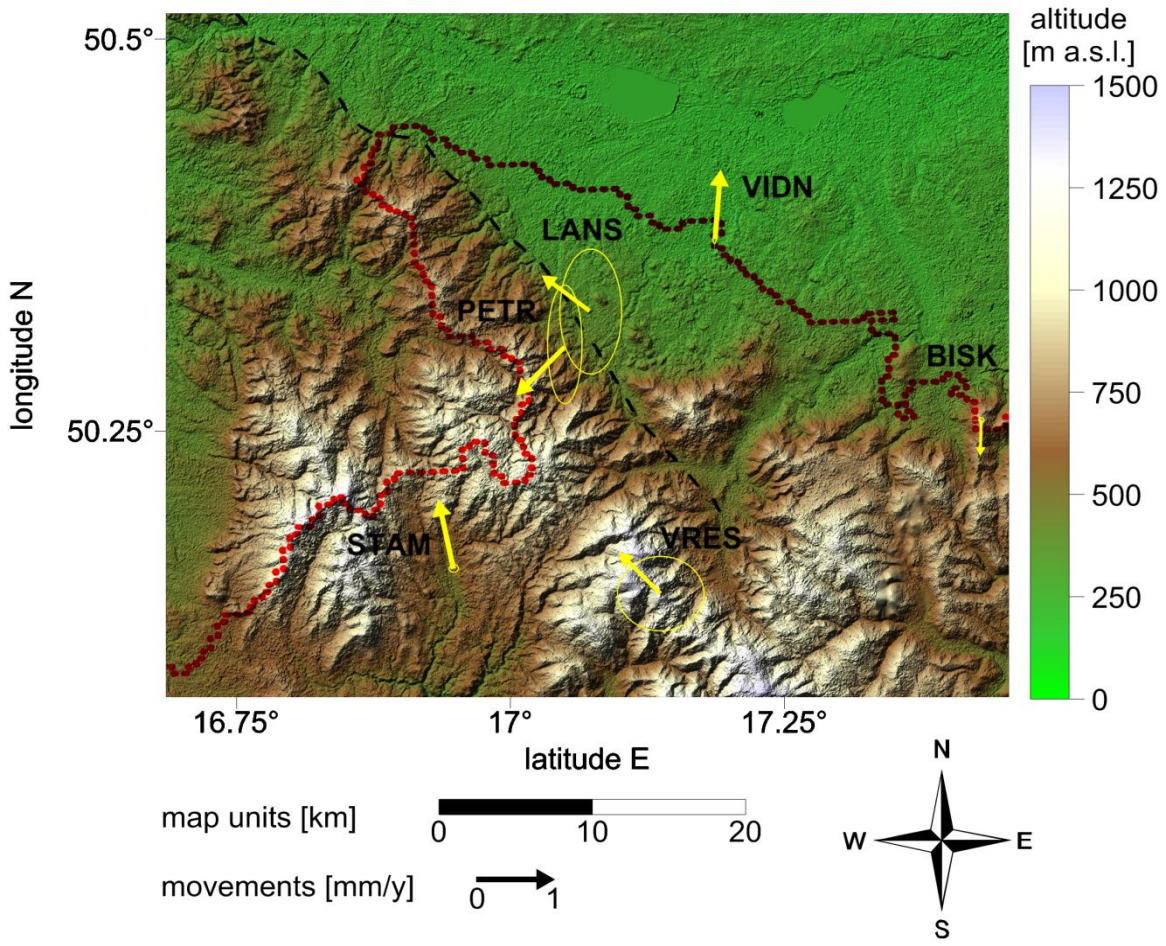

Fig. 22 Model 2: GPS stations with arrows showing strike of horizontal movements and 95% confidence error ellipses. The length of the arrow corresponds to the amplitude of the horizontal velocity.

To subtract the influence of movement of Euroasian tectonic plate, global motion model NNR-NUVEL 1A has been applied as a third model. The relative horizontal velocities (V_H) are not higher than 1.33 mm/y. The highest value represents the VIDN station, while the lowest velocity 0.49 mm/y represents the BISK station. The vertical velocities (V_{UP}) are more than four times higher than the horizontal. The maximum vertical velocity 2.54 mm/y upwards represents PETR station. Comparing to the whole area, stations BISK, PETR, STAM and VRES move downwards, while the stations LANS and VIDN move upwards (Tab. 5). The standard deviations are same for all three used models. The azimuths of the horizontal movements are marked in Fig. 23, as well as the 95% confidence error ellipses.

Tab. 5 Station movements and their uncertainties based on model 3, where V are velocities in N (north), E (east), H (horizontal) UP (up) direction and σ are standard deviations comes from least square estimation, A represents azimuth of the velocity

	Horizontal								Vertical	
Station	V_N [mm/y]	σ_{VN} [mm/y]	V_E [mm/y]	σ_{VE} [mm/y]	V_H [mm/y]	σ_{VH} [mm/y]	A [°]	σ_A [°]	V_{UP} [mm/y]	σ_{UP} [mm/y]
BISK	0.49	0.01	0.01	0.01	0.49	0.01	1	1	-0.68	0.02
LANS	1.01	0.51	-0.30	0.27	1.05	0.58	343	16	0.28	0.42
PETR	0.31	0.49	-0.30	0.13	0.43	0.51	316	47	-2.54	0.90
STAM	1.27	0.02	-0.04	0.02	1.27	0.03	358	1	-0.43	0.07
VIDN	1.32	0.02	0.14	0.01	1.33	0.02	6	1	0.61	0.06
VRES	1.07	0.30	-0.27	0.36	1.10	0.47	346	19	-0.08	0.64

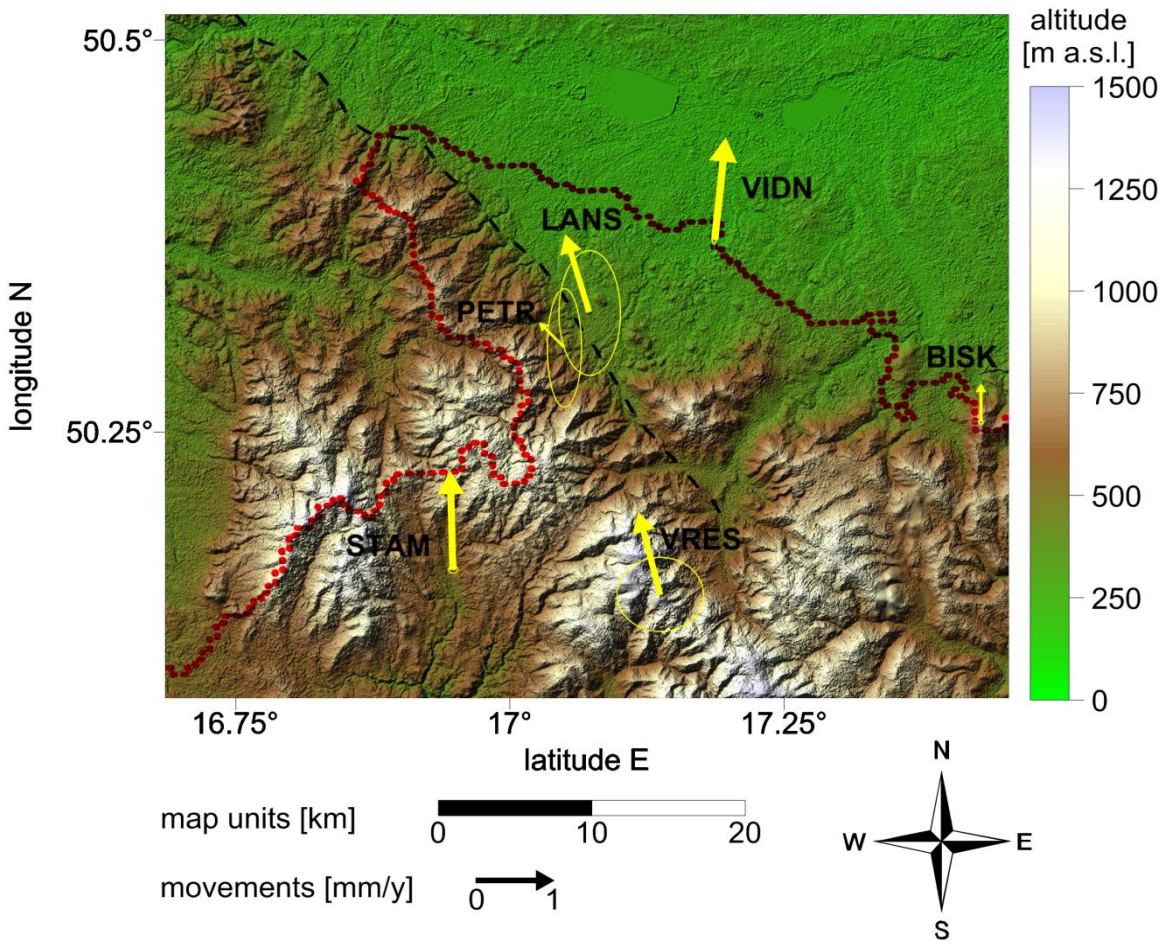

Fig. 23 Model 3: GPS stations with arrows showing strike of horizontal movements and 95% confidence error ellipses. The length of the arrow corresponds to the amplitude of the horizontal velocity.

All three models provided rather different results. The horizontal and vertical velocities differ in numbers, moreover in downward or upward movements. The azimuths of the stations are strongly dependent on the used model. Due to the complicated relative movements of all GPS stations, only PETR and LANS station have been chosen to determine the relative movement on the fault zone. The relative horizontal velocity of the stations is 0.7 mm/y. The relative movement between these two stations is left-lateral (Fig. 24).

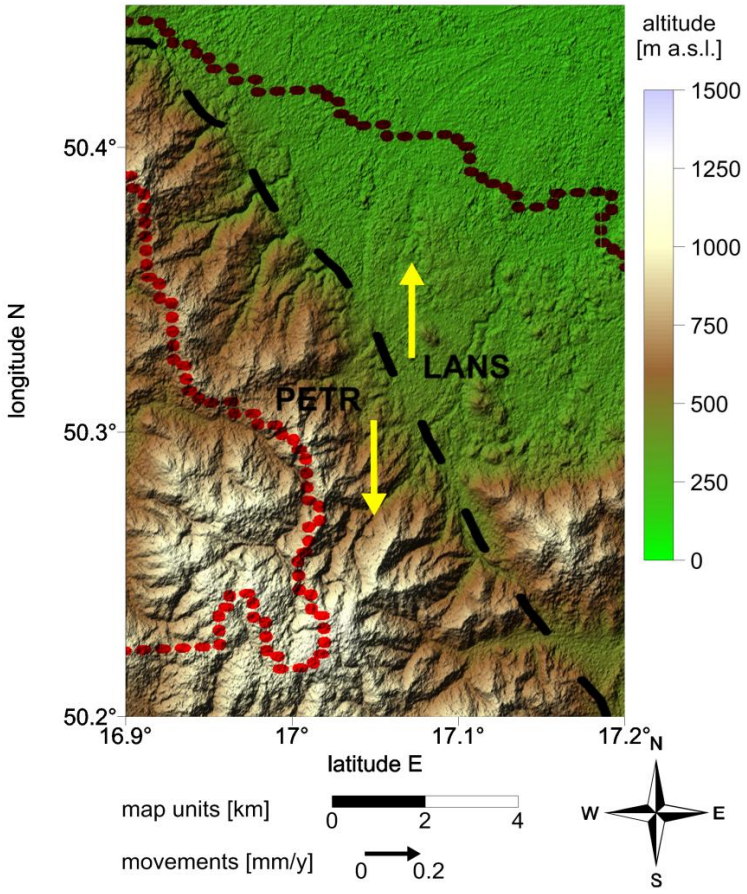

Fig. 24 GPS stations LANS and PETR with arrows showing strike of horizontal movements with respect to the movement to each other.

Results of brittle tectonic data and the results of the long-term GPS monitoring have been compiled and the ASTER GDEM of the studied area has been constructed. The stress conditions during the youngest tectonic phase have been compared with actual movements of GPS stations. Due to the differences of the movements in the used models, the relative movement between two GPS stations within the SMFZ has been considered. During the last youngest phase calculated by paleostress analysis the SMF has been a sinistral fault zone. The relative movement of the GPS stations is also left-lateral one. Thus, it means the SMF has been a sinistral fault zone recently and strike-slip regime prevails (Fig. 25).

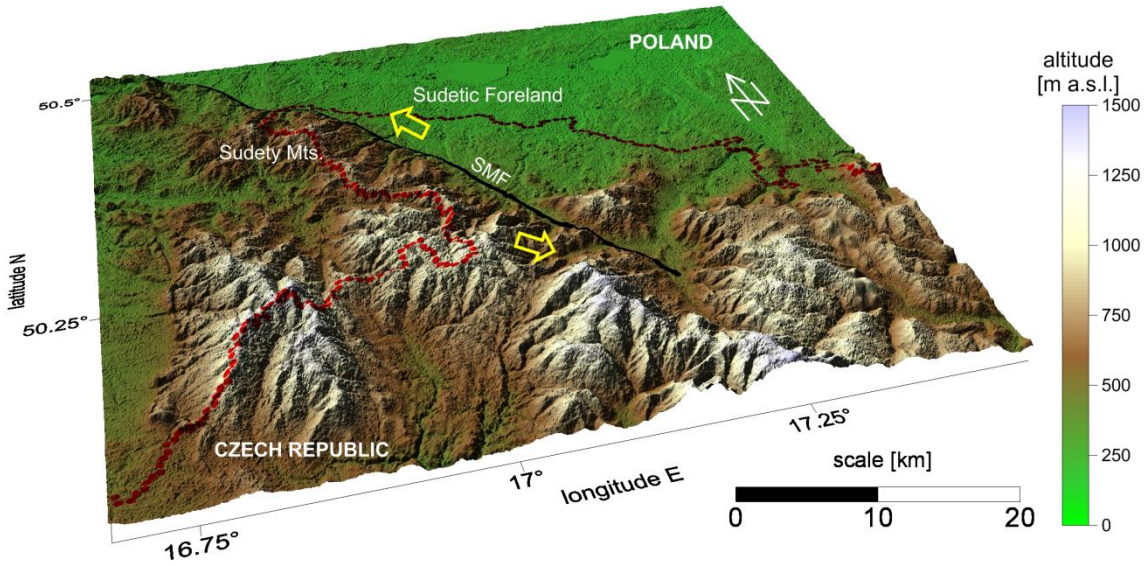

Fig. 25 The actual activity of the SMFZ area based on structural data and long-term GPS monitoring displayed on ASTER GDEM.

4.2 Hronov – Poříčí Fault Zone

Faults and fractures have been measured and described within the HPFZ in 52 localities. The last locality was placed to the gallery, while this gallery is crossing the HPFZ. There are mainly Cretaceous sandstones and Permo-Carboniferous conglomerates in the studied area (Tab. 6).

Tab. 6 List of the localities studied within the SMFZ with the GPS coordinates, description and lithology

Locality	N latitude	E longitude	Description	Lithology
L1	50°34'16"	16°06'06"	a small quarry	middle grained sandstone
L2	50°29'07"	16°10'32"	a small quarry	fine-grained sandstone
L3	50°30'24"	16°06'46"	a small quarry	arkose sandstone
L4	50°30'35"	16°06'28"	a small quarry	arkose sandstone, conglomerate
L5	50°32'19"	16°04'49"	a small natural outcrop	arkose sandstone
L6	50°32'21"	16°04'32"	a small natural outcrop	arkose sandstone
L7	50°32'59"	16°03'01"	rocks	arkose sandstone
L8	50°33'11"	16°01"33"	a small quarry	coarse grained conglomerate

L9	50°31'11"	16°04'02"	a small natural outcrop	silty marlstone
L10	50°31'37"	16°04'18"	a small natural outcrop	claystone
L11	50°32'00"	16°03'47"	a natural outcrop	conglomerate
L12	50°32'14"	16°02'31"	a midsize quarry	sandstone,phyllite,conglomerate
L13	50°32'47"	16°01'27"	a natural outcrop	siltstone
L14	50°33'54"	16°01'20"	a small natural outcrop	weathered conglomerate
L15	50°33'10"	16°03'06"	rocks	conglomerate, sandstone
L16	50°30' 00"	15°56'50"	a large quarry	basalt
L17	50°38'11"	15°55'15"	small rocks	rhyolite tuff
L18	50°38'27"	15°54'50"	a small natural outcrop	conglomerate
L19	50°38'29"	15°54'53"	a small natural outcrop	conglomerate
L20	50°38'46"	15°54'18"	rocks	phyllite
L21	50°25'07"	16°11'52"	a quarry	granodiorite porphyry
L22	50°30'42"	16°05'12"	a small natural outcrop	arkose, conglomerate
L23	50°35'53"	16°01'18"	a small natural outcrop	coarse grained sandstone
L24	50°36'04"	16°00'49"	a small natural outcrop	conglomerate
L25	50°35'30"	15°58'38"	a small quarry	arkose sandstone
L26	50°35'15"	15°59'07"	rocks	conglomerate
L27	50°35'01"	15°58'20"	a small natural outcrop	arkose
L28	50°34'56"	15°58'16"	a small natural outcrop	sandstone
L29	50°38'36"	15°54'13"	a natural outcrop	schist
L30	50°31'28"	16°14'14"	a natural outcrop	silty marlstone
L31	50°30'29"	16°12'59"	a midsize quarry	silty marlstone
L32	50°30'01"	16°12'11"	a natural outcrop	marlstone
L33	50°31'50"	16°04'41"	a small natural outcrop	siltstone
L34	50°31'39"	16°05'16"	a small natural outcrop	arkose sandstone
L35	50°28'37"	16°13'05"	a small natural outcrop	phyllite
L36	50°28'43"	16°13'34"	a small natural outcrop	sandstone
L37	50°29'06"	16°13'09"	a small natural outcrop	fine-grained sandstone
L38	50°29'58"	16°16'49"	a small natural outcrop	siltstone
L39	50°29'38"	16°13'40"	a natural outcrop	silty marlstone
L40	50°28'36"	16°14'04"	a small natural outcrop	middle grained sandstone
L41	50°28'20"	16°14'21"	a midsize quarry	middle grained sandstone
L42	50°26'40"	16°08'55"	a small natural outcrop	siltstone, sandstone
L43	50°27'36"	16°08'56"	a small natural outcrop	middle grained sandstone
L44	50°28'35"	16°08'41"	a small natural outcrop	siltstone
L45	50°29'57"	16°08'09"	a small natural outcrop	arkose sandstone
L46	50°29'43"	16°08'33"	a small natural outcrop	arkose sandstone
L47	50°29'27"	16°08'46"	a midsize quarry	sandstone

L48	50°28'20"	16°09'05"	a small natural outcrop	sandstone
L49	50°26'29"	16°10'32"	a natural outcrop	conglomerate
L50	50°25'21"	16°10'10"	a natural outcrop	conglomerate
L51	50°29'25"	16°03'21"	a large quarry	sandstone
L52	50°31'36"	16°03'54"	a gallery	sandstone, conglomerate

Five long-term GPS monitoring stations have been chosen to determine the actual movements within the area of HPFZ.

Tab. 7 shows the type of the station, its geographic coordinates, ellipsoidal heights and the information about observations. Figure 26 illustrate the studied localities, GPS stations and the HPFZ. The localities were chosen in the close vicinity of the fault zone, moreover some localities were measured in the main zone.

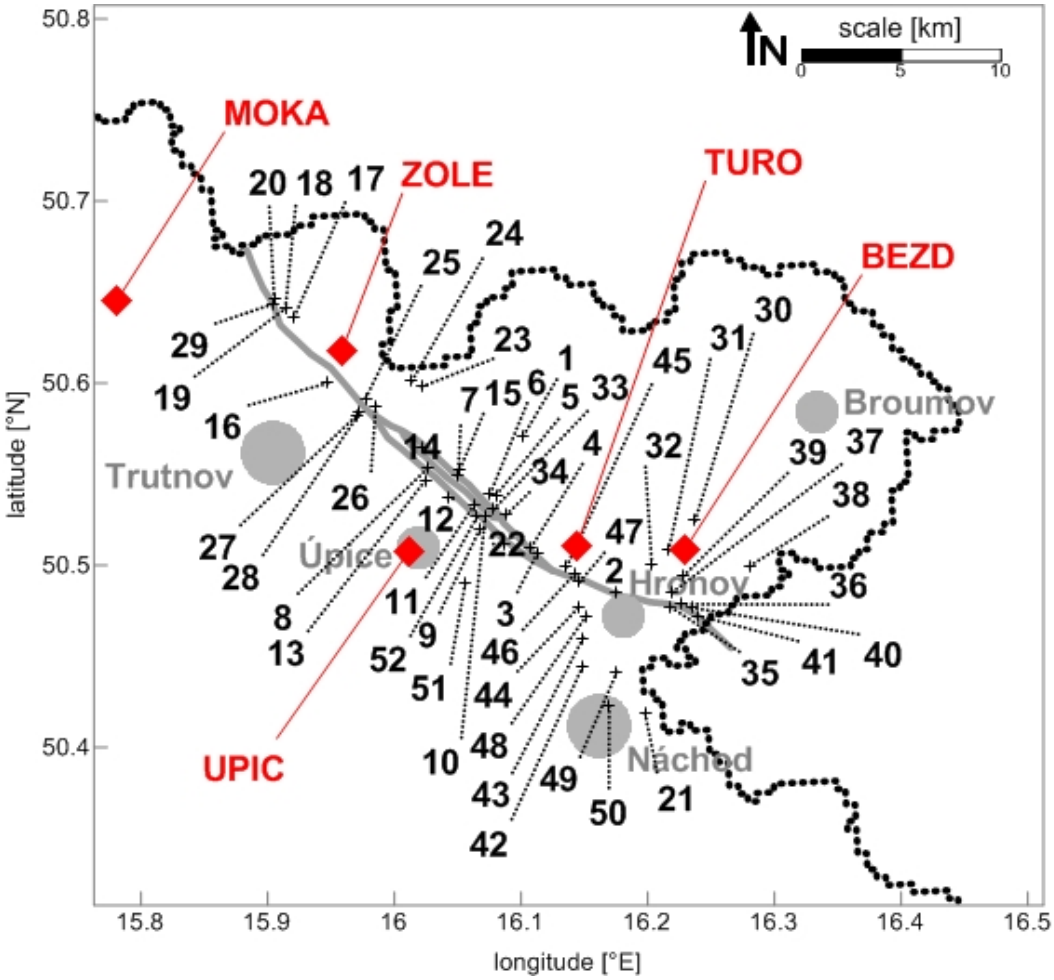

Fig. 26 The map of the HPFZ area. The studied localities are marked by crosses and numbers. The red squares represent GPS stations.

Tab. 7 Selected stations and their characteristics

		Station location			Observations
Station	**Type**	**N latitude**	**E longitude**	**Ellipsoid heigh [m]**	**Start**
BEZD	P	50° 30' 31.29"	16° 13' 45.31"	539.490	Dec 2005
MOKA	C	50° 38' 44.19"	15° 46' 51.68"	1007.485	Aug 2003
TURO	C	50° 30' 37.42"	16° 08' 37.58"	604.669	Dec 2005
UPIC	P	50° 30' 25.67"	16° 00' 39.36"	467.923	Aug 2003
ZOLE	C	50° 37' 02.25"	15° 57' 29.25"	600.508	Sep 2001

P: Permanent station, C: Campaign station

At total, 58 fault planes containing the kinematic indicators, mainly grooves and small steps with sharp borders (e.g. Doblas, 1998) have been measured within the HPFZ. The fault planes are mostly oriented in NW-SE direction, nevertheless they occur also in the second less significant direction NE-SW (Fig. 27 left). This principle orientation corresponds to the direction of the main fault zone. Subvertical to vertical faults have been found within the HPFZ mainly (Fig. 27 right).

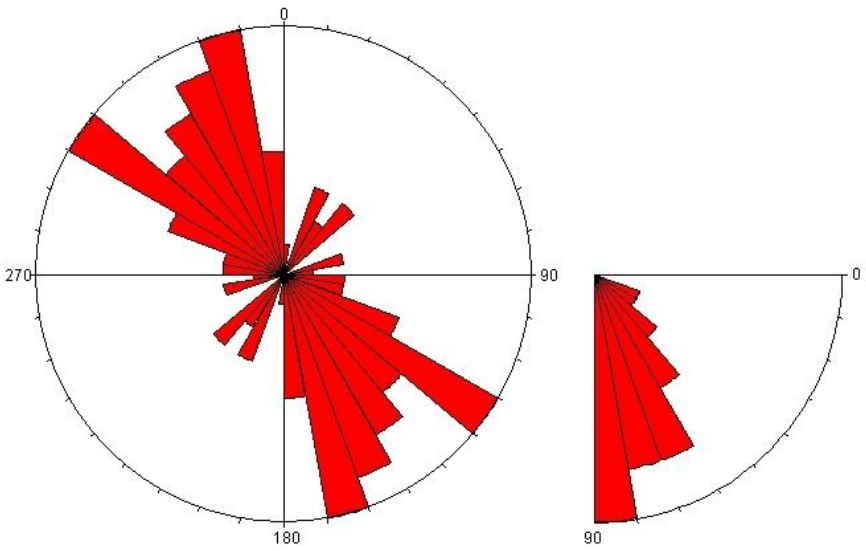

Fig. 27 Rose diagrams of the fault planes within the HPFZ. Left: strike of the planes. Right: dip of the planes. N=882.

The faults have vertical or subvertical dips, while no horizontal faults were found within the studied area (Fig. 28 left). The lineations found on the fault planes are mainly trending to the NE, S, SSW and SW. There are mainly subvertical lineations (50-60°) (Fig. 28 right). The kinematic analysis of the faults has been performed to separate the different

type of the faults and to determine the principle orientations of this types (Fig. 29). Only four normal faults have been measured, so they have not any preferential orientation. They occur in NW-SE, NE-SW and W-E directions. The reverse faults have one prevailing orientation – NW-SE. Dextral faults have also only one prevailing orientation – N-S. The sinistral faults were found in two principle directions – NW-SE and NE-SW. Rose diagram of all fractures displays one prevailing orientation. The fractures occur mostly in NW-SE direction (Fig. 30 left). This direction is same as the studied faults and the main fault zone. The dip of the fractures is mainly vertical 80-90° (Fig. 30 right).

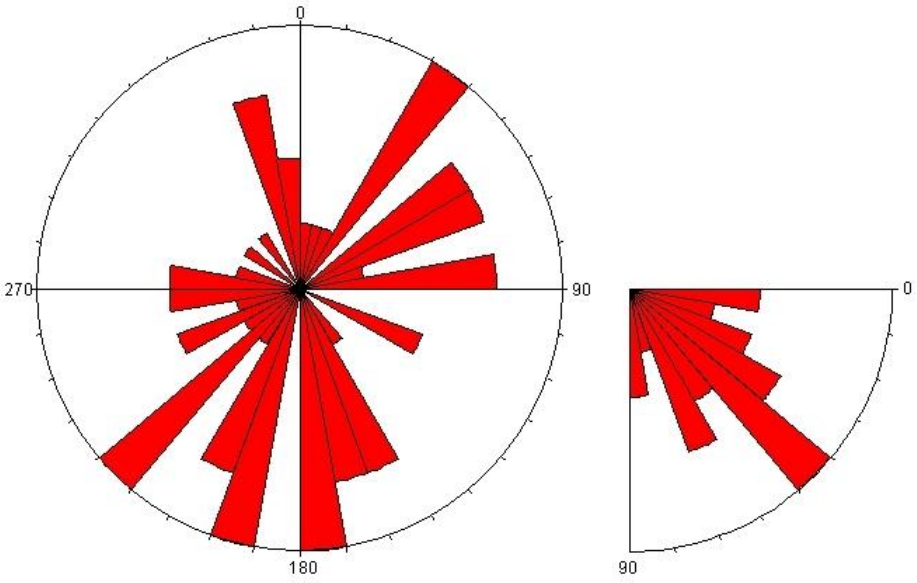

Fig. 28 Rose diagrams of the lineations on the fault planes within the HPFZ. Left: trend of the lineations. Right: plunge of the lineations. N=58.

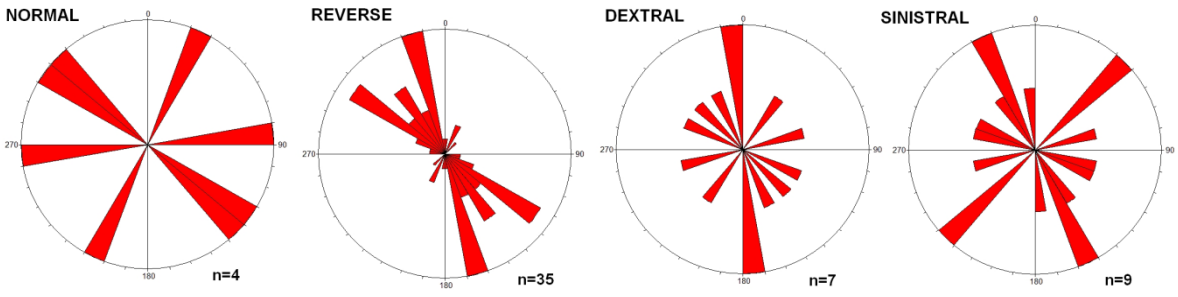

Fig. 29 Kinematic analysis of the fault types within the HPFZ.

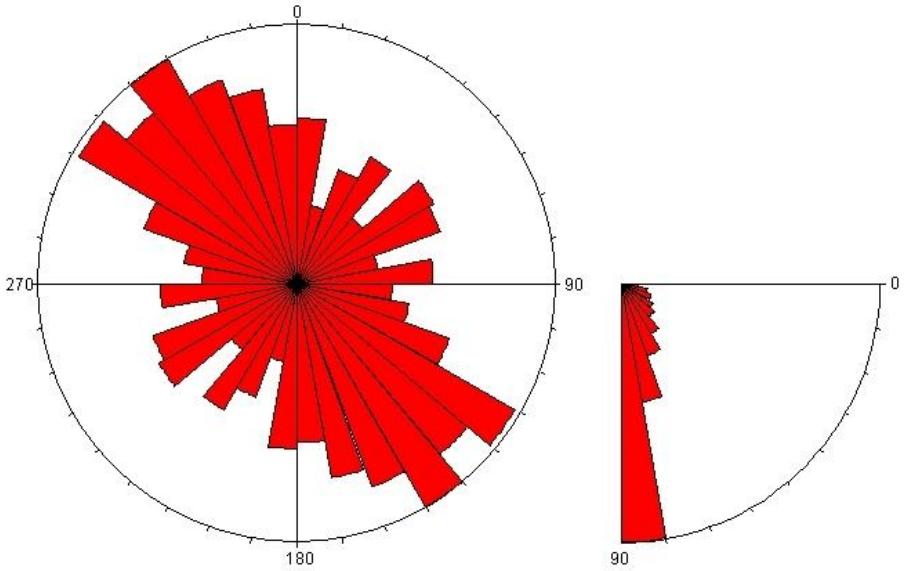

Fig. 30 Rose diagrams of the fracture planes within the HPFZ. Left: strike of the planes. Right: dip of the planes. N=940.

Paleostress analysis of the fault-slip data within the HPFZ resulted in separation of four tectonic phases. The phases have been ordered by the geological age on the base on the faults with multiple lineation systems and cross-cutting lineations from the first and youngest to the fourth and oldest. The youngest phase represents the actual stress conditions. This phase contains 35 faults that have been reactivated in the latest stress field. The maximum principle stress is oriented in NE-SW direction perpendicular to the main fault zone. Although the minimum compression is vertical, the intermediate principle stress is oriented in NW-SE direction (Fig. 31a). These conditions caused the HPFZ is under transpression with dextral component. The RDM provided the same results, when the T field is forming elongated cluster and the P fields are symmetrically oriented around the maximum compression and T field simultaneously (Fig. 31b). VGH method displays slightly different results. The only maximum principle stress is marked there (Fig. 31c). Nevertheless, the coloured clusters documenting the magnitudes of individual stresses are rather similar as for the RDM. The area where possible mechanically compatible faults could have been reactivated is rather small, while almost all "Mohr points" are positioned above the line representing Amontons's law of friction (Fig. 31d).

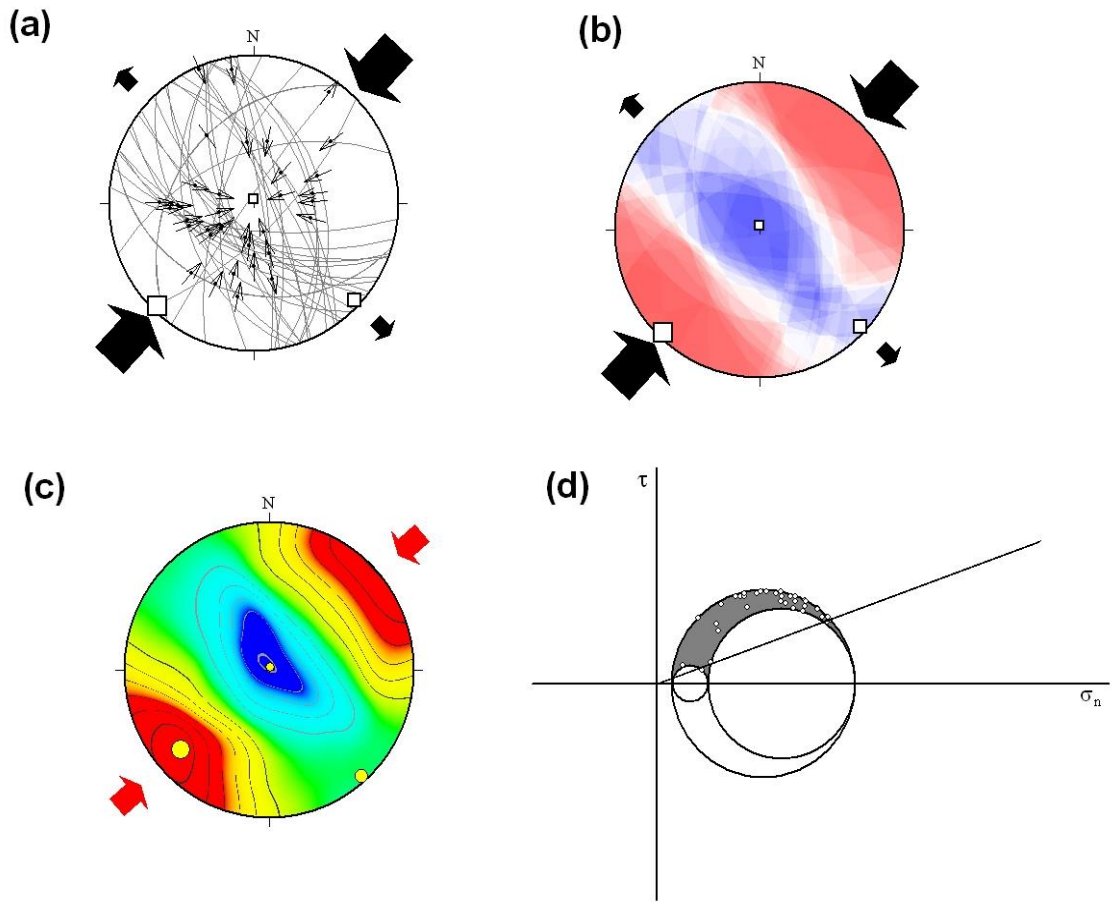

Fig. 31 The youngest phase of fault-slip data separation within the HPFZ. a) Paleostress analysis of the faults based on Gauss method (Žalohar and Vrabec, 2007), paleostress axes: σ_1-a large square, σ_2-a midsize square, σ_3-a small square, arrows are showing the maximum compression and maximum extension; b) Paleostress analysis of the faults based on Right Dihedra Method (Angelier and Mechler, 1977); c) VGF of the faults, kinematic axes: σ_1-a large circle, σ_2-a midsize circle, σ_3-a small circle, red arrows are showing the maximum compression; all stereonets represent lower hemisphere, equal angle projection; d) Mohr diagram. n=35.

The second phase of the calculated paleostress analysis was characterised by a compression. Eleven measured faults were developed or reactivated during this phase. The maximum principle stress was oriented WNW-ESE, and minimum principle stress was almost subvertical (Fig. 32a). The RDM provided totally the same results (Fig. 32b). On the other hand, the VGF method provided different results. The compressional arrows did not occur, moreover the extensional arrows are marked there. The maximum extension is oriented NE-SW, and the clusters around maximum and minimum principle stresses are

separated (Fig. 32c). The Mohr circles are almost same, although few "Mohr points" are positioned above the line representing Amontons's law of friction (Fig. 32d). During the second phase, the HPFZ was thrust with the compression oriented obliquely to the main fault zone. This is the only phase when no horizontal movements occurred.

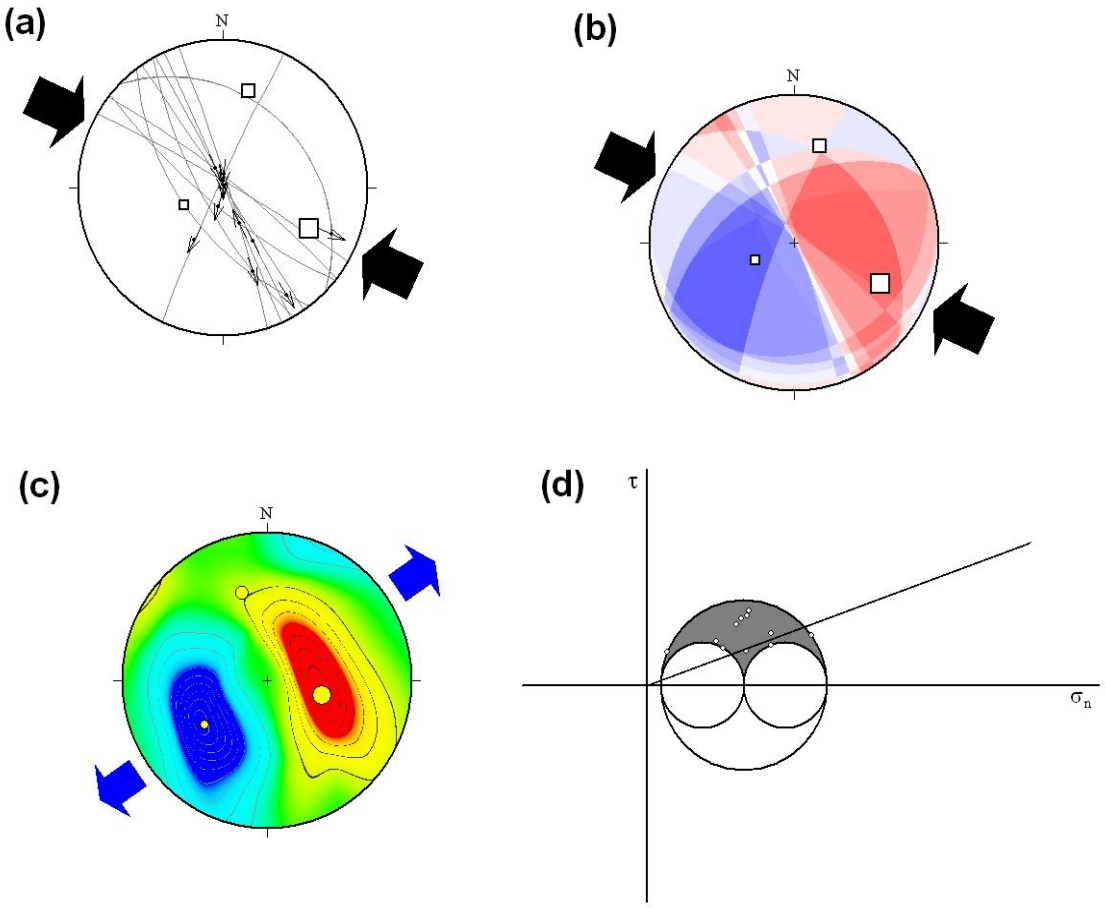

Fig. 32 The second phase of fault-slip data separation within the HPFZ. a) Paleostress analysis of the faults based on Gauss method (Žalohar and Vrabec, 2007), paleostress axes: σ_1-a large square, σ_2-a midsize square, σ_3-a small square, arrows are showing the maximum compression and maximum extension; b) Paleostress analysis of the faults based on Right Dihedra Method (Angelier and Mechler, 1977); c) VGF of the faults, kinematic axes: σ_1-a large circle, σ_2-a midsize circle, σ_3-a small circle, blue arrows are showing the maximum extension; all stereonets represent lower hemisphere, equal angle projection; d) Mohr diagram. n=11.

The third phase contains eight faults, while the fourth phase contains only three faults. The relative age of these two phases was not possible to determine. The relevance of phase with only three faults is debatable, nevertheless it has been covered to the results for the complex information. During the third phase, the HPFZ was under strike-slip regime. It

was a sinistral fault, with maximum principle stress oriented in NW-SE direction and minimum principle stress oriented in NE-SW direction (Fig. 33a). The RDM provided the same results with P and T quadrants typical for strike-slip conditions (Fig. 33b). The maximum principle stress calculated by the VGF method is oriented in the same direction, nevertheless in the opposite station of the stereogram. The stress conditions remained almost same (Fig. 33c). The Mohr circles have the same size, and the "Mohr points" are all situated above the line representing Amontons's law of friction (Fig. 33d).

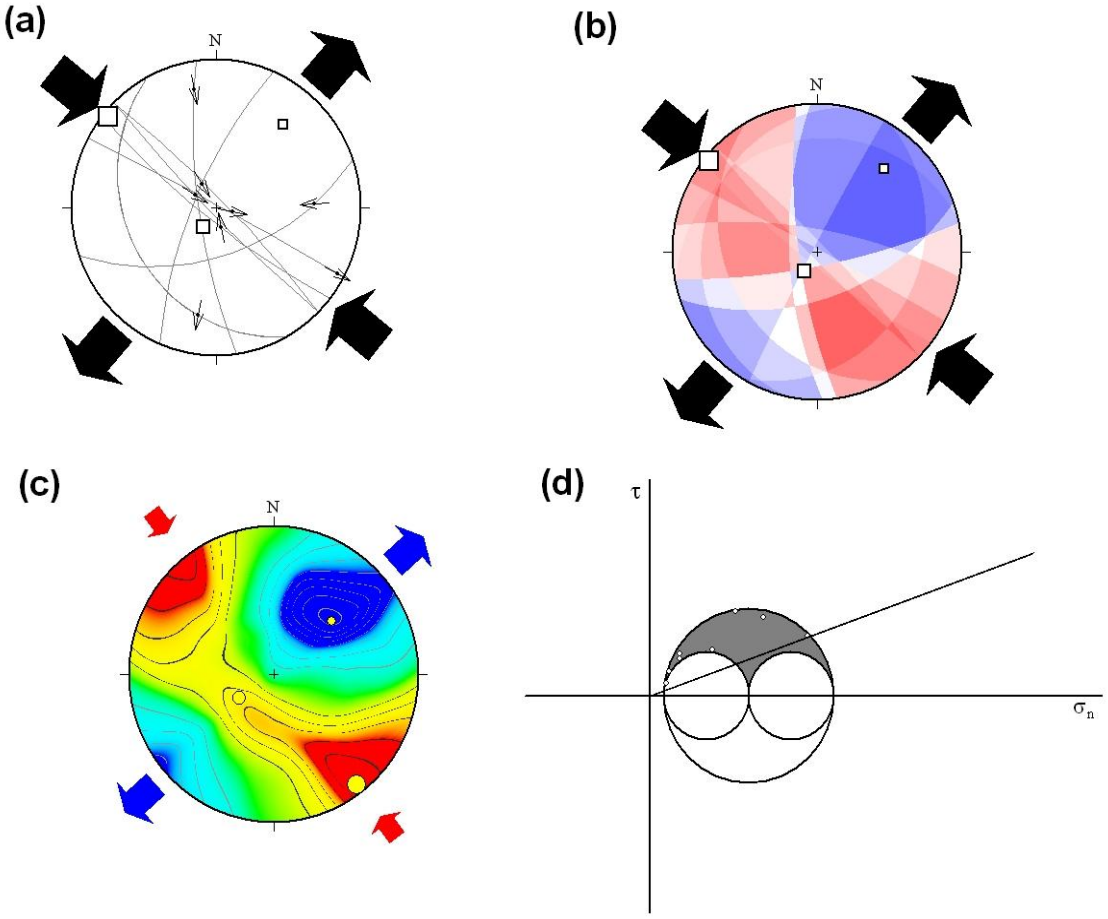

Fig. 33 The third phase of fault-slip data separation within the HPFZ. a) Paleostress analysis of the faults based on Gauss method (Žalohar and Vrabec, 2007), paleostress axes: σ_1-a large square, σ_2-a midsize square, σ_3-a small square, arrows are showing the maximum compression and maximum extension; b) Paleostress analysis of the faults based on Right Dihedra Method (Angelier and Mechler, 1977); c) VGF of the faults, kinematic axes: σ_1-a large circle, σ_2-a midsize circle, σ_3-a small circle, red arrows are showing the maximum compression, blue arrows are showing the maximum extension; all stereonets represent lower hemisphere, equal angle projection; d) Mohr diagram. n=8.

During the fourth phase the HPFZ was a dextral fault zone with maximum principle stress oriented NNE-SSW (Fig. 34a). The RDM provided same results, with P and T quadrants showing the strike-slip regime (Fig. 34b). The VGF method shows the same results with the axes oriented totally in same direction (Fig. 34c). All "Mohr points" are positioned above the line representing Amontons's law of friction. The area where possible mechanically compatible faults could have been reactivated is rather small (Fig. 34d).

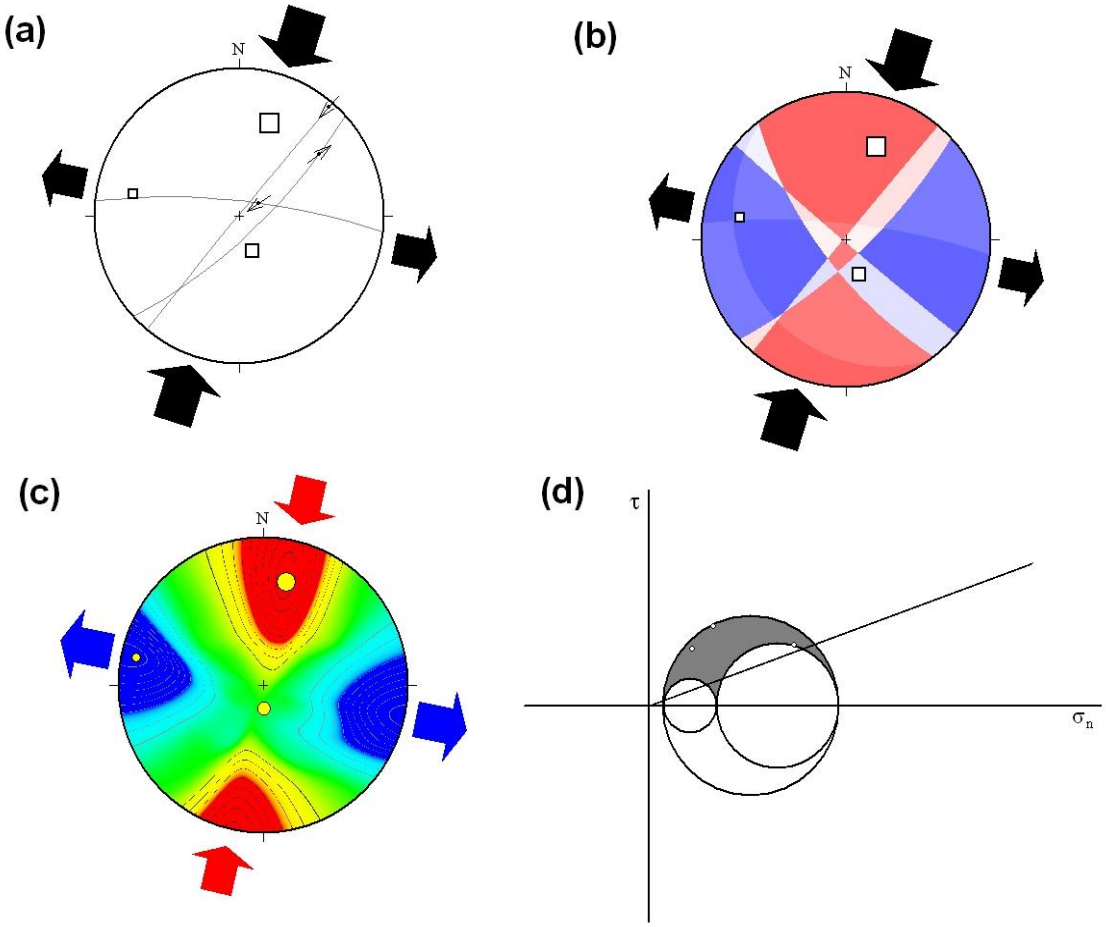

Fig. 34 The fourth phase of fault-slip data separation within the HPFZ. a) Paleostress analysis of the faults based on Gauss method (Žalohar and Vrabec, 2007), paleostress axes: σ_1-a large square, σ_2-a midsize square, σ_3-a small square, arrows are showing the maximum compression and maximum extension; b) Paleostress analysis of the faults based on Right Dihedra Method (Angelier and Mechler, 1977); c) VGF of the faults, kinematic axes: σ_1-a large circle, σ_2-a midsize circle, σ_3-a small circle, red arrows are showing the maximum compression, blue arrows are showing the maximum extension; all stereonets represent lower hemisphere, equal angle projection; d) Mohr diagram. n=3.

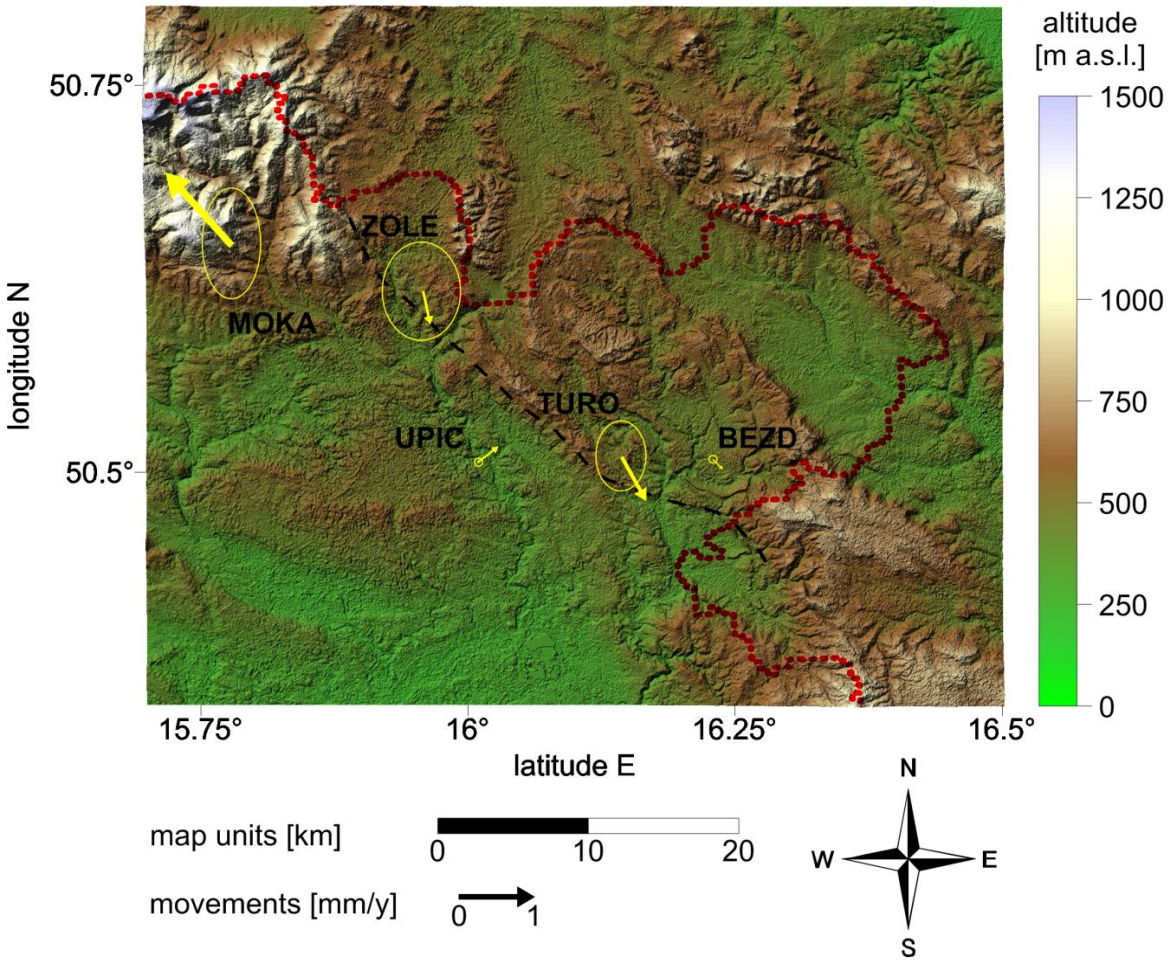

Fig. 35 Model 1: GPS stations with arrows showing strike of horizontal movements and 95% confidence error ellipses. The length of the arrow corresponds to the amplitude of the horizontal velocity.

Horizontal and vertical movements have been calculated for the five chosen long-term GPS monitoring stations within the HPFZ area. Three types of models have been used to test the variability and weight of the final movements and the azimuths as for the SMFZ area. First model is based on the deduction of arithmetic average movement of all individual station's movements from the primary GPS station velocities (Tab. 8). The arithmetic average movement for N velocities = 13.99 mm/y, for E velocities = 20.41 mm/y and for vertical velocities = 0.56 mm/y upwards. The relative horizontal velocities (V_H) are not higher than 1.22 mm/y. The highest value represents the MOKA station, the lowest velocity 0.19 mm/y represents the BEZD station. The vertical velocities (V_{UP}) are more than two times higher than the horizontal. The maximum vertical velocity 1.99 mm/y represents TURO station. Comparing to the whole area, stations MOKA and TURO move downwards, while the other stations move upwards. The azimuths of the horizontal movements are marked in (Fig. 35), as well as the 95% confidence error ellipses.

Tab. 8 Station movements and their uncertainties based on model 1, where V are velocities in N (north), E (east), H (horizontal) UP (up) direction and σ are standard deviations comes from least square estimation, A represents azimuth of the velocity

	Horizontal								Vertical	
Station	V_N [mm/y]	σ_{VN} [mm/y]	V_E [mm/y]	σ_{VE} [mm/y]	V_H [mm/y]	σ_{VH} [mm/y]	A [°]	σ_A [°]	V_{UP} [mm/y]	σ_{UP} [mm/y]
BEZD	-0.14	0.01	0.13	0.01	0.19	0.01	137	3	0.53	0.04
MOKA	0.92	0.46	-0.08	0.23	1.22	0.51	355	14	-0.28	2.03
TURO	-0.57	0.29	0.32	0.20	0.65	0.35	151	20	-1.99	1.02
UPIC	0.19	0.01	0.28	0.01	0.34	0.01	55	2	0.71	0.04
ZOLE	-0.42	0.40	0.09	0.35	0.42	0.53	168	47	1.02	0.83

Tab. 9 Station movements and their uncertainties based on model 2, where V are velocities in N (north), E (east), H (horizontal) UP (up) direction and σ are standard deviations comes from least square estimation, A represents azimuth of the velocity

	Horizontal								Vertical	
Station	V_N [mm/y]	σ_{VN} [mm/y]	V_E [mm/y]	σ_{VE} [mm/y]	V_H [mm/y]	σ_{VH} [mm/y]	A [°]	σ_A [°]	V_{UP} [mm/y]	σ_{UP} [mm/y]
BEZD	-0.16	0.01	-0.07	0.01	0.17	0.01	204	3	-0.09	0.04
MOKA	0.90	0.46	-1.00	0.23	1.17	0.51	312	16	-0.90	2.03
TURO	-0.59	0.29	0.12	0.20	0.59	0.35	169	19	-2.61	1.02
UPIC	0.17	0.01	0.08	0.01	0.32	0.01	25	3	0.09	0.04
ZOLE	-0.44	0.40	-0.11	0.35	0.41	0.53	194	45	0.40	0.83

Second model is a model based on the deduction of weighted average movement of all individual station's movements from the primary GPS station velocities. Supposing the results from permanent stations are more precise than from campaign stations, the high weight has been assigned to three used permanent stations. The highest value represents the MOKA station, the lowest velocity 0.17 mm/y represents the BEZD station. The vertical velocities (V_{UP}) are more than four times higher than the horizontal. The maximum vertical velocity 2.61 mm/y represents TURO station. Comparing to the whole area, stations BEZD, MOKA and TURO move downwards, while the other stations move upwards (Tab. 9). The azimuths of the horizontal movements are marked in Fig. 36, as well as the 95% confidence error ellipses (2σ).

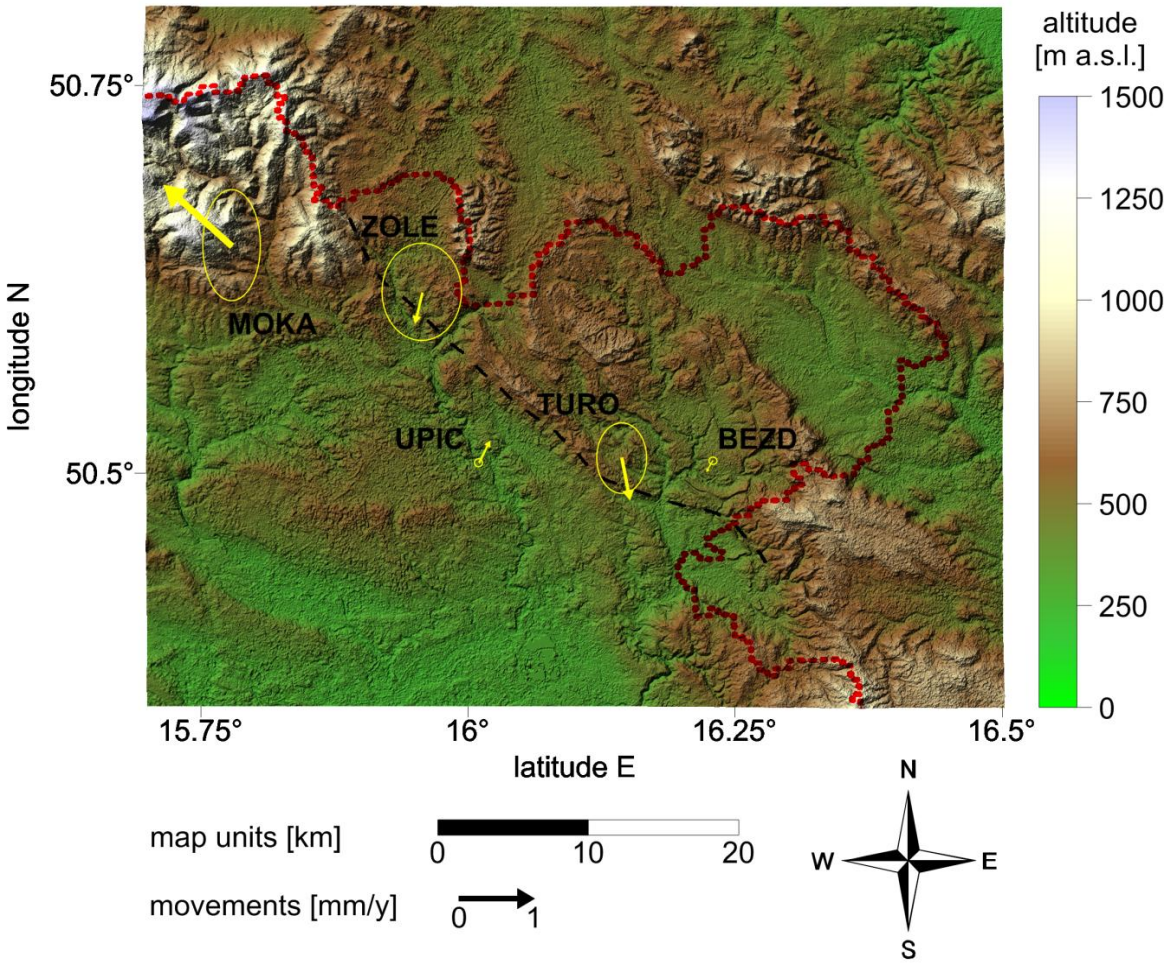

Fig. 36 Model 2: GPS stations with arrows showing strike of horizontal movements and 95% confidence error ellipses. The length of the arrow corresponds to the amplitude of the horizontal velocity.

Third model is based on the influence of movement of Euroasian tectonic plate subtraction by usage the global motion model NNR-NUVEL 1A. The maximum horizontal velocity goes to the MOKA station, which moves 2.18 mm/y. The minimum horizontal velocities and maximum vertical velocities were both calculated for the station TURO. The numbers for the vertical movements are not as precise as for the horizontal. The standard deviations are sometimes higher than the vertical velocities. Nevertheless, it can be stated, the stations BEZD, MOKA and TURO move downwards comparing to the stations ZOLE and UPIC (Tab. 10). The presence of HPF and other faults is probably the explanation. The directions of the movements of the GPS stations with 95% confidence error ellipses are displayed in the map showing the tectonic situation, main fault zone and less significant faults in the studied area (Fig. 37). The length of the arrow corresponds to the amplitude of the horizontal velocity.

Tab. 10 Station movements and their uncertainties based on model 3, where V are velocities in N (north), E (east), H (horizontal) UP (up) direction and σ are standard deviations comes from least square estimation, A represents azimuth of the velocity

Site	Horizontal								Vertical	
	V_N [mm/y]	σ_{VN} [mm/y]	V_E [mm/y]	σ_{VE} [mm/y]	V_H [mm/y]	σ_{VH} [mm/y]	A [°]	σ_A [°]	V_{UP} [mm/y]	σ_{UP} [mm/y]
BEZD	0.96	0.01	-0.17	0.01	0.97	0.01	170	3	-0.03	0.04
MOKA	1.94	0.46	-1.00	0.23	2.18	0.51	333	16	-0.84	2.03
TURO	0.51	0.29	0.03	0.20	0.51	0.35	177	19	-2.55	1.02
UPIC	1.25	0.01	0.02	0.01	1.25	0.01	1	3	0.15	0.04
ZOLE	0.63	0.40	-0.15	0.35	0.65	0.53	167	45	0.46	0.83

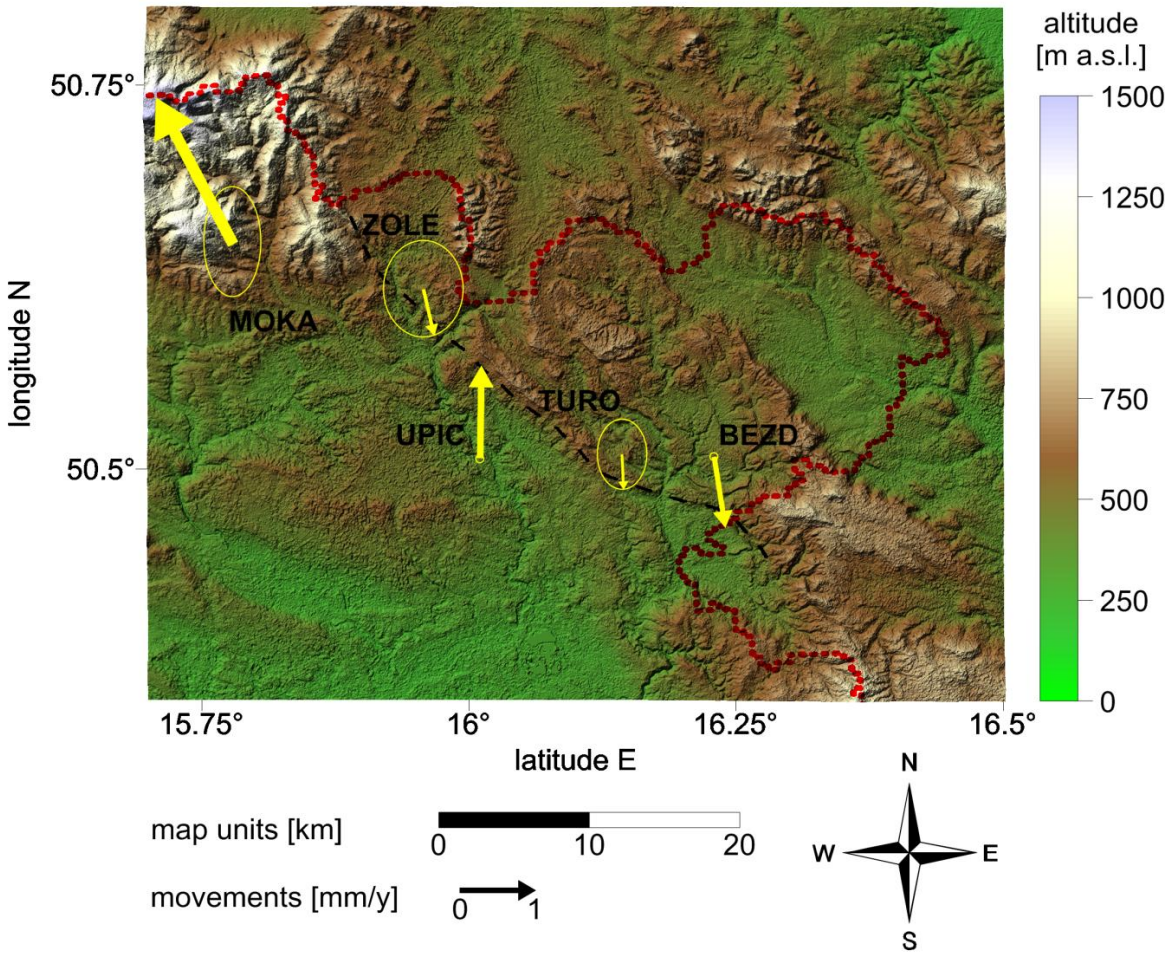

Fig. 37 Model 3: GPS stations with arrows showing strike of horizontal movements and 95% confidence error ellipses. The length of the arrow corresponds to the amplitude of the horizontal velocity.

Both structural and GPS data were compared and the actual activity and stress conditions of the HPFZ area were constructed. The ASTER GDEM shows the 3D situation of the geomorfological situation. The HPFZ goes along the foothill of the Jestřebí hory Mts. The stations ZOLE and UPIC move towards the main fault zone, which causes the thrusting of the NW part over the SE part. In the same time, the stations TURO and MOKA go along the fault zone, moreover against each other. This situation causes the transpressional conditions with dextral movements along the fault zone. The actual movements of the GPS stations in the used models are rather similar. During the last youngest phase calculated by paleostress analysis the HPF has been a reverse fault zone with dextral component. The relative movements of the GPS stations provided the same results. Thus, it means HPFZ has been a dextral transpressive fault zone in compressional regime recently (Fig. 38).

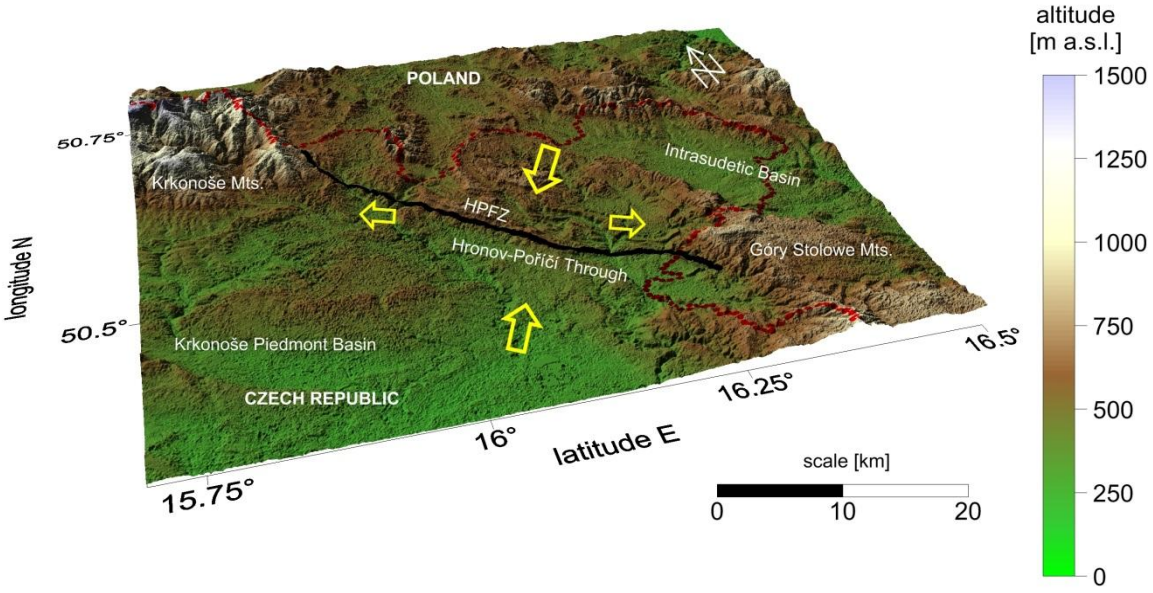

Fig. 38 The actual activity of the HPFZ area based on structural data and long-term GPS monitoring displayed on ASTER GDEM.

Chapter 5

Discussion

This thesis combines and correlates brittle tectonic field study and GPS long-term monitoring. It is a time consuming process to collect a representative brittle tectonic data set describing large area. The field work involve identification of kinematic indicators (Nováková, 2008; Appendix 1) to decide whether they are relevant, which movements it is, to determine the relative age of crosscutting faults (Nováková et al., 2010; Appendix 4) or of two or more sets or lineations on one fault plane. This decision is more or less subjective particularly depending on a geologist's experience. Kinematic data analyses could delineate the stress history of the area. Obviously, the method describes history only. GPS monitoring, on the other hand, depicts actual movements in the monitored area. Combination of the methods thus might draw a complete picture. GPS monitoring needs time to attain reliable results too. Usually, several years of monitoring are required. The process of interpretation is, however, somehow similar.

The paleostress analysis is a useful tool enabling a geologist to distinguish various tectonic phases during which faults were developed or reactivated. Consequently is is possible to calculate stress field and conditions every individual phase. Nováková (2010; Appendix 3) described the process of fault separation into tectonic phases on data collected in two great quarries near the village of Vápenná. Nováková (Appendix 5) describes the reactivation of brittle tectonic structures within the SMFZ using the data set including the earlier attained limestone quarries data. Four tectonic phases have been determined for the area analysing both data sets. Consistency of the results points out the limestone quarries are, in terms of stress history, representative site for all the SMFZ area.

The youngest tectonic phase determined by paleostress analysis in the SMFZ area suggests the SMF was a sinistral fault zone during the last active period. This finding corresponds to the present relative movement observed between GPS station LANS and PETR (see Fig. 24). The stations are sited close to each other on the different sides of the SMF. Both methods combined point out the last and recent movement along the SMF is sinistral fault zone. It seems this area is rather geologically complicated, full of affiliated faults (e.g. Opletal and Pecina, 2004; Skácel, 2004). On the other hand, the observed GPS movements of all stations in the area evince the area moves almost as a compact block. The observed movement along the SMF (LANS vs. PETR movement) and similar relative movement between VRES and PETR or STAM and PETR sited on same side of the SMF indicate the SMF is either terminated or at least dislocated between the stations. Data suggests, a fault

or set faults, the Ramzová overthrust (Opletal and Pecina, 2004) for example, probably compensates the movement along the SMF. Using GPS measurements, Kontny (2004) based on studies in Poland and Nováková and Schenk (2008) based on studies in the Czech Republic, documented transpressional left-lateral movements along the SMF. Sinistral movements along the SMF have been also confirmed by Schenková et al. (2009). Using geomorfological investigations, Badura et al. (2004) concluded that the SMF represents a sinistral-normal fault reactivated in the late Neogene and Quaternary.

In the HPFZ area, the youngest tectonic phase determined by paleostress analysis shows the HPF was a reverse fault zone with dextral movement lately (Nováková and Balek; Appendix 6). Actual movement according to GPS monitoring corresponds to the finding (see Fig. 37). The GPS measurements provided rather similar results, moreover for all three used models. Transpressional conditions with dextral component within the HPFZ caused the observed movements. The development of the HPFZ as a thrust fault has been described by Tásler et al. (1979). According to Aleksandrowski et al. (1993) the HPFZ movements have been ranging from dip-slip to strike-slip transpressional. Using DEM, Wojewoda (2007) described the HPFZ was a right-lateral fault zone during the Neogene.

Separation of the faults and various analyses of data from SMFZ and HPFZ areas allowed to determine the history of kinematics and stress conditions within the studied fault zones. The GPS measurements provided the complementary results of the actual movements of the GPS stations in the studied areas. Both applied methods thus completed the kinematics and stress history record. The procedure of comparing the brittle tectonic data and GPS monitoring data confirmed complementary character of the method and advantage of the multidisciplinary approach.

Chapter 6

Conclusions

The extensional study of the brittle tectonics in the NE part of the Bohemian Massif provided complex view of the tectonic development and the stress conditions during various tectonic phases of the Sudetic Marginal Fault Zone and the Hronov – Poříčí Fault Zone. Almost 5000 faults and fractures have been measured in 116 localities. Strike and dip of the faults have been measured within the studied areas, as well as trend and plunge of the lineations occurring on the reactivated planes. Two principle sets of faults within the SMFZ are oriented in the N-S and W-E directions. The faults are mainly dipping under 80-90°. In general, the horizontal or subhorizontal faults almost do not occur in the area. The lineations found on the fault planes are mainly trending to the SW and W. The kinematic frequent analysis was performed due to the distribution of the fault types in the orientations. Strike-slip faults (dextral and sinistral) are mainly oriented in N-S and W-E directions. On the other hand, normal and reverse faults occur in two perpendicular directions NW-SE and NE-SW. The fractures within the SMFZ have a predominant W-E orientation, nevertheless they occur in all directions.

Paleostress analysis of the fault-slip data within the SMFZ resulted in separation of six tectonic phases:

- The first and the youngest phase is characterised by the strike-slip regime with maximum compression (σ_1) in the NNW-SSE direction and maximum extension (σ_3) in NW-SE direction. This phase is supposed to be the recent one, whereas there is no evidence of other younger kinematic indicators. The SMFZ has been a sinistral fault zone with the maximum compression oblique to the main direction of the fault during this phase.
- The second phase was characterised by the compressional tectonic regime. The maximum compression (σ_1) was oriented in WNW-ESE direction. These stress conditions resulted the SMF was a reverse fault zone during this phase.
- The third phase is characterised by the extensional stress conditions. The maximum compression (σ_1) was subvertical to the main fault zone. The maximum extension (σ_3) was oriented ENE-WSW almost perpendicular to the main fault zone. The SMF was a normal fault during the third phase.

- The fourth phase was characterised by the extensional stress conditions. The maximum extension (σ_3) was oriented ENE-WSW, the intermediate stress axis (σ_2) was oriented NNW-SSE. During this phase the SMF was a normal fault and extensional tectonic regime occurred.
- The fifth phase was characterised by the strike-slip regime. The maximum compression (σ_1) was oriented NNE-SSW, the maximum extension (σ_3) was oriented in WNW-ESE direction. These stress conditions resulted during this phase the SMF was a dextral fault.
- The sixth phase was characterised by the strike-slip regime. The maximum compression (σ_1) was oriented NW-SE almost parallel to the main fault. The maximum extension (σ_3) was oriented NE-SW almost perpendicular to the main fault. During this last phase, the SMF was a normal fault zone with sinistral component.

The faults within the HPFZ are mostly oriented in NW-SE direction, nevertheless in minor they also occur in the NE-SW direction. The faults are mainly vertical or subvertical dipping 70-90°. The lineations found on the fault planes are mainly trending to the NE, S, SSW and SW. Normal faults of NW-SE, NE-SW and W-E directions have been found. The reverse faults are mainly oriented in NW-SE direction. Dextral faults are mainly oriented in N-S direction. Two principle sets of sinistral faults were found in NW-SE and NE-SW directions. The fractures within the HPFZ are oriented mainly in NW-SE direction.

Paleostress analysis of the fault-slip data within the HPFZ resulted in separation of four tectonic phases:

- The first and the youngest phase is characterised by compressional regime. The maximum compression (σ_1) is oriented in NE-SW direction perpendicular to the main fault zone. Although the maximum extension (σ_3) is vertical, the intermediate principle stress is oriented in NW-SE direction. These conditions caused that the HPFZ is under transpression with dextral component recently.
- The second phase was characterised by compression. The maximum compression (σ_1) was oriented WNW-ESE and the maximum extension (σ_3) was almost subvertical. During this phase, the HPFZ was thrust with the compression oriented obliquely to the main fault zone.
- The third phase was characterised by strike-slip regime. The maximum compression (σ_1) was oriented NW-SE, the maximum extension (σ_3) was

oriented in NE-SW direction. As a result of these stress conditions the HPFZ was a sinistral fault zone.

- The fourth phase was characterised by strike-slip regime. The maximum compression (σ_1) was oriented NNE-SSW, the maximum extension (σ_3) was oriented in WNW-ESE direction. During this tectonic phase the HPFZ was a dextral fault zone.

Data from campaign and permanent GPS stations were used to calculate the horizontal and vertical movements, azimuths (strikes) of the horizontal movements and the standard deviations within the SMFZ and HPFZ areas. Three types of models have been used to test the variability and weight of the final movements and the azimuths. First model is based on the deduction of arithmetic average movement of all individual station's movements from the primary GPS station velocities. Second model is based on the deduction of weighted average movement of all individual station's movements from the primary GPS station velocities. Supposing that the results from permanent stations are more precise than from the campaign stations, the high weight has been assigned to three used permanent stations. To subtract the influence of movement of Euroasian tectonic plate, global motion model NNR-NUVEL 1A model was applied as the third model.

The lowest local horizontal velocities within the SMFZ area were calculated for GPS stations BISK = 0.29 mm/y and VRES = 0.2 mm/y. The lowest local vertical velocities within the SMFZ area were calculated for GPS stations STAM = 0.04 mm/y upwards and BISK = -0.14 mm/y downwards. The highest local horizontal velocity within the SMFZ area was calculated for GPS station VIDN = 1.33 mm/y. The highest local vertical velocity within the SMFZ area was calculated for GPS station PETR = 2.54 mm/y upwards. Generally, comparing to the whole area, stations BISK and PETR move downwards, while the stations LANS, VIDN, STAM and VRES move upwards.

The lowest local horizontal velocities within the HPFZ area were calculated for GPS stations BEZD = 0.17 mm/y and UPIC = 0.32 mm/y. The lowest local vertical velocities within the HPFZ area were calculated for GPS stations BEZD = 0.03 mm/y upwards and UPIC = 0.09 mm/y upwards. The highest local horizontal velocity within the HPFZ area was calculated for GPS station MOKA = 2.18 mm/y. The highest local vertical velocity within the HPFZ area was calculated for GPS station TURO = 2.61 mm/y upwards. Generally, comparing to the whole area, stations BEZD, MOKA and TURO move downwards, while the stations UPIC and ZOLE move upwards. The standard deviations for both horizontal and vertical movements are much lower for permanent stations than for the campaign stations.

The brittle tectonic data has been related to the recent tectonic movements indicated by the GPS measurements. Both structural and GPS data were compared and the actual activity and stress conditions of the SMFZ and HPFZ area were constructed. The tectonic situation within the SMFZ determined by various methods is rather complicated and disparate. To determine the relative movement within the SMFZ, PETR and LANS stations have been chosen. The relative horizontal velocity between the stations is 0.7 mm/y. The relative movement between these two stations is left-lateral.

The tectonic situation within the HPFZ determined by various methods is rather identical. The stations ZOLE and UPIC move towards the HPFZ, that causes the thrusting of the northwestern part over the southeastern part. In the same time, the stations TURO and MOKA go along the fault zone. This situation causes the transpressional conditions with dextral movements within the HPFZ.

The research demonstrated abundant tectonic activity in the NE part of the Bohemian Massif. The variations associated with different tectonic regimes provide further evidence of complicated behaviour of the Sudetic Marginal Fault Zone and the Hronov – Poříčí Fault Zone. The SMFZ has been a sinistral fault zone with strike-slip regime recently. The HPFZ has been a dextral transpressive fault zone in compressional regime recently. In both studied areas, the youngest tectonic phase defined by the paleostress analysis corresponds to the actual movements found by the GPS monitoring. Both employed methods the paleostress analysis of brittle tectonics data and long-term GPS monitoring, provided complementary results. The application of multidisciplinary approach proved to be a promising tool for reconstruction an actual stress conditions and recent tectonic movements of complex fault zones and structures.

References

Alexandrowski, P., Kryza, R., Mazur, S., Zaba, J., 1997. Kinematic data on major Variscan strike-slip faults and shear zones in the Polish Sudetes, northeast Bohemian Massif. Geological Magazine, 134, 727–739.

Arlegui, L.E., Simón, J.L., Lisle, R.J., Orife, T., 2006. Analysis of non-striated faults in a recent extensional setting: the Plio-Pleistocene Concud fault (Jiloca graben, eastern Spain). Journal of Structural Geology, 28, 1019–1027.

Angelier, J., 1979. Tectonic analysis of fault slip data sets. Journal of Geophysical Research, 89, B7, 5835–5848.

Angelier, J., 1984. Determination of the mean principle directions of stresses for a given fault population. Tectonophysics, 56, T17–T26.

Angelier, J., 1994. Fault Slip Analysis and Paleostress Reconstruction. In: Hancock, P.L. (Ed.), Continental Deformation. Pergamon Press, Oxford, 53–100.

Angelier, A., Mechler, P., 1977. Sur une méthode graphique de recherche de constraintes principales également utilisable et en séismologie: la méthode des dièdres droits. Bulletin Société Géologique de la France, 19, 1309–1318.

Badura, J., Zuchiewicz, W., 2008. The Sudetic Marginal Fault as one of principal morphotectonic structures of the eastern portion of the European Cenozoic Rift System. 6–14th August 2008, International Geological Congress Oslo.

Badura, J., Zuchiewicz, W., Przybylski, B., 2004. The Sudetic Marginal Fault, SW Poland: a reactivated sinistral-normal fault. Geolines, 17, 17–18.

Badura, J., Zuchiewicz, W., Štěpančíková, P., Przybylski, B., Kontny, B., Cacoń, S., 2007. The Sudetic Marginal Fault: A young morphotectonic feature at the NE margin of the Bohemian Massif, Central Europe. Acta Geodynamica et Geomaterialia, 4, 4, 148, 7–29.

Barlik, M., 2002. 4th Czech–Polish Workshop on recent Geodynamics of the Sudety Mts. and Adjacent Areas. November 7–9, 2002, Lubawka, Poland, 9.

Barlik, M., Olszak, T., Pachuta, A., 2004. Ten years of gravimetric monitoring on the points of geodynamic networks in the Sudety Mts. Acta Geodynamica et Geomaterialia, 1, 3, 135, 91–95.

Bergerat, F., Angelier, J., Andereasson, P., 2007. Evolution of paleostress fields and brittle deformation of the Tornquist Zone in Scania (Sweden) during Permo-Mesozoic and Cenozoic times. Tectonophysics, 444, 93–110.

Bechtold M., Battaglia, M., Tanner, D.C., Zuliani, D., 2009. Constraints on the active tectonics of the Friuli/NW Slovenia area from CGPS measurements and three-dimensional kinematic modelling. Journal of Geophysical Research, 114, B03408, doi:10.1029/2008JB005638.

Beutler, G., Bock, H., Dach, R, Friedz, P., Gäde, A., Hugentobler, U., Jäggi, A., Mendl, M., Mervart, L., Prange, L., Schaer, S., Springer, T., Uschl, C., Walser, P., 2007. User manual of the Bernese software Version 5.0.

Bistachi, A., Eva, E., Massironi, M., Solarino, S., 2000. Miocene to Present kinematics of the NW-Alps: evidences from remote sensing, structural analysis, seismotectonics and thermochronology. Journal of Geodynamics, 30, 1–2, 205–228.

Bistachi, A., Massironi, M., 2000. Post-nappe brittle tectonics and kinematic evolution of the north-western Alps: an integrated approach. Tectonophysics, 327, 3–4, 267–292.

Blachowski, J., Cacoń, S., 2002. Mobility of Local Tectonic Structures in Western Part of the Paczków Graben (Sudetic Foreland) on the Grounds of Present Investigations. 4th Czech–Polish Workshop on recent Geodynamics of the Sudety Mts. and Adjacent Areas. November 7–9, 2002, Lubawka, Poland, 10.

Bock, Y., Wdowinski, S., Fang, P., Zhang, J., Behr, J., Genrich, J., Williams, S., Agnew, D., Wyatt, F., Johnson, H., Stark, K., Oral, B., Hudnut, K., Dinardo, S., Young, W., Jackson, D., Gurtner, W., 1997. Southern California Permanent GPS Geodetic Array: Continuous measurements of crustal deformation between the 1992 Landers and 1994 Northridge earthquakes. Journal of Geophysical Research, 102, 18.013–18.033.

Bosy, J., Kontny, B., Cacoń, S., Schenk, S., Schenková, Z., Kottnauer, P., 2002. GPS Data Processing and Geodynamic Movement Assessment. 4th Czech–Polish Workshop on recent Geodynamics of the Sudety Mts. and Adjacent Areas. November 7–9, 2002, Lubawka, Poland, 12.

Bott, M.H.P., 1959. The mechanisms of oblique slip faulting. Geological Magazine, 96, 109–117.

Brož, M., Málek, J., Stejskal, V., Štěpančíková, P., Štrunc, J., Kolínský, P., 2009. Hydro-geological effects of seismicity in the Hronov – Poříčí Fault Zone area. Acta Research Reports, 18, 61–63.

Bruyninx, C., 2004. The EUREF Permanent Network: a multi-disciplinary network serving surveyors as well as scientists. GeoInformatics, 7, 32–35.

Bruyninx, C., 2006. GPS and GLONASS data analysis using stations from the EUREF Permanent Network. EUREF Symposium 2006, 14–17 June 2006, Riga.

Bruyninx, C., Becker, M., Stangl, G., 2001. Regional Densification of the IGS in Europe Using the EUREF Permanent GPS Network (EPN). Physical and Chemical Earth, 26, 6–8, 531–538.

Buday, T., Ďurica, D., Opletal, M., Šebesta, J., 1995. Significance of the Bělský and Klepáčovský fault system and its continuation to the Carpathian Mts. [in Czech]. Geologický průzkum 2, 9, 275–281.

Burg ,J.P. Paleostress calculations. 2012.

http://www.files.ethz.ch/structuralgeology/JPB/files/English/5paleostress.pdf.

Cacoń, S., Kontny, B., Bosy, J., 2007. 3D monitoring of the selected active tectonic structures in Poland, Italy and Greece. Acta Geodynamica et Geomaterialia, 4, 1, 145, 7–17.

Cajthamlová M, 2010. Geokinematics of the Bohemian Massif determined by the satellite geodesy data [in Czech]. PhD thesis. Czech Technical University. Prague.

Calais, E., Bayer, R., Chéry, J., Cotton, F., Doerflinger, E., Flouzat, M., Jouanne, F., Kasser, M., Laplanche, M., Maillard, D., Martinod, J., Matthieu, F., Nicolon, P., Nocquet, J.-M., Scotti, O., Serrurier, L., Tardy, M., Vigny, C., 2000. REGAL: A permanent GPS network in the western Alps and foreland, first results, Comptes Rendus de l'Académie des Sciences.

Caporali, A., Martin, S., Massironi, M., 2003. Average strain rate in the Italian crust inferred from a permanent GPS network–II. Strain rate versus seismicity and structural geology. Geophysical Journal International, 155, 254–268.

Cloos, H., 1922. Der Gebirgsbau Schlesiens und die Stellung seiner Bodenschätze, Berlin.

Cháb, J., 1987. Zhodnocení geologických a technických prací provedených v předpolí ložiska Zlatý Chlum u Jeseníka, In: Hauk, J. ed., MS archív ČGS Praha a Jeseník.

Carey, E., Brunier, B., 1974. Analyse theorique et numerique d'un modele elementaire applique a l'etude d'une population de faille. Comptes Rendus de I Ycademie des Sciences, Paris, D, 279, 891–894.

Chlupáč, I., 1994. Regional geological subdivision of the Bohemian Massif on the territory of the Czech Republic. Journal of the Czech Geological Society, 39, 1, 127–144.

Chlupáč, I., Brzobohatý, R., Kovanda, J., Stráník, Z., 2002. Geological history of the Czech Republic [in Czech]. Academia Praha.

Cymermann, Z., Piasecki, M.A.J., Seston, R., 1997. Terranes and terrane boundaries in the Sudetes, northeast Bohemian Massif. Geological Magazine 134, 717–725.

Cymermann, Z., 1999. Alpine transpression in the Sudetes. [in Polish] Przegląd Geologiczny, 47, 10, 942–945.

Dach, R., Brockmann, E., Schaer, S., Beutler, G., Meindl, M., Prange, L., Bock, H., Jaggi, A., Ostini, L., 2009. GNSS processing at CODE: status report. Journal of Geodesy, 83, 3–4, 353–365.

Dach, R., Hugentobler, U., Fridez, P., Meindl, M., 2007. Bernese GPS software version 5.0. Astronomical Institute, University of Bern.

Danišík, M., Štěpančíková, P., Evans, N.J., 2012. Constraining long-term denudation and faulting history in intraplate regions by multisystem thermochronology: An example of the Sudetic Marginal Fault (Bohemian Massif, central Europe). Tectonics, 31, 1–19.

D'Agostino, N., Avallone, A., Cheloni, D., D´Anastasio, E., Mantenuto, S., Selvagi, G., 2008. Active tectonics of the Adriatic region from GPS and earthquake slip vectors. Journal of Geophysical Research. 113, B12413, 19.

Dixon, T. H., Mao, A., 1997. A GPS estimate of relative motion between North and South America, Geophysical Research Letters, 24, 535–538,.

Doblas, M., 1998. Slickenside kinematic indicators. Tectonophysics, 295, 187–197.

Drake, S. P., 2002. Converting GPS coordinates to navigation coordinates. Electronics and Surveillance Research Laboratory, Edinburgh, Australia.

Fejes, I., Barlik, M., Busics, I., Packelski, W., Rogowsky, J., Sledzinsky, J., Zielinsky, J.B., 1993. The Central Europe Regional Geodynamics Project, paper presented at 2nd International Seminar on GPS in Central Europe, Hungary Academy of Sciences, Penc, Hungary.

Grácová, M., Mantlík, F., Schenk, V., Schenková, Z., Zajac, M., 2005. Preliminary West Sudeten site movements determined by the GAMIT/GLOBK and BERNESE GPS software. Abstracts of the 7th Czech-Polish Workshop "Recent Geodynamics of the Sudeten and Adjacent Areas", 18.

Grácová, M., Mantlík, F., Schenk, V., Schenková, Z., 2007. Data processing of GNSS observation of the GEONAS network – Effects of extréme meteorological conditions. Acta Geodynamica et Geomaterialia, 4, 4, 148, 153–161.

Grenerczy, G., Sella, G., Stein, S., Kenyeres, A., 2005. Tectonic implications of the GPS velocity field in the northern Adriatic region. Geophysical Rechearch Letters. 32, L16311.

Grocholski, A., 1977. Uskok sudecki brzeżny a zagadnienie wulkanotektoniki trzeciorzędowej, Acta Univ.Wratislaviensis, No 378, Prace Geol.- Miner. 6, Wroclaw, 89–103.

Guterch, B., Lewandowska-Marciniak, H., 2002. Seismicity and seismic hazard in Poland. Folia Quaternaria 73, 85–99.

Hancock, P.L., 1985. Brittle microtectonics: principles and practise. Journal of Structural Geology 7, 437–457.

Havíř, J., 2002. Variscan and Post-Variscan Paleostresses on the Southeastern Margin of the Nízký Jeseník Region (Czech Republic). Geolines, 14, 33–34.

Havíř, J., 2004. Orientations of recent principal stress axes in the Jeseníky region. Acta Geodynamica et Geomaterialia 1, 3, 135, 31–33.

Havíř, J., 2011. Principal stress axes orientations in the NE part of the Bohemian Massif during cainozoic – present knowledge, difficulties and limits. On recent geodynamics of the Sudety Mts. and adjacent areas, abstracts. 12th Czech-Polish Workshop, 20–22 October, Jugowice, 2011. 26.

Havíř, J., Špaček, P., 2004. Recent tectonic activity and orientations of the principal stresses in the Jeseníky region. Geolines 17, 38–39.

Kaláb, Z., Krejzlík, J., Holub, K., 2002. Decade of seismological observations in the northern part of Moravo-Silesian region. Acta Geodynamica et Geomaterialia, 4, 4, 148, 43–49.

Kaplon, J., Cacoń, S., 2008. Geodetic monitoring of recent tectonic activity of the Marginal Sudetic Fault. EGU General Assembly 2008, Vienna. A–07487.

Kernstocková, M., Melichar, R., 2006. Do you separate sets of reactivated faults manually? Geolines 20, 66.

Khanbari, K. and Huchton, P., 2010. Paleostress analysis of the volcanic margins of Yemen. Arabian Journal of Geosciences 3, 529–538.

Kolínský, P., Valenta, J., Gaždová, R., 2012. Seismicity, groumdwater level variations and earth tides in the Hronov – Poříčí Fault Zone, Czech Republic. Acta Geodynamica et Geomaterialia, 9, 2, 166, 191–209.

Komárek, L., 2009. Paleostress analysis of Gijón-Villavicio Jurrasic Basin (Spain) [in Czech]. Bc thesis. Masaryk University Brno. pp. 31.

Kontny, B., 2004. Is the Sudetic Marginal Fault still active? Results of the GPS monitoring 1996-2002. Acta Geodynamica et Geomaterialia 1, 3,135, 31–33.

Kounov, A., Burg, J.P., Bernoulli, D., Seward, D., Ivanov, Z., Dimov, D., Gerdjikov, I., 2011. Paleostress analysis of Cenozoic faulting in the Kraishte area, SW Bulgaria. Journal of Structural Geology, 33, 859–874.

Krzyszkowski, D., Bowman, D., 1997. Neotectonic Deformation of Pleistocene Deposits Along the Sudetic Marginal Fault, Southwestern Poland. Earth Surface Processes and Landforms, 22, 6, 545–562.

Krzyszkowski, D., Migoń, P., Sroka, W., 1995. Neotectonic Quarternary history of the Sudetic Marginal Fault, SW Poland. In Neotectonics of Poland: Some New Achievements (ed. W. Zuchiewicz), Folia Quaternaria, 66, 73–98.

Lee, J.Ch., Lu, Ch.Y., Chu H.T., Delcaillau, B., Angelier, J., Deffontaines, B., 1996. Active Deformation and Paleostress Analysis in the Pakua Anticline Area of Western Taiwan. TAO, 7, 4, 431–446.

Liesa, C.L., Lisle, R.J., 2004. Reliability of methods to separate stress tensors from heterogeneous fault-slip data. Journal of Structural Geology, 26, 559–572.

Likhar, S., Madhav, N., Kulkarni, V., Tomar, S., Pillai, P., 2002. A comparative study of results from GPS data processing software. Trends in GPS data processing, 24 - 25 October 2002. India International Centre, New Delhi, India, 1–5.

Mantlík, F., Schenk, V., Schenková, Z., Kottnauer, P., Grácová, M., Fučík, Z., 2005. GEONAS – The GEOdynamic Network of the Academy of Sciences of the Czech Republic: Permanent GNSS observations and routine data processing in the IRS operational centre. EUREF Publication No. 14, Mitteilungen desBundesamtes für Kartographie and Geodäsie, 35, Frankfurt am Main, 140–142.

Málek, J., Stejskal, V., Zedník, J., 2008. Seismological swarm in the Hronov – Poříčí Fault Zone area in January 2008. [in Czech]. In Marková, E. (Ed.) Human in its nature and space. Proceedings from the conference in Úpice town, 20-22.5.2008, 84–91.

Melichar, R., Kernstocková, M., 2008. 9D Space - The best way to understand paleostress analysis. Programme & Extended Abstracts. International Meeting of Young Researchers in Structural Geology and Tectonics, YORSGET-08, 1-3 July 2008, Universidad de Oviedo (Spain), 327–331.

Nemčok, M., Lisle, R.J., 1995. A stress inversion procedure for polyphase fault/slip data sets. Journal of Structural Geology 17, 1445–1453.

Nieto-Samaniego, A.F., 1998. Stress, strain and fault patterns. Journal of Structural Geology, 21, 1065–1070.

Nováková, L., 2008. Main directions of the fractures in the limestone and granite quarries along the Sudetic Marginal Fault near Vápenná village, NE Bohemian Massif, Czech Republic. Acta Geodynamica et Geomaterialia 5, 1, 149, 49–55.

Nováková, L., Schenk, V., 2008. Recent tectonic movements in the NE part of the Bohemian Massif, Czech Republic, indicated by the brittle tectonic approach. Geophysical Research Abstracts 10, 07801.

Nováková, L., 2010. Detailed brittle tectonic analysis of the limestones in the quarries near Vápenná village. Acta Geodynamica et Geomaterialia 7, 2, 158, 1–8.

Nováková, L., Hájek, P., Šťastný, M., 2010. Determining the relative age of fault activity through analyses of gouge mineralogy and geochemistry: a case study from Vápenná (Rychlebské hory Mts.), Czech Republic. International Journal of Geosciences, 1, 2, 66–69.

Oberc, J., 1967. Sudetic marginal flexure and tectonics of the Rychlebské hory Mts.. [in Polish]. Časopis pro Mineralogii a Geologii 12, 2–12.

Oberc, J., 1977. The Late Alpine Campaign in south-west Poland. In: W. Pozaryski (Ed.), Geology of Poland IV, Tectonics. Wydawna Geologika, Warszawa, 451–475.

Oberc, J., Dyjor, S., 1969. Sudetic Marginal Fault [in Polish]. Buletyn Instytutu Geologicznego 236, 41–142.

Opletal, M., Pecina, V., 2004. The Ramzová tectonic zone: the contact between Lugian and Silesicum. Acta Geodynamica et Geomaterialia, 1, 3, 135, 41–47.

Popotnig, A., Decker, K., Graseman, B., 2007. Active kinematics and tectonic geomorphology of the Lavanttal Fault. EGU General Assembly, Vienna 2008.

Salvini, F., Brancolini, G., Buseti, M., Storti, F., Mazzarini, F., Coren, F., 1997. Cenozoic geodynamics of the Ross Sea region, Antarctica: Crustal extension, intraplate strike-slip faulting, and tectonic inheritance. Journal of Geophysical Research, 102, B11, 24.669–24.696.

Salvini, F., Storti, F., 2005. Kinematicly - versus dynamically - induced brittle deformations: the Chinese box ambiguity and solution. Application to the Antarctica Cenozoic Tectonics. Geophysical Research Abstracts, 7, 09455.

Scheck, M., Bayer, U., Otto, V., Lamarch, J., 2002. The Elbe Fault System in North Central Europe-a basement controlled zone of crustal weakness. Tectonophysics, 360, 281–299.

Schenk, V., Cacoń, S., Bosy, J., Kontny, B., Schenková, Z., Kottnauer, P., 2000. GPS network „SUDETEN" – Preliminary results of the campaigns 1997–1999. Report of Geodesy, 53, 7, 25–33.

Schenk, V., Kottnauer, P., Schenková, Z., Hájek, P., 2004. Czech permanent GPS obsertvatories for geodynamic investigations of the Bohemian Massif operated by the

Institute of Rock Structure and Mechanics, Prague. Acta Geodynamica et Geomaterialia, 1, 3, 135, 111–114.

Schenk, V., Schenková, Z., Cacoń, S., Kontny, B., Bosy, J., Kottnauer, P., 2003. The geodynamic interpretation of the GPS data monitored at the East Sudeten network. Acta Montana A 24, 131, 87–97.

Schenk, V., Schenková, Z., Cajthamlová, M., Fučík, F., 2010. GEONAS - Geodynamic network of Permanent GNNS stations within the Czech Republic. Acta Geodynamica et Geomaterialia, 7, 1, 157, 99–111.

Schenk, V., Schenková, Z., Pospíšil, L., 1989. Fault system dynamics and seismic activity - examples from the Bohemian Massif and the Western Carpathians. Geophysical Transactions, 35, 1–2, 101–116.

Schenková, Z., Kottnauer, P., Schenk, V., Cajthamlová-Grácová, M., Mantlík , F., Kujal, R., 2009. Investigation of the recent crustal movements of the eastern part of the Bohemian Massif using GPS technology. Acta Research Reports, 18, 17–25.

Schulmann, K., Gayer, R., 2000. A model for a continental accretionary wedge developed by oblique collision: the NE Bohemian Massif. Journal of the Geological Society, 157, 401–416.

Skácel, J., 1989. Crossing of the Sudetic Marginal Fault and Nýznerov overthrust between Vápenná and Javorník in Silesia [in Czech]. Acta Universitatis Palackyanae Olomoucensis, 95, 31–45.

Skácel, J., 2004. The Sudetic Marginal Fault between Bílá voda and Lipová Lázně. Acta Geodynamica et Geomaterialia 1, 3, 135, 31-33.

Skácelová, D., Skácelová, Z., Havíř, J., 1997. Earthquakes in the Northeastern Part of the Bohemian Massif Recorded by the MORC Station during the Period October 1994 – March 1995. Věstník Českého geologického ústavu, 72, 1, 49-53.

Skácelová, Z., Mlčoch, B., Tasáryová, Z., 2009. Digital elevation model of the crystalline basement and Permo-Carboniferous surface (Bohemian Massif, NE part of the Czech Republic). Acta Geodynamica et Geomaterialia, 6, 3, 155, 265–271.

Stejskal, V., Kašpárek, L., Kopylova, G.N., Lyubyshin, A.A., Skalský, L., 2009. Precursory groundwater level changes in the period of activation of the weak intraplate seismic activity on the NE margin of the Bohemian Massif (Central Europe) in 2005. Studia Geophysica et Geodetica, 53, 215−238.

Stejskal, V., Skalský, L., Kašpárek, L., 2007. Results of two years' seismo-hydrological monitoring in the area of the Hronov – Poříčí Fault Zone, Western Sudetes. Acta Geodynamica et Geomaterialia, 4, 4, 148, 59–76.

Stejskal, V., Štěpančíková, P., Vilímek, V., 2006. Selected geomorphological methods assessing neotectonic evolution of the seismoactive Hronov – Poříčí Fault Zone. Geomorphologica Slovaca, 6, 14−22.

Stemberk, J., Štěpančíková, P., 2003. Tectonic setting and newly organised monitoring of recent tectonic deformation in the Rychlebské Hory Mts. Acta Montana, A 24, 131, 153–161.

Strzerzynski, P., Guillot, S., Leloup, P.H., Ledru, P., Courrioux, G., Darmendrail, X., 2004. Brittle deformations between the Ambin and Vanoise domes in the frame of the structural evolution of the internal Alpine belt. Virtual Explorer, 16.

Styron, R.H., Taylor, M.H., 2009. Kinematics of the Himalayan arc from GPS geodesy and structural geology. American Geophysical Union, Fall Meeting 2009, T41D–07.

Styron, R.H., Taylor, M.H., Murphy, M.A., 2011. Oblique convergence, arc-parallel extension, and the role of strike-slip faulting in the High Himalaya. Geosphere, 7, 2, 582–596.

Styron, R.H., Taylor, M.H., Okoronkwo, K., 2010. Database of Active Structures From the Indo-Asian Collision. EOS, Transactions AGU, 91, 20, 181.

Suess, F.E., 1912. Die moravischen Fenster und ihre Beziehung zum Grundgebirge des Hohen Gesenkes. Denkschrichte des Koeniglischen Akademie der Wissenscahft, Math. Naturwiss 83, 541–631.

Špaček, P., Sýkorová, Z., Pazdírková, J., Švancara, J., Havíř, J., 2006. Present-day seismicity of the south-eastern Elbe Fault System (NE Bohemian Massif). Studia Geophysica et Geodaetica, 50, 2, 233–258.

Štěpančíková, P., 2005. Selected analyses of the morphostructure of the NE part of the Rychlebské hory Mts. (Czech Republic). Acta Geodynamica et Geomaterialia, 2, 1, 137, 59–67.

Štěpančíková, P., 2008. Morphostructural development of the north-eastern part of the Rychlebské hory Mts. Acta Research Reports, 17, 55–61.

Štěpančíková, P., Hók, J., 2009. Tectonic hazard and paleoseismological research within the Sudetic Marginal Fault zone (NE Bohemian Massif, Czech Republic). 17th Conference on Engineering Geology with Forum for Young Engineering Geologists, 439–441.

Štěpančíková, P., Rowberry, M., 2008. Rock landforms that reflect differential relief development in the North-eastern sector of the Rychlebské hory and the adjacent area of Žulovská pahorkatina (SE Sudeten Mts., Czech Republic). Acta Geodynamica et Geomaterialia, 5, 151, 297–321.

Štěpančíková P., Dohnal J., Pánek T., Łój M., Smolková V., Šilhán K., 2011. The application of electrical resistivity tomography and gravimetric survey as useful tools in an active tectonics study of the Sudetic Marginal Fault (Bohemian Massif, central Europe). Journal of Applied Geophysics, 74, 69–80.

Štěpančíková, P., Hók, J., Nývlt, D., Dohnal, J., Sýkorová, I., Stemberk, J., 2010. Active tectonics research using trenching technique on the south-eastern section of the Sudetic Marginal Fault (NE Bohemian Massif, central Europe). Tectonophysics, 485, 269–282.

Štěpančíková, P., Stemberk, J., Vilímek, V., Košťák, B., 2008a. Neotectonic development of drainage network in the East Sudeten Mountains and monitoring of recent fault displacements (Czech Republic). Geomorphology, 102, 68–80.

Štěpančíková, P., Hók, J., Stemberk, J., Nývlt, D., 2008b. Results of active tectonics research in the Sudetic Marginal Fault zone: Vlčice u Javorníka. Abstracts of the 9th Czech-Polish Workshop on Recent Geodynamics of the Sudety Mts. and Adjacent Areas, 18.

Švábenský,O., Weigel, J., Machotka,R., Podstavek, J., 2002. Last Geodetic Activities of BUT in Sudety Mts. Region. 4th Czech–Polish Workshop on recent Geodynamics of the Sudety Mts. and Adjacent Areas. November 7–9, 2002, Lubawka, Poland, 43.

Švábenský, O., Weigel, J., 2007. Long- term positional monitoring of station VYHL of the Sněžník network. Acta Geodynamica et Geomaterialia, 4, 4, 201–206.

Tásler, R., Čadková, Z., Dvořák, J., Fediuk, F., Chaloupský, J., Jetel, J., Kaiserová-Kalibová, M., Prouza, V., Schovánková-Hrdličková, D., Středa, J., Střída, M. and Šetlík, J., 1979. Geology of the Czech part of the Intra-Sudetic Basin [in Czech]. ÚÚG, Praha, pp. 292.

Valenta, J., Stejskal, V., Štěpančíková, P., 2008. Tectonic pattern of the Hronov – Poříčí Trough as seen from pole-dipole geoelectrical measurements. Acta Geodynamica et Geomaterialia, 5, 2, 150, 185–195.

Valenta, J., Gazdova, R., Kolinsky, P., 2011. Seismo-hydrological monitoring in the area of the Hronov-Poříčí Fault Zone, Northern Czech Republic, Central Europe. American Geophysical Union, Fall Meeting 2011, S11B–2211.

Viola, G., Kounov, A., Andreoli, M.A.G., Mattila, J., 2011. Brittle tectonic evolution along the western margin of South Africa: More than 500 Myr continued reactivation. Tectonophysics, 514–517, 93–114.

Vyskočil, P., 1988. The dynamics of the Hronov – Poříčí seismoactive fault. Proceedings of the Research Institute of Geodesy. Topographie et de la Cartographie, 17, 93–111.

Woldřich, J.N. 1901 Earthquake in the north-eastern Bohemia on January 10, 1901 [in Czech]. Transactions of the Czech Academy of Sciences, series II 10, 25, 1–33.

Wojewoda, J., 2007. Neotectonic aspect of the Intrasudetic shear zone. Acta Geodynamica et Geomaterialia, 4, 4, 148, 31–41.

Yamaji, A., 2000. The multiple inverse method: a new technique to separate stresses from heterogeneous fault-slip data. Journal of Structural Geology, 22, 441–452.

Zachariáš, J., Hübst, Z., 2012. Structural evolution of the Roudný gold deposit, Bohemian Massif: a combination of paleostress analysis and review of historical documents. Journal of Geosciences, 57, 87–103.

Zedník, J., Hudová, Z., 2008. Earthquake M=3.3 in Hronov area 25.10.2005. In Marková, E. (Ed.) Human in its nature and space. [in Czech]. Proceedings from the conference in Úpice town 20-22.5.2008, Úpice, 129–133.

Žalohar, J., Vrabec, M., 2007. Paleostress analysis of heterogeneous fault-slip data: The Gauss method. Journal of Structural Geology 29, 1798–1810.

Žalohar, J., 2009. T-TECTO 3.0 Professional Integrated Software for Structural Analysis of Fault-Slip Data, Introductory Tutorial, pp 56.

Appendices

Appendices

Appendix 1

Nováková, L., 2008. Main Directions of the Fractures in the Limestone and Granite Quarries along the Sudetic Marginal fault near Vápenná village, NE Bohemian Massif, Czech Republic. Acta Geodynamica et Geomaterialia, 5, 1, 149, 49–55.

Peer – reviewed article

Appendices

Appendix 2

Nováková, L., 2009. Brittle tectonic investigations in the north-eastern part of the Bohemian Massif, Czech Republic. 71st EAGE Annual Conference & Exhibition in Amsterdam 2009.

Peer – reviewed extended abstract

Appendices

Appendix 3

Nováková, L., 2010. Detailed brittle tectonic analysis of the limestones in the quarries near Vápenná village. Acta Geodynamica et Geomaterialia, 7, 2, 158, 1–8.

Peer – reviewed article in journal with IF

Appendices

Appendix 4

Nováková, L., Hájek, P., Šťastný, M., 2010. Determining the relative age of fault activity through analyses of gouge mineralogy and geochemistry: a case study from Vápenná (Rychlebské hory Mts.), Czech Republic. International Journal of Geosciences, 1, 2, 66–69.

Peer – reviewed article

Appendices

Appendix 5

Nováková, L., Methods of tectonic phase separation applied to the Sudetic Marginal Fault Zone (NE Bohemian Massif, Czech Republic). Geologica Acta. Under review.

Peer – reviewed article in journal with IF

Appendices

Appendix 6

Nováková, L., Balek, J., What can GPS monitoring and brittle tectonic studies tell us about a fault reactivation: the Hronov-Poříčí Fault Zone, Bohemian Massif. Studia Geophysica et Geodetica. Under review.

Peer – reviewed article in journal with IF

Appendices